Orbital functionals in density functional theory: the optimized effective potential method

T. Grabo[a], T. Kreibich[a], S. Kurth[b], and E.K.U. Gross[a]

[a] Institut für Theoretische Physik, Universität Würzburg, Am Hubland, 97074 Würzburg, Germany

[b] Department of Physics and Quantum Theory Group, Tulane University, New Orleans, LA 70118, USA

Contents

1 Introduction **1**

2 The OEP method, basic formalism **6**
2.1 Derivation of the OEP equations 6
2.2 Approximation of Krieger, Li and Iafrate 9
2.3 Rigorous properties of the OEP and KLI potentials 13
2.3.1 An important lemma 13
2.3.2 Asymptotic form 18
2.3.3 Derivative discontinuities 22
2.4 Hartree-Fock versus x-only OEP, a comparison 27

3 Relativistic generalization of the OEP and KLI methods **28**
3.1 Relativistic optimized effective potential method 29
3.2 Relativistic KLI approximation 31
3.3 Relativistic OEP in the electrostatic case 34

4 Numerical results **35**
4.1 Exchange-only calculations for nonrelativistic systems 35
4.1.1 Atomic systems 35
4.1.2 Diatomic molecules 47
4.2 Comparison of nonrelativistic with relativistic results 52
4.3 Inclusion of correlation contributions for nonrelativistic systems 60
4.3.1 Atomic systems 63
4.3.2 Diatomic molecules 72
4.4 Solids 78

5 Beyond the OEP - a connection with Many-Body Perturbation Theory **85**

1 Introduction

Density functional theory (DFT) is a powerful quantum mechanical method for calculating the electronic structure of atoms, molecules and solids [1, 2, 3]. The success of DFT hinges on the availability of good approximations for the total-energy functional. In this article we shall review a particular approach to the construction of such approximations

which involves explicitly orbital-dependent functionals. Before describing the nature of this approach we first briefly review the foundations of DFT.

We are concerned with Coulomb systems described by Hamiltonians of the type

$$\hat{H} = \hat{T} + \hat{W}_{\rm Clb} + \hat{V} \tag{1}$$

where (atomic units are used throughout this article)

$$\hat{T} = \sum_{i=1}^{N} \Big(-\frac{1}{2} \nabla_i^2 \Big) \tag{2}$$

denotes the kinetic-energy operator,

$$\hat{W}_{\rm Clb} = \frac{1}{2} \sum_{\substack{i,j=1 \\ i \neq j}}^{N} \frac{1}{|\mathbf{r_i} - \mathbf{r_j}|} \tag{3}$$

represents the Coulomb interaction between the particles, and

$$\hat{V} = \sum_{i=1}^{N} v(\mathbf{r}_i) \tag{4}$$

contains all external potentials of the system, typically the Coulomb potentials of the nuclei.

Modern DFT is based on the celebrated theorem of Hohenberg and Kohn (HK) [4] which, for systems with nondegenerate ground states, may be summarized by the following three statements:

1. The ground-state density ρ uniquely determines the ground-state wave function $\Psi[\rho]$ as well as the external potential $v = v[\rho]$. As a consequence, any observable of a static many-particle system is a functional of its ground-state density.

2. The total-energy functional

$$E_{v_0}[\rho] := < \Psi[\rho] | \hat{T} + \hat{W}_{\rm Clb} + \hat{V}_0 | \Psi[\rho] > \tag{5}$$

of a particular physical system characterized by the external potential v_0 is equal to the exact ground-state energy E_0 if and only if the exact ground-state density ρ_0 is inserted. For all other densities $\rho \neq \rho_0$ the inequality

$$E_0 < E_{v_0}[\rho] \tag{6}$$

holds. Consequently, the exact ground-state density ρ_0 and the exact ground-state energy E_0 can be determined by solving the Euler-Lagrange equation

$$\frac{\delta}{\delta \rho(\mathbf{r})} E_{v_0}[\rho] = 0. \tag{7}$$

3. The functional

$$F[\rho] := < \Psi[\rho] | \hat{T} + \hat{W}_{\rm Clb} | \Psi[\rho] > \tag{8}$$

is universal in the sense that it is independent of the external potential v_0 of the particular system considered, i.e. it has the same functional form for all systems with a fixed particle-particle interaction ($\hat{W}_{\rm Clb}$ in our case).

The proof of the HK theorem does not depend on the particular form of the particle-particle interaction. It is valid for *any* given particle-particle interaction $\hat{W}$, in particular also for $\hat{W} \equiv 0$, i.e. for non-interacting systems described by Hamiltonians of the form

$$\hat{H}_S = \hat{T} + \hat{V}_S. \tag{9}$$

Hence the potential $V_S(\mathbf{r})$ is uniquely determined by the ground-state density:

$$V_S(\mathbf{r}) = V_S[\rho](\mathbf{r}). \tag{10}$$

As a consequence, all single-particle orbitals satisfying the Schrödinger equation

$$\left(-\frac{\nabla^2}{2} + V_S[\rho](\mathbf{r})\right) \varphi_j(\mathbf{r}) = \varepsilon_j \varphi_j(\mathbf{r}) \tag{11}$$

are functionals of the density as well:

$$\varphi_j(\mathbf{r}) = \varphi_j[\rho](\mathbf{r}). \tag{12}$$

The HK total-energy functional of non-interacting particles is given by

$$E_S[\rho] = T_S[\rho] + \int d^3r\, \rho(\mathbf{r}) V_S(\mathbf{r}) \tag{13}$$

where $T_S[\rho]$ is the kinetic-energy functional of non-interacting particles:

$$T_S[\rho] = \sum_{\substack{i=1 \\ \text{lowest } \varepsilon_i}}^{N} \int d^3r\, \varphi_i^*[\rho](\mathbf{r}) \left(-\frac{\nabla^2}{2}\right) \varphi_i[\rho](\mathbf{r}). \tag{14}$$

We emphasize that the quantity (14) really represents a *functional of the density:* Functional means that we can assign a unique number $T_S[\rho]$ to any function $\rho(\mathbf{r})$. This is done by first calculating that very potential $V_S(\mathbf{r})$ which uniquely corresponds to $\rho(\mathbf{r})$. Several numerical schemes have been devised to achieve this task [5, 6, 7, 8, 9, 10]. Then we take this potential, solve the Schrödinger equation (11) with it to obtain a set of orbitals $\{\varphi_j(\mathbf{r})\}$ and use those to calculate the number T_S by evaluating the right-hand side of Eq. (14). As a matter of fact, by the same chain of arguments, *any orbital functional is an (implicit) functional of the density,* provided the orbitals come from a local, i.e. multiplicative potential.

Returning to the *interacting* system of interest we now define the so-called exchange-correlation (xc) energy functional by

$$E_{\text{xc}}[\rho] := F[\rho] - \frac{1}{2} \int d^3r \int d^3r'\, \frac{\rho(\mathbf{r})\rho(\mathbf{r}')}{|\mathbf{r} - \mathbf{r}'|} - T_S[\rho]. \tag{15}$$

The HK total-energy functional (5) can then be written as

$$E_{v_0}[\rho] = T_S[\rho] + \int d^3r\, \rho(\mathbf{r}) v_0(\mathbf{r}) + \frac{1}{2} \int d^3r \int d^3r'\, \frac{\rho(\mathbf{r})\rho(\mathbf{r}')}{|\mathbf{r} - \mathbf{r}'|} + E_{\text{xc}}[\rho]. \tag{16}$$

In historical retrospective we may identify three generations of density functional schemes which may be classified according to the level of approximations used for the universal functionals $T_S[\rho]$ and $E_{\text{xc}}[\rho]$.

In what we call the *first generation of DFT, explicitly* density-dependent functionals are used to approximate both $T_S[\rho]$ and $E_{\rm xc}[\rho]$. The simplest approximation of this kind is the Thomas-Fermi model, where $E_{\rm xc}[\rho]$ is neglected completely and $T_S[\rho]$ is approximated by

$$T_S^{\rm TF}[\rho] = \frac{3}{10}\left(3\pi^2\right)^{2/3}\int d^3r\,\rho(\mathbf{r})^{5/3} \tag{17}$$

yielding

$$E_{v_0}^{\rm TF}[\rho] = \frac{3}{10}\left(3\pi^2\right)^{2/3}\int d^3r\,\rho(\mathbf{r})^{5/3} + \int d^3r\,v_0(\mathbf{r})\rho(\mathbf{r}) + \frac{1}{2}\int d^3r\int d^3r'\,\frac{\rho(\mathbf{r})\rho(\mathbf{r}')}{|\mathbf{r}-\mathbf{r}'|} \tag{18}$$

as approximate expression for the total-energy functional. For functionals of this type the HK variational principle (7) can be used directly, leading to equations of the Thomas-Fermi type. As these equations only contain one basic variable, namely the density $\rho(\mathbf{r})$ of the system, they are readily solved numerically. The results obtained in this way, however, are generally of only moderate accuracy in T_S, yielding unacceptably large errors in E_0.

The *second generation* of DFT employs the *exact* functional (14) for the non-interacting kinetic energy and an approximate density functional for the xc energy:

$$E_{v_0}^{\rm KS}[\rho] = T_{\rm S}^{\rm exact}[\rho] + \int d^3r\,v_0(\mathbf{r})\rho(\mathbf{r}) + \frac{1}{2}\int d^3r\int d^3r'\,\frac{\rho(\mathbf{r})\rho(\mathbf{r}')}{|\mathbf{r}-\mathbf{r}'|} + E_{\rm xc}[\rho]. \tag{19}$$

This total-energy expression leads to the Kohn-Sham (KS) version of DFT [11] as will be shown in the following. Plugging Eq. (19) into the variational principle (7) yields

$$0 = \frac{\delta T_{\rm S}^{\rm exact}[\rho]}{\delta\rho(\mathbf{r})} + v_0(\mathbf{r}) + \int d^3r'\,\frac{\rho(\mathbf{r}')}{|\mathbf{r}-\mathbf{r}'|} + \frac{\delta E_{\rm xc}[\rho]}{\delta\rho(\mathbf{r})}. \tag{20}$$

The variation of the non-interacting kinetic energy functional is given by

$$\begin{aligned}\delta T_S^{\rm exact}[\rho] &= \delta\sum_{i=1}^{N} < \varphi_i[\rho]| -\frac{\nabla^2}{2}|\varphi_i[\rho] > \\ &= \delta\left[\sum_{i=1}^{N}\varepsilon_i[\rho] - \int d^3r'\,V_S[\rho](\mathbf{r}')\rho(\mathbf{r}')\right]\end{aligned} \tag{21}$$

where the single-particle equation (11) has been used. Since the HK theorem ensures a one-to-one mapping between the density and the single-particle potential, a variation $\delta\rho$ of the former corresponds to a unique variation δV_S of the latter. Therefore, the variation of the single-particle energies ε_i can be calculated using first-order perturbation theory yielding

$$\delta\varepsilon_i = < \varphi_i[\rho]|\delta V_S[\rho]|\varphi_i[\rho] > . \tag{22}$$

Using this result in (21) gives

$$\delta T_S^{\rm exact}[\rho] = -\int d^3r'\,V_S[\rho](\mathbf{r}')\delta\rho(\mathbf{r}') \tag{23}$$

which, combined with Eq. (20) leads to

$$V_S[\rho](\mathbf{r}) = v_0(\mathbf{r}) + \int d^3r'\,\frac{\rho(\mathbf{r}')}{|\mathbf{r}-\mathbf{r}'|} + V_{\rm xc}[\rho](\mathbf{r}) \tag{24}$$

where we have defined the xc potential as

$$V_{\rm xc}[\rho](\mathbf{r}) := \frac{\delta E_{\rm xc}[\rho]}{\delta \rho(\mathbf{r})}. \tag{25}$$

Being the HK variational equation of the *interacting* system, Eq. (20) determines the exact ground-state density of the interacting system. Since Eq. (24), on the other hand, is equivalent to Eq. (20), the density

$$\rho(\mathbf{r}) = \sum_{\substack{i=1 \\ N \text{ lowest } \varepsilon_i}}^{N} |\varphi_i(\mathbf{r})|^2 \tag{26}$$

resulting from the solution of the Schrödinger equation (11) with the potential (24) must be identical with the ground-state density of the *interacting* system of interest. Eqs. (11), (24), (25) and (26) are known as Kohn-Sham equations. In practice, these equations have to be solved self-consistently employing approximate but explicitly density-dependent functionals for $E_{\rm xc}[\rho]$. The resulting scheme is still easy to solve numerically and gives – especially for sophisticated density-gradient-dependent approximations of $E_{\rm xc}[\rho]$ – excellent results for a wide range of atomic, molecular and solid-state systems.

Finally, in the *third generation of DFT,* one employs, in addition to the *exact* expression for T_S, also the *exact* expression for the exchange energy given by

$$E_{\rm x}^{\rm exact}[\rho] = -\frac{1}{2} \sum_{\sigma=\uparrow,\downarrow} \sum_{j,k=1}^{N_\sigma} \int d^3r \int d^3r' \, \frac{\varphi^*_{j\sigma}(\mathbf{r}) \varphi^*_{k\sigma}(\mathbf{r}') \varphi_{k\sigma}(\mathbf{r}) \varphi_{j\sigma}(\mathbf{r}')}{|\mathbf{r}-\mathbf{r}'|}. \tag{27}$$

Only the correlation part of $E_{\rm xc}[\rho]$ needs to be approximated in this approach. In contrast to the conventional second-generation KS scheme, the third generation allows for the treatment of explicitly orbital-dependent functionals for $E_{\rm c}$ as well, giving more flexibility in the construction of such approximations.

The central equation in the third generation of DFT is still the KS equation (11). The difference between the second and third generation lies in the level of approximation to the xc-energy. As a consequence of the orbital dependence of $E_{\rm xc}$ in the third generation of DFT the calculation of $V_{\rm xc}[\rho](\mathbf{r})$ from Eq. (25) is somewhat more complicated. A detailed derivation will be given in the following section for the spin-dependent version of DFT. The result is an integral equation determining the xc potential. This integral equation, known as the optimized effective potential (OEP) equation [12, 13], is difficult to solve. To avoid a full-scale numerical solution, Krieger, Li and Iafrate (KLI) [14, 15, 16, 17, 18, 19, 20, 21, 22] have devised a semi-analytical scheme for solving the OEP integral equation approximately. This scheme is described in the subsequent section. After that, some rigorous properties of the OEP and KLI solutions will be deduced and the relation of the OEP method to the Hartree-Fock (HF) scheme will be discussed.

For heavier systems, relativistic effects become more and more important. For example, the nonrelativistic (x-only) ground-state energy of the mercury atom is 18408 a.u. while the relativistic value is 19649 a.u. This demonstrates that a relativistic treatment is indispensable for heavier systems. In section 3 a relativistic generalization of the OEP and KLI methods will be developed. A selection of numerical results for atoms, molecules and solids, including both relativistic and nonrelativistic calculations, will be presented in section 4.

The total-energy functional (16) can also be written as

$$E_{v_0}[\rho] = G[\rho] + \frac{1}{2}\int d^3r \int d^3r' \; \frac{\rho(\mathbf{r})\rho(\mathbf{r}')}{|\mathbf{r}-\mathbf{r}'|} + \int d^3r \, \rho(\mathbf{r}) v_0(\mathbf{r}) \tag{28}$$

where $G[\rho]$ encompasses all the non-trivial parts of the functional $E_{v_0}[\rho]$. The functional $G[\rho]$ can be expanded in powers of the particle-particle interaction $\hat{W}_{\mathrm{Clb}}$:

$$G[\rho] = G^{(0)}[\rho] + G^{(1)}[\rho] + G^{(2)}[\rho] + \ldots \tag{29}$$

where the superscript denotes the order in the coupling constant e^2. (The densities ρ that are inserted in these functionals may or may not depend on e^2 as well. This latter dependence is not of interest here). In the first generation of DFT, the whole functional $G[\rho]$ is approximated by a simple explicit functional of the density. The logical development of DFT towards more and more accurate functionals requires that more and more parts of $G[\rho]$ be treated exactly. This inevitably leads to the use of orbital functionals because all the *exact* functionals of DFT are explicitly orbital-dependent and thereby only implicit functionals of the density. The second generation of DFT, equivalent to the Kohn-Sham method, treats the zero-order term of $G[\rho]$ exactly:

$$G^{(0)}[\rho] = T_S^{\mathrm{exact}}[\rho]. \tag{30}$$

The third generation of DFT, leading to the OEP method, additionally employs the exact first-order term of $G[\rho]$:

$$G^{(1)}[\rho] = E_{\mathrm{x}}^{\mathrm{exact}}[\rho] \tag{31}$$

Since the expressions (30) and (31) are easily expressed in terms of the KS Green function, the expansion (29) suggests that a systematic orbital representation of the correlation energy

$$E_{\mathrm{c}}[\rho] = G^{(2)}[\rho] + G^{(3)}[\rho] + \ldots \tag{32}$$

can be achieved using the techniques of many-body perturbation theory. Some future directions along these lines will be presented in section 5.

We finally mention that a time-dependent generalization of the OEP has recently been developed [23] to deal with explicitly time-dependent situations such as atoms in strong laser pulses [24]. In the linear-response regime this method has led to a successful procedure [25] to calculate excitation energies from the poles of the frequency-dependent density response. Time-dependent applications of this kind will not be discussed in the present article. The interested reader is referred to recent reviews of time-dependent DFT [26, 27, 28].

2 The OEP method, basic formalism

2.1 Derivation of the OEP equations

We are going to derive the OEP equations for the spin-dependent version of DFT [29, 30], where the basic variables are the spin-up and spin-down densities $\rho_\uparrow(\mathbf{r})$ and $\rho_\downarrow(\mathbf{r})$, respectively. They are obtained by self-consistently solving the single-particle Schrödinger equations

$$\left(-\frac{\nabla^2}{2} + V_{S\sigma}[\rho_\uparrow, \rho_\downarrow](\mathbf{r})\right) \varphi_{j\sigma}(\mathbf{r}) = \varepsilon_{j\sigma}\varphi_{j\sigma}(\mathbf{r}) \qquad j = 1, \ldots, N_\sigma \qquad \sigma = \uparrow, \downarrow \tag{33}$$

where

$$\rho_\sigma(\mathbf{r}) = \sum_{i=1}^{N_\sigma} |\varphi_{i\sigma}(\mathbf{r})|^2. \tag{34}$$

For convenience we shall assume in the following that infinitesimal symmetry-breaking terms have been added to the external potential to remove any possible degeneracies. The KS orbitals can then be labeled such that

$$\varepsilon_{1\sigma} < \varepsilon_{2\sigma} < \ldots < \varepsilon_{N_\sigma\sigma} < \varepsilon_{(N_\sigma+1)\sigma} < \ldots \tag{35}$$

The Kohn-Sham potentials $V_{S\sigma}(\mathbf{r})$ may be written in the usual way as

$$V_{S\sigma}(\mathbf{r}) = v_0(\mathbf{r}) + \int d^3r' \, \frac{\rho(\mathbf{r}')}{|\mathbf{r}-\mathbf{r}'|} + V_{\mathrm{xc}\sigma}(\mathbf{r}), \tag{36}$$

where

$$\rho(\mathbf{r}) = \sum_{\sigma=\uparrow,\downarrow} \rho_\sigma(\mathbf{r}) \tag{37}$$

and

$$V_{\mathrm{xc}\sigma}(\mathbf{r}) := \frac{\delta E_{\mathrm{xc}}\left[\rho_\uparrow, \rho_\downarrow\right]}{\delta \rho_\sigma(\mathbf{r})}. \tag{38}$$

The starting point of the OEP method is the total-energy functional

$$\begin{aligned} E_{v_0}^{\mathrm{OEP}}\left[\rho_\uparrow, \rho_\downarrow\right] &= \sum_{\sigma=\uparrow,\downarrow} \sum_{i=1}^{N_\sigma} \int d^3r \; \varphi_{i\sigma}^*(\mathbf{r}) \left(-\frac{1}{2}\nabla^2\right) \varphi_{i\sigma}(\mathbf{r}) \\ &\quad + \int d^3r \; v_0(\mathbf{r})\rho(\mathbf{r}) + \frac{1}{2}\int d^3r \int \; d^3r' \; \frac{\rho(\mathbf{r})\rho(\mathbf{r}')}{|\mathbf{r}-\mathbf{r}'|} \\ &\quad + E_{\mathrm{xc}}^{\mathrm{OEP}}\left[\{\varphi_{j\tau}\}\right] \end{aligned} \tag{39}$$

where, in contrast to ordinary spin DFT, the xc energy is an *explicit* (approximate) functional of spin orbitals and therefore only an *implicit* functional of the spin densities $\rho_\uparrow$ and $\rho_\downarrow$. In order to calculate the xc potentials defined in Eq. (38) we use the chain rule for functional derivatives to obtain

$$\begin{aligned} V_{\mathrm{xc}\sigma}^{\mathrm{OEP}}(\mathbf{r}) &= \frac{\delta E_{\mathrm{xc}}^{\mathrm{OEP}}\left[\{\varphi_{j\tau}\}\right]}{\delta \rho_\sigma(\mathbf{r})} \\ &= \sum_{\alpha=\uparrow,\downarrow} \sum_{i=1}^{N_\alpha} \int d^3r' \; \frac{\delta E_{\mathrm{xc}}^{\mathrm{OEP}}\left[\{\varphi_{j\tau}\}\right]}{\delta \varphi_{i\alpha}(\mathbf{r}')} \frac{\delta \varphi_{i\alpha}(\mathbf{r}')}{\delta \rho_\sigma(\mathbf{r})} + \text{c.c.} \end{aligned} \tag{40}$$

and, by applying the functional chain rule once more,

$$V_{\mathrm{xc}\sigma}^{\mathrm{OEP}}(\mathbf{r}) = \sum_{\alpha=\uparrow,\downarrow} \sum_{\beta=\uparrow,\downarrow} \sum_{i=1}^{N_\alpha} \int d^3r' \int d^3r'' \; \left(\frac{\delta E_{\mathrm{xc}}^{\mathrm{OEP}}\left[\{\varphi_{j\tau}\}\right]}{\delta \varphi_{i\alpha}(\mathbf{r}')} \frac{\delta \varphi_{i\alpha}(\mathbf{r}')}{\delta V_{S\beta}(\mathbf{r}'')} + \text{c.c.} \right) \frac{\delta V_{S\beta}(\mathbf{r}'')}{\delta \rho_\sigma(\mathbf{r})}. \tag{41}$$

The last term on the right-hand side is the inverse $\chi_S^{-1}(\mathbf{r}, \mathbf{r}')$ of the static density response function of a system of non-interacting particles

$$\chi_{S\alpha,\beta}(\mathbf{r}, \mathbf{r}') := \frac{\delta \rho_\alpha(\mathbf{r})}{\delta V_{S\beta}(\mathbf{r}')}. \tag{42}$$

This quantity is diagonal with respect to the spin variables so that Eq. (41) reduces to

$$V_{\mathrm{xc}\sigma}^{\mathrm{OEP}}(\mathbf{r}) = \sum_{\alpha=\uparrow,\downarrow} \sum_{i=1}^{N_\alpha} \int d^3r' \int d^3r'' \left(\frac{\delta E_{\mathrm{xc}}^{\mathrm{OEP}}\left[\{\varphi_{j\tau}\}\right]}{\delta \varphi_{i\alpha}(\mathbf{r}')} \frac{\delta \varphi_{i\alpha}(\mathbf{r}')}{\delta V_{S\sigma}(\mathbf{r}'')} + \mathrm{c.c.} \right) \chi_{S\sigma}^{-1}\left(\mathbf{r}'', \mathbf{r}\right). \quad (43)$$

Acting with the response operator (42) on both sides of Eq. (43) one obtains

$$\int d^3r' \; V_{\mathrm{xc}\sigma}^{\mathrm{OEP}}(\mathbf{r}') \chi_{S\sigma}\left(\mathbf{r}', \mathbf{r}\right) = \sum_{\alpha=\uparrow,\downarrow} \sum_{i=1}^{N_\alpha} \int d^3r' \; \frac{\delta E_{\mathrm{xc}}^{\mathrm{OEP}}\left[\{\varphi_{j\tau}\}\right]}{\delta \varphi_{i\alpha}(\mathbf{r}')} \frac{\delta \varphi_{i\alpha}(\mathbf{r}')}{\delta V_{S\sigma}(\mathbf{r})} + \mathrm{c.c.} \quad (44)$$

To further evaluate this equation, we note that the first functional derivative on the right-hand side of Eq. (44) is readily computed once an explicit expression for $E_{\mathrm{xc}}^{\mathrm{OEP}}$ in terms of single-particle orbitals is given. The remaining functional derivative on the right-hand side of Eq. (44) is calculated using first-order perturbation theory. This yields

$$\frac{\delta \varphi_{i\alpha}(\mathbf{r}')}{\delta V_{S\sigma}(\mathbf{r})} = \delta_{\alpha,\sigma} \sum_{\substack{k=1 \\ k\neq i}}^{\infty} \frac{\varphi_{k\sigma}(\mathbf{r}')\varphi_{k\sigma}^*(\mathbf{r})}{\varepsilon_{i\sigma} - \varepsilon_{k\sigma}} \varphi_{i\sigma}(\mathbf{r}). \quad (45)$$

Using this equation, the response function

$$\chi_{S\alpha,\beta}\left(\mathbf{r}, \mathbf{r}'\right) = \frac{\delta}{\delta V_{S\beta}(\mathbf{r}')} \left(\sum_{i=1}^{N_\alpha} \varphi_{i\alpha}^*(\mathbf{r}) \varphi_{i\alpha}(\mathbf{r}) \right) \quad (46)$$

is readily expressed in terms of the orbitals as

$$\chi_{S\sigma}\left(\mathbf{r}, \mathbf{r}'\right) = \sum_{i=1}^{N_\sigma} \sum_{\substack{k=1 \\ k\neq i}}^{\infty} \frac{\varphi_{i\sigma}^*(\mathbf{r})\varphi_{k\sigma}(\mathbf{r})\varphi_{k\sigma}^*(\mathbf{r}')\varphi_{i\sigma}(\mathbf{r}')}{\varepsilon_{i\sigma} - \varepsilon_{k\sigma}} + \mathrm{c.c.} \quad (47)$$

Inserting (45) and (47) in Eq. (44), we obtain the standard form of the OEP integral equation:

$$\sum_{i=1}^{N_\sigma} \int d^3r' \varphi_{i\sigma}^*(\mathbf{r}') \left(V_{\mathrm{xc}\sigma}^{\mathrm{OEP}}(\mathbf{r}') - u_{\mathrm{xc}i\sigma}(\mathbf{r}') \right) G_{Si\sigma}\left(\mathbf{r}', \mathbf{r}\right) \varphi_{i\sigma}(\mathbf{r}) + \mathrm{c.c.} = 0 \quad (48)$$

where

$$u_{\mathrm{xc}i\sigma}(\mathbf{r}) := \frac{1}{\varphi_{i\sigma}^*(\mathbf{r})} \frac{\delta E_{\mathrm{xc}}^{\mathrm{OEP}}\left[\{\varphi_{j\tau}\}\right]}{\delta \varphi_{i\sigma}(\mathbf{r})} \quad (49)$$

and

$$G_{Si\sigma}\left(\mathbf{r}, \mathbf{r}'\right) := \sum_{\substack{k=1 \\ k\neq i}}^{\infty} \frac{\varphi_{k\sigma}(\mathbf{r})\varphi_{k\sigma}^*(\mathbf{r}')}{\varepsilon_{i\sigma} - \varepsilon_{k\sigma}}. \quad (50)$$

The derivation of the OEP integral equation (48) described here was given by Shaginyan [31] and by Görling and Levy [32]. It is important to note that the same expression results [12, 13, 16, 19, 33, 34] if one demands that the local single-particle potential appearing in Eq. (33) be the *optimized* one yielding orbitals minimizing the total-energy functional (39), i.e. that

$$\left. \frac{\delta E_{v_0}^{\mathrm{OEP}}}{\delta V_{S\sigma}(\mathbf{r})} \right|_{V_{S\sigma}=V^{\mathrm{OEP}}} = 0. \quad (51)$$

This equation is the historical origin [12] of the name *optimized effective potential.* As was first pointed out by Perdew and co-workers [35, 36], Eq. (51) is equivalent to the HK variational principle. This is most easily seen by applying the functional chain rule to Eq. (51) yielding

$$0 = \frac{\delta E_{v_0}^{\rm OEP}}{\delta V_{S\sigma}(\mathbf{r})} = \sum_\alpha \int d^3r' \, \frac{\delta E_{v_0}^{\rm OEP}}{\delta \rho_\alpha(\mathbf{r}')} \frac{\delta \rho_\alpha(\mathbf{r}')}{\delta V_{S\sigma}(\mathbf{r})}. \tag{52}$$

Once again, the last term on the right-hand side of Eq. (52) can be identified with the static KS response function (42). Hence, acting with the inverse response operator on Eq. (52) leads to the HK variational principle

$$0 = \frac{\delta E_{v_0}^{\rm OEP}}{\delta \rho_\sigma(\mathbf{r})}. \tag{53}$$

2.2 Approximation of Krieger, Li and Iafrate

In order to use the OEP method derived in the previous section, Eq. (48) has to be solved for the xc potential $V_{{\rm xc}\sigma}^{\rm OEP}$. Unfortunately, there is no known analytic solution of $V_{{\rm xc}\sigma}^{\rm OEP}$ depending explicitly on the set of single-particle orbitals $\{\varphi_{j\tau}\}$. Thus, one needs to solve the full integral equation numerically, which is a rather demanding task and has been achieved so far only for systems of high symmetry such as spherical atoms [15, 19, 21, 13, 37, 38] and for solids within the linear muffin tin orbitals atomic sphere approximation [39, 40, 41].

However, Krieger, Li and Iafrate [14, 16] recently proposed a transformation of Eq. (48) that leads to an alternative but still exact form of the OEP integral equation which lends itself as a starting point for a highly accurate approximation for $V_{{\rm xc}\sigma}^{\rm OEP}$. Following Krieger, Li and Iafrate [14, 16], we define

$$\psi_{i\sigma}^*(\mathbf{r}) := \int d^3r' \varphi_{i\sigma}^*(\mathbf{r}') \left(V_{{\rm xc}\sigma}^{\rm OEP}(\mathbf{r}') - u_{{\rm xc}i\sigma}(\mathbf{r}') \right) G_{Si\sigma}(\mathbf{r}', \mathbf{r}), \tag{54}$$

such that the OEP integral equation (48) can be rewritten as

$$\sum_{i=1}^{N_\sigma} \psi_{i\sigma}^*(\mathbf{r}) \varphi_{i\sigma}(\mathbf{r}) + \text{c.c.} \; = \; 0 \, . \tag{55}$$

Since the KS orbitals $\{\varphi_{j\tau}\}$ span an orthonormal set, one readily concludes from Eq. (54) that the function $\psi_{i\sigma}(\mathbf{r})$ is orthogonal to $\varphi_{i\sigma}(\mathbf{r})$:

$$\int d^3r \, \psi_{i\sigma}^*(\mathbf{r}) \varphi_{i\sigma}(\mathbf{r}) = 0 \, . \tag{56}$$

The quantity $G_{Si\sigma}(\mathbf{r}', \mathbf{r})$ given by Eq. (50) is the Green function of the KS equation projected onto the subspace orthogonal to $\varphi_{i\sigma}(\mathbf{r})$, i.e. it satisfies the equation

$$\left(\hat{h}_{S\sigma}(\mathbf{r}) - \varepsilon_{i\sigma} \right) G_{Si\sigma}(\mathbf{r}', \mathbf{r}) = -\Big(\delta(\mathbf{r}' - \mathbf{r}) - \varphi_{i\sigma}(\mathbf{r}') \varphi_{i\sigma}^*(\mathbf{r}) \Big) \tag{57}$$

where $\hat{h}_{S\sigma}(\mathbf{r})$ is a short-hand notation for the KS Hamiltonian

$$\hat{h}_{S\sigma}(\mathbf{r}) := -\frac{\nabla^2}{2} + V_{S\sigma}[\rho_\uparrow, \rho_\downarrow](\mathbf{r}). \tag{58}$$

Using Eq. (57), we can act with the operator $(\hat{h}_{S\sigma} - \varepsilon_{i\sigma})$ on Eq. (54), leading to

$$\left(\hat{h}_{S\sigma}(\mathbf{r}) - \varepsilon_{i\sigma} \right) \psi_{i\sigma}^*(\mathbf{r}) = -\Big(V_{{\rm xc}\sigma}^{\rm OEP}(\mathbf{r}) - u_{{\rm xc}i\sigma}(\mathbf{r}) - (\bar{V}_{{\rm xc}i\sigma}^{\rm OEP} - \bar{u}_{{\rm xc}i\sigma}) \Big) \varphi_{i\sigma}^*(\mathbf{r}) \tag{59}$$

where $\bar{V}_{\mathrm{xc}i\sigma}$ denotes the average of $V_{\mathrm{xc}\sigma}(\mathbf{r})$ with respect to the ith orbital, i.e.

$$\bar{V}^{\mathrm{OEP}}_{\mathrm{xc}i\sigma} := \int d^3r\, \varphi^*_{i\sigma}(\mathbf{r}) V^{\mathrm{OEP}}_{\mathrm{xc}\sigma}(\mathbf{r}) \varphi_{i\sigma}(\mathbf{r}) \tag{60}$$

and

$$\bar{u}_{\mathrm{xc}i\sigma} := \int d^3r\, \varphi^*_{i\sigma}(\mathbf{r}) u_{\mathrm{xc}i\sigma}(\mathbf{r}) \varphi_{i\sigma}(\mathbf{r}). \tag{61}$$

The differential equation (59) has the structure of a KS equation with an additional inhomogeneity term. Eq. (59) plus the boundary condition that $\psi^*_{i\sigma}(\mathbf{r})$ tends to zero as $r \to \infty$ uniquely determines $\psi^*_{i\sigma}(\mathbf{r})$. We can prove this statement by assuming that there are two independent solutions $\psi^*_{i\sigma,1}(\mathbf{r})$ and $\psi^*_{i\sigma,2}(\mathbf{r})$ of Eq. (59). Then the difference between these two solutions, $\Psi^*_{i\sigma}(\mathbf{r}) := \psi^*_{i\sigma,1}(\mathbf{r}) - \psi^*_{i\sigma,2}(\mathbf{r})$, satisfies the homogeneous KS equation

$$(\hat{h}_{S\sigma} - \varepsilon_{i\sigma}) \Psi^*_{i\sigma}(\mathbf{r}) = 0, \tag{62}$$

which has a unique solution

$$\Psi^*_{i\sigma}(\mathbf{r}) = \varphi^*_{i\sigma}(\mathbf{r}), \tag{63}$$

if the above boundary condition is fulfilled. However, this solution leads to a contradiction with the orthogonality relation (56) so that $\Psi^*_{i\sigma}(r)$ can only be the trivial solution of Eq. (62),

$$\Psi^*_{i\sigma}(\mathbf{r}) \equiv 0\,. \tag{64}$$

This completes the proof.

At this point it is useful to attach some physical meaning to the quantity $\psi_{i\sigma}$: From Eq. (54) it is obvious that $\psi_{i\sigma}$ is the usual first-order shift in the wave function caused by the perturbing potential $\delta V_{i\sigma} = V^{\mathrm{OEP}}_{\mathrm{xc}\sigma} - u_{\mathrm{xc}i\sigma}$. This fact also motivates the boundary condition assumed above. In x-only theory, $u_{\mathrm{x}i\sigma}$ is the local, orbital-dependent HF exchange potential so that $\psi_{i\sigma}$ is the first order shift of the KS wave function towards the HF wave function. One has to realize, however, that the first-order change of the orbital dependent potential $u_{\mathrm{x}i\sigma}[\{\varphi_{j\tau}\}]$ has been neglected. This change can be expected to be small compared to $\delta V_{i\sigma}$ [16].

To further transform the OEP integral equation (55), we solve Eq. (59) for $V_{S\sigma}(\mathbf{r})\psi^*_{i\sigma}(\mathbf{r})$:

$$V_{S\sigma}(\mathbf{r})\psi^*_{i\sigma}(\mathbf{r}) = -\Big(V^{\mathrm{OEP}}_{\mathrm{xc}\sigma}(\mathbf{r}) - u_{\mathrm{xc}i\sigma}(\mathbf{r}) - (\bar{V}^{\mathrm{OEP}}_{\mathrm{xc}i\sigma} - \bar{u}_{\mathrm{xc}i\sigma})\Big)\varphi^*_{i\sigma}(\mathbf{r}) + \left(\frac{\nabla^2}{2} + \varepsilon_{i\sigma}\right)\psi^*_{i\sigma}(\mathbf{r})\,. \tag{65}$$

We then multiply Eq. (55) by the KS potential $V_{S\sigma}(\mathbf{r})$:

$$\sum_{i=1}^{N_\sigma} V_{S\sigma}(\mathbf{r})\psi^*_{i\sigma}(\mathbf{r})\varphi_{i\sigma}(\mathbf{r}) + \text{c.c.} \;=\; 0\,, \tag{66}$$

and employ Eq. (65) to obtain

$$0 = \sum_{i=1}^{N_\sigma} \left\{ \Big(V^{\mathrm{OEP}}_{\mathrm{xc}\sigma}(\mathbf{r}) - u_{\mathrm{xc}i\sigma}(\mathbf{r}) - (\bar{V}^{\mathrm{OEP}}_{\mathrm{xc}i\sigma} - \bar{u}_{\mathrm{xc}i\sigma})\Big)\varphi^*_{i\sigma}(\mathbf{r}) - \left(\frac{\nabla^2}{2} + \varepsilon_{i\sigma}\right)\psi^*_{i\sigma}(\mathbf{r}) \right\} \varphi_{i\sigma}(\mathbf{r}) + \text{ c.c.} \tag{67}$$

Solving this equation for $V_{\mathrm{xc}\sigma}^{\mathrm{OEP}}$ yields

$$V_{\mathrm{xc}\sigma}^{\mathrm{OEP}}(\mathbf{r}) = \frac{1}{2\rho_\sigma(\mathbf{r})}\sum_{i=1}^{N_\sigma}\Big\{|\varphi_{i\sigma}(\mathbf{r})|^2\Big(u_{\mathrm{xc}i\sigma}(\mathbf{r}) + (\bar{V}_{\mathrm{x}i\sigma}^{\mathrm{OEP}} - \bar{u}_{\mathrm{x}i\sigma})\Big) + \left(\frac{\nabla^2}{2}\psi_{i\sigma}^*(\mathbf{r}) + \varepsilon_{i\sigma}\psi_{i\sigma}^*(\mathbf{r})\right)\varphi_{i\sigma}(\mathbf{r})\Big\} + \text{c.c.} \tag{68}$$

The second term in the curled brackets may be rewritten by using the KS and the OEP equation again, leading to

$$\begin{aligned}
&\sum_{i=1}^{N_\sigma}\left(\frac{\nabla^2}{2}\psi_{i\sigma}^*(\mathbf{r}) + \varepsilon_{i\sigma}\psi_{i\sigma}^*(\mathbf{r})\right)\varphi_{i\sigma}(\mathbf{r}) + \text{c.c.} \\
&= \sum_{i=1}^{N_\sigma}\left[\left(\frac{\nabla^2}{2}\psi_{i\sigma}^*(\mathbf{r})\right)\varphi_{i\sigma}(\mathbf{r}) - \psi_{i\sigma}^*(\mathbf{r})\left(\frac{\nabla^2}{2}\varphi_{i\sigma}(\mathbf{r})\right)\right] + \text{c.c.} \\
&= -\sum_{i=1}^{N_\sigma}\nabla\cdot(\psi_{i\sigma}^*(\mathbf{r})\nabla\varphi_{i\sigma}(\mathbf{r})) + \text{c.c.}
\end{aligned} \tag{69}$$

In this way Eq. (68) may be written as

$$V_{\mathrm{xc}\sigma}^{\mathrm{OEP}}(\mathbf{r}) = \frac{1}{2\rho_\sigma(\mathbf{r})}\sum_{i=1}^{N_\sigma}|\varphi_{i\sigma}(\mathbf{r})|^2\Big(v_{\mathrm{xc}i\sigma}(\mathbf{r}) + (\bar{V}_{\mathrm{x}i\sigma}^{\mathrm{OEP}} - \bar{u}_{\mathrm{x}i\sigma})\Big) + \text{c.c.} \tag{70}$$

with

$$v_{\mathrm{xc}i\sigma}(\mathbf{r}) = u_{\mathrm{xc}i\sigma}(\mathbf{r}) - \frac{1}{|\varphi_{i\sigma}(\mathbf{r})|^2}\nabla\cdot(\psi_{i\sigma}^*(\mathbf{r})\nabla\varphi_{i\sigma}(\mathbf{r}))\ . \tag{71}$$

Eq. (70) is an exact transformation of the original OEP integral equation (48). The advantage of Eq. (70), although still being an integral equation, lies in the fact that it may serve as a starting point for constructing approximations of $V_{\mathrm{xc}\sigma}^{\mathrm{OEP}}$: We only need to approximate $\psi_{i\sigma}^*$ in Eq. (71) by a suitable functional of the orbitals.

The simplest possible approximation is obtained by completely neglecting the terms involving $\psi_{i\sigma}^*$, i.e. by replacing $v_{\mathrm{xc}i\sigma}$ by $u_{\mathrm{xc}i\sigma}$. At first sight, this approximation might appear rather crude. It can be interpreted [14, 16], however, as a mean-field approximation in the sense that the neglected terms averaged over the ground-state spin density $\rho_\sigma(\mathbf{r})$ vanish. To demonstrate this, we investigate the quantity

$$I = \int d^3r\,\nabla\cdot\frac{1}{2}\sum_{i=1}^{N_\sigma}\Big(\psi_{i\sigma}^*(\mathbf{r})\nabla\varphi_{i\sigma}(\mathbf{r})\Big) + \text{c.c.} \tag{72}$$

which amounts to the difference between the exact $V_{\mathrm{xc}\sigma}^{\mathrm{OEP}}(\mathbf{r})$ and the approximated xc potential averaged over $\rho_\sigma(\mathbf{r})$. From Eq. (54) one easily derives

$$\begin{aligned}
\frac{\nabla^2}{2}\psi_{i\sigma}^*(\mathbf{r}) &= \sum_{\substack{k=1\\k\neq i}}^{\infty}A_{ik\sigma}\left(\frac{\nabla^2}{2}\right)\varphi_{k\sigma}^*(\mathbf{r}) \\
&= \sum_{\substack{k=1\\k\neq i}}^{\infty}A_{ik\sigma}\left(V_{S\sigma}(\mathbf{r})\varphi_{k\sigma}^*(\mathbf{r}) - \varepsilon_{k\sigma}\varphi_{k\sigma}^*(\mathbf{r})\right) = V_{S\sigma}(\mathbf{r})\psi_{i\sigma}^*(\mathbf{r}) - \sum_{\substack{k=1\\k\neq i}}^{\infty}A_{ik\sigma}\varepsilon_{k\sigma}\varphi_{k\sigma}^*(\mathbf{r})
\end{aligned} \tag{73}$$

where we have used the abbreviation

$$A_{ik\sigma} = \frac{1}{\varepsilon_{i\sigma} - \varepsilon_{k\sigma}} \int d^3r' \varphi^*_{i\sigma}(\mathbf{r}') \left(V^{\mathrm{OEP}}_{\mathrm{xc}\sigma}(\mathbf{r}') - u_{\mathrm{xc}i\sigma}(\mathbf{r}') \right) \varphi_{k\sigma}(\mathbf{r}') \quad . \tag{74}$$

Insertion of Eq. (73) in Eq. (69) leads to

$$\begin{aligned} I = -\frac{1}{2} \int d^3r \sum_{i=1}^{N_\sigma} \Big(& V_{S\sigma}(\mathbf{r}) \psi^*_{i\sigma}(\mathbf{r}) \varphi_{i\sigma}(\mathbf{r}) \\ & - \sum_{\substack{k=1 \\ k\neq i}}^{\infty} A_{ik\sigma} \varepsilon_{k\sigma} \varphi^*_{k\sigma}(\mathbf{r}) \varphi_{i\sigma}(\mathbf{r}) + \varepsilon_{i\sigma} \psi^*_{i\sigma}(\mathbf{r}) \varphi_{i\sigma}(\mathbf{r}) + \mathrm{c.c.} \Big) = 0 \end{aligned} \tag{75}$$

where the last step follows from the orthogonality of the KS orbitals together with Eqs. (55) and (56). Hence, the neglected terms have zero average value.

The resulting equation, known as the KLI approximation, is given by [14, 15, 16, 17, 18, 19, 20, 21, 22, 42, 43, 44]

$$V^{\mathrm{KLI}}_{\mathrm{xc}\sigma}(\mathbf{r}) = \frac{1}{2\rho_\sigma(\mathbf{r})} \sum_{i=1}^{N_\sigma} |\varphi_{i\sigma}(\mathbf{r})|^2 \left(u_{\mathrm{xc}i\sigma}(\mathbf{r}) + (\bar{V}^{\mathrm{KLI}}_{\mathrm{xc}i\sigma} - \bar{u}_{\mathrm{xc}i\sigma}) \right) + \mathrm{c.c.} \tag{76}$$

which has proven to be an excellent approximation to the full xc potential $V^{\mathrm{OEP}}_{\mathrm{xc}\sigma}(\mathbf{r})$, as will be shown in section 4. We immediately recognize that this form is very similar to the Slater potential. It should be noted that – in contrast to the work of Krieger [16] – we did *not* use any asymptotic properties of $\psi_{i\sigma}$ or $\varphi_{i\sigma}$ in the derivation of Eq. (75). This implies that the KLI approximation is also justified for solid state systems.

In contrast to the full OEP equation (48), the KLI equation, still being an integral equation, can be solved explicitly in terms of the orbitals $\{\varphi_{j\tau}\}$: Multiplying Eq. (76) by $|\varphi_{j\sigma}(\mathbf{r})|^2$ and integrating over space yields

$$\bar{V}^{\mathrm{KLI}}_{\mathrm{xc}j\sigma} = \bar{V}^{S}_{\mathrm{xc}j\sigma} + \sum_{i=1}^{N_\sigma - 1} M_{ji\sigma} \left(\bar{V}^{\mathrm{KLI}}_{\mathrm{xc}i\sigma} - \frac{1}{2} \left(\bar{u}_{\mathrm{xc}i\sigma} + \bar{u}^*_{\mathrm{xc}i\sigma} \right) \right), \tag{77}$$

where

$$\bar{V}^{S}_{\mathrm{xc}j\sigma} := \int d^3r \, \frac{|\varphi_{j\sigma}(\mathbf{r})|^2}{\rho_\sigma(\mathbf{r})} \sum_{i=1}^{N_\sigma} |\varphi_{i\sigma}(\mathbf{r})|^2 \frac{1}{2} \left(u_{\mathrm{xc}i\sigma}(\mathbf{r}) + u^*_{\mathrm{xc}i\sigma}(\mathbf{r}) \right) \tag{78}$$

and

$$M_{ji\sigma} := \int d^3r \, \frac{|\varphi_{j\sigma}(\mathbf{r})|^2 |\varphi_{i\sigma}(\mathbf{r})|^2}{\rho_\sigma(\mathbf{r})}. \tag{79}$$

The term corresponding to the highest occupied orbital $\varphi_{N_\sigma\sigma}$ has been excluded from the sum in Eq. (77) because $\bar{V}^{\mathrm{KLI}}_{\mathrm{xc}N_\sigma\sigma} = \bar{u}_{\mathrm{xc}N_\sigma\sigma}$, which will be proven in the next section. The remaining unknown constants $(\bar{V}^{\mathrm{KLI}}_{\mathrm{xc}i\sigma} - \bar{u}_{\mathrm{xc}i\sigma})$ are determined by the linear equation

$$\sum_{i=1}^{N_\sigma - 1} (\delta_{ji} - M_{ji\sigma}) \left(\bar{V}^{\mathrm{KLI}}_{\mathrm{xc}i\sigma} - \frac{1}{2} \left(\bar{u}_{\mathrm{xc}i\sigma} + \bar{u}^*_{\mathrm{xc}i\sigma} \right) \right) = \left(\bar{V}^{S}_{\mathrm{xc}j\sigma} - \frac{1}{2} \left(\bar{u}_{\mathrm{xc}j\sigma} + \bar{u}^*_{\mathrm{xc}j\sigma} \right) \right), \tag{80}$$

with $j = 1, \ldots N_\sigma - 1$. Solving Eq. (80) and substituting the result into Eq. (76), we obtain an explicitly orbital-dependent functional.

We conclude this section in remarking that the derivation given here differs slightly from the one given by Krieger, Li and Iafrate [14, 16]. The main difference is that we

choose to work with the quantity $\psi_{i\sigma}$, which is related to $p_{i\sigma}$ introduced in Ref. [14, 16] by $\psi_{i\sigma} = p_{i\sigma}\varphi_{i\sigma}$. Since both $\psi_{i\sigma}$ and $\varphi_{i\sigma}$ are well-behaved functions, $p_{i\sigma}$ has poles where $\varphi_{i\sigma}$ becomes zero. It is therefore more convenient to work with the well-behaved function $\psi_{i\sigma}$, especially for the considerations of the next section.

We finally note that the KLI equation (76) can also be obtained by a less rigorous derivation, namely by approximating the energy dominator in the Green function (57) by a single constant as was first suggested by Sharp and Horton [12] and further elaborated by Krieger, Li, and Iafrate [15, 17, 19, 20, 21, 22].

2.3 Rigorous properties of the OEP and KLI potentials

2.3.1 An important lemma

In this section a number of rigorous statements on the optimized effective potential of finite systems will be derived [45]. For this purpose, the exchange-only potential and the correlation potential have to be treated separately. The exact exchange potential of DFT is defined as

$$V_{\mathrm{x}\sigma}[\rho_\uparrow,\rho_\downarrow](\mathbf{r}) = \frac{\delta E_{\mathrm{x}}^{\mathrm{exact}}}{\delta\rho_\sigma(\mathbf{r})}\,, \qquad\qquad \sigma=\uparrow,\downarrow \tag{81}$$

where the exact exchange-energy functional is given by Eq. (27). In an ordinary OEP calculation, one only determines the potential $V_{\mathrm{x}\sigma}[\rho_{\uparrow 0},\rho_{\downarrow 0}](\mathbf{r})$ corresponding to the self-consistent ground-state spin densities $(\rho_{\uparrow 0},\rho_{\downarrow 0})$ of the system considered. If one were to calculate $V_{\mathrm{x}\sigma}[\rho_\uparrow,\rho_\downarrow]$ *for an arbitrary given set* $(\rho_\uparrow,\rho_\downarrow)$ *of spin densities* one would have to perform the following three steps:

1. Determine the unique potentials $V_{S\sigma}[\rho_\uparrow,\rho_\downarrow](\mathbf{r}),\sigma=\uparrow,\downarrow$, corresponding to the given spin densities $(\rho_\uparrow,\rho_\downarrow)$
2. Solve the Schrödinger equation (33) for the spin-up and spin-down orbitals with the potentials of step (1)
3. Plug the orbitals obtained in step (2) into the OEP integral equation

$$\sum_{i=1}^{N_\sigma}\int d^3r'\,\varphi_{i\sigma}^*(\mathbf{r}')\Big(V_{\mathrm{x}\sigma}(\mathbf{r}')-u_{\mathrm{x}i\sigma}(\mathbf{r}')\Big)G_{Si\sigma}(\mathbf{r}',\mathbf{r})\varphi_{i\sigma}(\mathbf{r})+\mathrm{c.c.}=0 \tag{82}$$

   and solve this equation for $V_{\mathrm{x}\sigma}$ keeping the orbitals of step (2) fixed.

In this way Filippi, Umrigar and Gonze [46] have recently calculated the exchange potentials corresponding to the *exact* (not the x-only) densities of some atoms where the exact densities were determined in a quantum Monte-Carlo calculation. Likewise, for any given approximate functional $E_{\mathrm{c}}[\{\varphi_{i\sigma}\}]$, the corresponding correlation potential

$$V_{\mathrm{c}\sigma}[\rho_\uparrow,\rho_\downarrow](\mathbf{r}) = \frac{\delta E_{\mathrm{c}}}{\delta\rho_\sigma(\mathbf{r})} \tag{83}$$

is obtained by the above steps (1) and (2), and step (3) replaced by the solution of

$$\sum_{i=1}^{N_\sigma}\int d^3r'\,\varphi_{i\sigma}^*(\mathbf{r}')\Big(V_{\mathrm{c}\sigma}(\mathbf{r}')-u_{\mathrm{c}i\sigma}(\mathbf{r}')\Big)G_{Si\sigma}(\mathbf{r}',\mathbf{r})\varphi_{i\sigma}(\mathbf{r})+\mathrm{c.c.}=0\,. \tag{84}$$

Whenever, in the following derivations, the OEP equations (82) and (84) are used or transformed it is understood that the orbitals $\{\varphi_{i\sigma}\}$ are kept fixed so that they always correspond to a unique fixed set $(\rho_\uparrow, \rho_\downarrow)$ of spin densities.

We first prove an important *lemma* concerning the constants defined by Eqs. (60) and (61). The lemma states that

(i)

$$\bar{u}_{\mathrm{x}N_\sigma\sigma} = \bar{V}_{\mathrm{x}N_\sigma\sigma}$$

is satisfied for

$$u_{\mathrm{x}i\sigma}(\mathbf{r}) = \frac{1}{\varphi^*_{i\sigma}(\mathbf{r})}\frac{\delta E_{\mathrm{x}}^{\mathrm{exact}}}{\delta\varphi_{i\sigma}(\mathbf{r})} \tag{85}$$

with the exact exchange-energy functional;

(ii)

$$\bar{u}_{\mathrm{c}N_\sigma\sigma} = \bar{V}_{\mathrm{c}N_\sigma\sigma}$$

is satisfied for any approximate correlation energy functional $E_{\mathrm{c}}[\{\varphi_{i\sigma}\}]$ *having the property*

$$u_{ci\sigma}(\mathbf{r}) = \frac{1}{\varphi^*_{i\sigma}(\mathbf{r})}\frac{\delta E_{\mathrm{c}}}{\delta\varphi_{i\sigma}(\mathbf{r})} \stackrel{r\to\infty}{\longrightarrow} \text{const}\,, i = 1...N_\sigma\,. \tag{86}$$

We begin with the proof of statement (ii). To this end we use Eq. (59) for the correlation part only:

$$\left(-\frac{\nabla^2}{2} + V_{S\sigma}(\mathbf{r}) - \varepsilon_{i\sigma}\right)\psi^*_{i\sigma}(\mathbf{r}) = \left(V_{\mathrm{c}\sigma}(\mathbf{r}) - u_{ci\sigma}(\mathbf{r}) - C_{i\sigma}\right)\varphi^*_{i\sigma}(\mathbf{r}) \tag{87}$$

where we have introduced the abbreviation

$$C_{i\sigma} = \bar{V}_{\mathrm{c}i\sigma} - \bar{u}_{\mathrm{c}i\sigma} \tag{88}$$

(dropping the superscript OEP for notational simplicity). If Eq. (87) is satisfied with potentials $V_{S\sigma}(\mathbf{r})$, $V_{\mathrm{c}\sigma}(\mathbf{r})$ and $u_{\mathrm{c}i\sigma}(\mathbf{r})$ it will also be satisfied with the constantly shifted potentials

$$\tilde{V}_{S\sigma}(\mathbf{r}) := V_{S\sigma}(\mathbf{r}) + B_{S\sigma} \tag{89}$$

$$\tilde{V}_{\mathrm{c}\sigma}(\mathbf{r}) := V_{\mathrm{c}\sigma}(\mathbf{r}) + B_{\mathrm{c}\sigma} \tag{90}$$

$$\tilde{u}_{ci\sigma}(\mathbf{r}) := u_{ci\sigma}(\mathbf{r}) + B_{i\sigma} \tag{91}$$

and the corresponding eigenvalues $\tilde{\varepsilon}_{i\sigma}$ and the constants $\bar{\tilde{V}}_{ci\sigma}$, $\bar{\tilde{u}}_{ci\sigma}$. The constants $B_{S\sigma}$, $B_{\mathrm{c}\sigma}$, $B_{i\sigma}$ cancel out in Eq. (87) because the eigenvalues $\tilde{\varepsilon}_{i\sigma}$ resulting from solving the Schrödinger equation (33) with the potential (89) are given by

$$\tilde{\varepsilon}_{i\sigma} = \varepsilon_{i\sigma} + B_{S\sigma} \tag{92}$$

and the constants $\bar{\tilde{V}}_{\mathrm{c}\sigma}$, $\bar{\tilde{u}}_{ci\sigma}$ obtained from the correlation parts of Eqs. (60), (61) with the potentials (90), (91) are

$$\bar{\tilde{V}}_{ci\sigma} = \bar{V}_{ci\sigma} + B_{\mathrm{c}\sigma} \tag{93}$$

$$\bar{\tilde{u}}_{ci\sigma} = \bar{u}_{ci\sigma} + B_{i\sigma}\,. \tag{94}$$

Hence we can assume *without restriction* that

$$V_{S\sigma}(\mathbf{r}) \stackrel{r\to\infty}{\longrightarrow} 0 \tag{95}$$

$$V_{c\sigma}(\mathbf{r}) \stackrel{r\to\infty}{\longrightarrow} 0 \tag{96}$$

$$u_{ci\sigma}(\mathbf{r}) \stackrel{r\to\infty}{\longrightarrow} 0\,. \tag{97}$$

In the following we shall investigate the asymptotic behavior of the KS orbitals $\varphi_{i\sigma}(\mathbf{r})$ and of the quantities $\psi_{i\sigma}(\mathbf{r})$ determined by Eq. (87). As a shorthand we write

$$\varphi_{i\sigma}(\mathbf{r}) \stackrel{r\to\infty}{\longrightarrow} \Phi_{i\sigma}(r) f_{i\sigma}(\Omega) \tag{98}$$

$$\psi_{i\sigma}(\mathbf{r}) \stackrel{r\to\infty}{\longrightarrow} \Psi_{i\sigma}(r) g_{i\sigma}(\Omega)\,. \tag{99}$$

The aim is to determine the asymptotically dominant functions $\Phi_{i\sigma}(r)$ and $\Psi_{i\sigma}(r)$. The angular parts $f_{i\sigma}(\Omega)$ and $g_{i\sigma}(\Omega)$ are not of interest in the present context. Using the fact that the KS potential of finite neutral systems behaves asymptotically as [47]

$$V_{S\sigma}(\mathbf{r}) \stackrel{r\to\infty}{\longrightarrow} -\frac{1}{r} \tag{100}$$

the KS equation (33) leads to the following asymptotic equation

$$\left(-\frac{1}{2}\,\frac{1}{r}\,\frac{d^2}{dr^2}r - \frac{1}{r} - \varepsilon_{i\sigma}\right)\Phi_{i\sigma}(r) = 0\,. \tag{101}$$

The asymptotic form of $\Phi_{i\sigma}(r)$ is easily found to be

$$\Phi_{i\sigma}(r) \stackrel{r\to\infty}{\longrightarrow} r^{1/\beta_{i\sigma}}\,\frac{\mathrm{e}^{-\beta_{i\sigma}r}}{r} \tag{102}$$

with

$$\beta_{i\sigma} := \sqrt{-2\varepsilon_{i\sigma}}\,. \tag{103}$$

By virtue of Eqs. (87) and (102), $\Psi_{i\sigma}(r)$ must satisfy the asymptotic equation

$$\left(-\frac{1}{2}\,\frac{1}{r}\,\frac{d^2}{dr^2}r - \frac{1}{r} - \varepsilon_{i\sigma}\right)\Psi_{i\sigma}(r) = \left(W_{i\sigma}(r) - C_{i\sigma}\right) r^{1/\beta_{i\sigma}}\,\frac{\mathrm{e}^{-\beta_{i\sigma}r}}{r} \tag{104}$$

where we have introduced the quantity $W_{i\sigma}(r)$ defined by

$$\Big(V_{c\sigma}(\mathbf{r}) - u_{ci\sigma}(\mathbf{r})\Big) \stackrel{r\to\infty}{\longrightarrow} W_{i\sigma}(r) w_{i\sigma}(\Omega)\,. \tag{105}$$

From Eqs. (96) and (97) we know that

$$W_{i\sigma}(r) \stackrel{r\to\infty}{\longrightarrow} 0\,. \tag{106}$$

Inserting the ansatz

$$\Psi_{i\sigma}(r) = p_{i\sigma}(r)\frac{\mathrm{e}^{-\beta_{i\sigma}r}}{r} \tag{107}$$

in Eq. (104) we find that the function $p_{i\sigma}(r)$ must satisfy the equation

$$\frac{1}{2}p''_{i\sigma} - \beta_{i\sigma}p'_{i\sigma} + \frac{p_{i\sigma}}{r} = C_{i\sigma}r^{1/\beta_{i\sigma}} \qquad \text{if} \quad C_{i\sigma} \neq 0 \tag{108}$$

and

$$\frac{1}{2}p''_{i\sigma} - \beta_{i\sigma}p'_{i\sigma} + \frac{p_{i\sigma}}{r} = -W_{i\sigma}(r)r^{1/\beta_{i\sigma}} \qquad \text{if} \quad C_{i\sigma} = 0\,. \tag{109}$$

The asymptotic solution of Eq. (108) is immediately recognized as

$$p_{i\sigma}(r) \stackrel{r\to\infty}{\longrightarrow} -\frac{C_{i\sigma}}{\beta_{i\sigma}}\, r^{(1/\beta_{i\sigma}+1)} \tag{110}$$

so that

$$\Psi_{i\sigma}(r) = -\frac{C_{i\sigma}}{\beta_{i\sigma}}\, r^{1/\beta_{i\sigma}}\, \mathrm{e}^{-\beta_{i\sigma}r} \qquad \text{if} \quad C_{i\sigma} \neq 0\,. \tag{111}$$

Writing

$$p_{i\sigma}(r) = F_{i\sigma}(r)r^{1/\beta_{i\sigma}+1} \qquad \text{if} \quad C_{i\sigma} = 0 \tag{112}$$

one readily verifies by insertion in Eq. (109) that

$$F_{i\sigma}(r) \stackrel{r\to\infty}{\longrightarrow} 0 \tag{113}$$

as a consequence of (106).

We now prove statement (ii) of the lemma by reductio ad absurdum: Assume that $C_{N_\sigma\sigma} \neq 0$. Then the asymptotic form of $\Psi_{N_\sigma\sigma}(r)$ is given by (111) and we conclude that

$$\psi^*_{N_\sigma\sigma}(\mathbf{r})\varphi_{N_\sigma\sigma}(\mathbf{r}) \stackrel{r\to\infty}{\longrightarrow} -\frac{C_{N_\sigma\sigma}}{\beta_{N_\sigma\sigma}} r^{\left(\frac{2}{\beta_{N_\sigma\sigma}}-1\right)} \mathrm{e}^{-2\beta_{N_\sigma\sigma}r} \cdot g^*_{N_\sigma\sigma}(\Omega) f_{N_\sigma\sigma}(\Omega)\,. \tag{114}$$

For $i \neq N_\sigma$, on the other hand, we obtain

$$\psi^*_{i\sigma}(\mathbf{r})\varphi_{i\sigma}(\mathbf{r}) \stackrel{r\to\infty}{\longrightarrow} G_{i\sigma}(r) r^{\left(\frac{2}{\beta_{i\sigma}}-1\right)} \mathrm{e}^{-2\beta_{i\sigma}r} \cdot g^*_{i\sigma}(\Omega) f_{i\sigma}(\Omega) \tag{115}$$

where

$$G_{i\sigma}(r) = \begin{cases} -C_{i\sigma}/\beta_{i\sigma} & \text{if} \quad C_{i\sigma} \neq 0 \\ F_{i\sigma}(r) \stackrel{r\to\infty}{\longrightarrow} 0 & \text{if} \quad C_{i\sigma} = 0 \end{cases}\,. \tag{116}$$

From this we conclude that the OEP integral equation

$$\psi^*_{N_\sigma\sigma}(\mathbf{r})\varphi_{N_\sigma\sigma}(\mathbf{r}) + \sum_{i=1}^{N_\sigma-1} \psi^*_{i\sigma}(\mathbf{r})\varphi_{i\sigma}(\mathbf{r}) + \text{c.c.} \equiv 0 \tag{117}$$

is not satisfied for $r \to \infty$ because the dominant term given by (114) cannot be canceled by any of the other contributions (115) which all fall off more rapidly (cf. Eq. (35)). Consequently the $\psi_{j\sigma}$ cannot be solutions of the OEP equation which is the desired contradiction. This implies that $C_{N_\sigma\sigma} = 0$ which completes the proof of statement (ii).

In order to prove statement (i) of the lemma we first investigate the asymptotic form of the quantities $u_{\mathrm{x}i\sigma}(\mathbf{r})$. Employing the exact exchange-energy functional (27) we find

$$u_{\mathrm{x}i\sigma}(\mathbf{r}) = -\sum_{j=1}^{N_\sigma} \frac{\varphi^*_{j\sigma}(\mathbf{r})}{\varphi^*_{i\sigma}(\mathbf{r})} K_{ji\sigma}(\mathbf{r}) \tag{118}$$

with

$$K_{ji\sigma}(\mathbf{r}) := \int d^3r' \, \frac{\varphi_{j\sigma}(\mathbf{r}')\varphi^*_{i\sigma}(\mathbf{r}')}{|\mathbf{r}-\mathbf{r}'|} \, . \tag{119}$$

Performing a multipole expansion of $K_{ji\sigma}(\mathbf{r})$ and using the orthonormality of the KS orbitals we find

$$K_{ii\sigma}(\mathbf{r}) \stackrel{r\to\infty}{\longrightarrow} \frac{1}{r} \tag{120}$$

$$K_{ji\sigma}(\mathbf{r}) \stackrel{r\to\infty}{\longrightarrow} \frac{1}{r^m} k_{ji\sigma}(\Omega) \qquad i \neq j \tag{121}$$

with some integer $m \geq 2$ that depends on i and j. Hence the sum in Eq. (118) must be dominated asymptotically by the $j = N_\sigma$ term:

$$u_{\mathrm{x}i\sigma}(\mathbf{r}) \stackrel{r\to\infty}{\longrightarrow} -\frac{\varphi^*_{N_\sigma\sigma}(\mathbf{r})}{\varphi^*_{i\sigma}(\mathbf{r})} K_{N_\sigma i\sigma}(\mathbf{r}) \, . \tag{122}$$

Using Eqs. (120), (121) and the asymptotic behavior (102) of the KS orbitals we obtain

$$u_{\mathrm{x}N_\sigma\sigma}(\mathbf{r}) \stackrel{r\to\infty}{\longrightarrow} -\frac{1}{r} \tag{123}$$

and for $i \neq N_\sigma$

$$u_{\mathrm{x}i\sigma}(\mathbf{r}) \stackrel{r\to\infty}{\longrightarrow} -r^{\left(\frac{1}{\beta_{N_\sigma\sigma}} - \frac{1}{\beta_{i\sigma}} - m\right)} \mathrm{e}^{(\beta_{i\sigma}-\beta_{N_\sigma\sigma})r} \omega_{i\sigma}(\Omega) \, . \tag{124}$$

We recognize that $u_{\mathrm{x}i\sigma}(\mathbf{r})$ diverges exponentionally to $-\infty$ for $i < N_\sigma$. In the x-only case, the quantities $\psi_{i\sigma}(\mathbf{r})$ satisfy the equation

$$\left(-\frac{\nabla^2}{2} + V_{S\sigma}(\mathbf{r}) - \varepsilon_{i\sigma}\right) \psi^*_{i\sigma}(\mathbf{r}) = \left(V_{\mathrm{x}\sigma}(\mathbf{r}) - u_{\mathrm{x}i\sigma}(\mathbf{r}) - C_{i\sigma}\right) \varphi^*_{i\sigma}(\mathbf{r}) \tag{125}$$

where

$$C_{i\sigma} = \bar{V}_{\mathrm{x}i\sigma} - \bar{u}_{\mathrm{x}i\sigma} \, . \tag{126}$$

In the following we prove statement (i) of the lemma by reductio ad absurdum: Assume that $C_{N_\sigma\sigma} \neq 0$. Then, by Eq. (123), the right-hand side of Eq. (125) for $i = N_\sigma$ is asymptotically dominated by $-C_{N_\sigma\sigma}\varphi^*_{N_\sigma\sigma}(\mathbf{r})$ and we obtain, in complete analogy to the correlation-only case:

$$\Psi_{N_\sigma\sigma}(r) = -\frac{C_{N_\sigma\sigma}}{\beta_{N_\sigma\sigma}} r^{1/\beta_{N_\sigma\sigma}} \mathrm{e}^{-\beta_{N_\sigma\sigma} r} \qquad \text{for} \quad C_{N_\sigma\sigma} \neq 0 \, . \tag{127}$$

For $i < N_\sigma$, the right-hand side of Eq.(125) is dominated by $-u_{\mathrm{x}i\sigma}(\mathbf{r})\varphi^*_{i\sigma}(\mathbf{r})$. Using Eqs. (102) and (124) $\Psi_{i\sigma(r)}$ satisfies the asymptotic differential equation

$$\left(-\frac{1}{2}\frac{1}{r}\frac{d^2}{dr^2}r - \frac{1}{r} - \varepsilon_{i\sigma}\right) \Psi_{i\sigma}(r) = r^{\left(\frac{1}{\beta_{N_\sigma\sigma}} - 1 - m\right)} \mathrm{e}^{-\beta_{N_\sigma\sigma} r} \, . \tag{128}$$

From this equation one readily concludes that

$$\Psi_{i\sigma}(r) \stackrel{r\to\infty}{\longrightarrow} \frac{1}{\varepsilon_{N_\sigma\sigma} - \varepsilon_{i\sigma}} r^{\left(\frac{1}{\beta_{N_\sigma\sigma}} - 1 - m\right)} \mathrm{e}^{-\beta_{N_\sigma\sigma} r} \, , \qquad i < N_\sigma \, . \tag{129}$$

We note in passing that all the functions $\psi_{i\sigma}$, $i = 1...N_\sigma$, have the *same* exponential decay, $\mathrm{e}^{-\beta_{N_\sigma\sigma}r}$, determined by the highest occupied orbital energy $\beta_{N_\sigma\sigma} = \sqrt{-2\varepsilon_{N_\sigma\sigma}}$. This fact further supports the interpretation of the quantities $\psi_{i\sigma}$ (in the x-only case) as a shift from the KS orbitals towards the HF orbitals: The HF orbitals $\varphi_{i\sigma}^{\mathrm{HF}}$ are known [48] to be asymptotically dominated by the exponential decay $\mathrm{e}^{-\beta_{N_\sigma\sigma}r}$ of the highest occupied orbital. The same holds true for the shifted KS orbitals $(\varphi_{i\sigma} + \psi_{i\sigma})$.

From Eqs. (102), (127) and (129) we obtain

$$\psi^*_{N_\sigma\sigma}(\mathbf{r})\varphi_{N_\sigma\sigma}(\mathbf{r}) \stackrel{r\to\infty}{\longrightarrow} -\frac{C_{N_\sigma\sigma}}{\beta_{N_\sigma\sigma}}\, r^{\left(\frac{2}{\beta_{N_\sigma\sigma}}-1\right)} \mathrm{e}^{-2\beta_{N_\sigma\sigma}r} \cdot g^*_{N_\sigma\sigma}(\Omega) f_{N_\sigma\sigma}(\Omega)\,. \tag{130}$$

and

$$\psi^*_{i\sigma}(\mathbf{r})\varphi_{i\sigma}(\mathbf{r}) \stackrel{r\to\infty}{\longrightarrow} \frac{1}{\varepsilon_{N_\sigma\sigma} - \varepsilon_{i\sigma}} r^{\left(\frac{1}{\beta_{N_\sigma\sigma}}+\frac{1}{\beta_{i\sigma}}-2-m\right)} \mathrm{e}^{-(\beta_{N_\sigma\sigma}+\beta_{i\sigma})r} \cdot g^*_{i\sigma}(\Omega) f_{i\sigma}(\Omega)\,, i < N_\sigma\,. \tag{131}$$

Once again we conclude that in the OEP equation (117) the asymptotically dominant term (130) cannot be canceled by any of the other terms (131), leading to the contradiction that the $\psi_{j\sigma}(\mathbf{r})$ are not solutions of the OEP integral equation. Hence we conclude that $C_{N_\sigma\sigma} = 0$ which completes the proof of the lemma.

The original proof [13] of statement (i) was based on the asymptotic form of the Green function which is easily accessible only in 1D. Considering the 3D Green function, Krieger, Li and Iafrate [19] made it plausible that the statement holds true in the 3D case as well. An alternative proof was recently given [49] for the x-only case. This proof is based on the scaling properties of the exchange-energy functional and can therefore not be generalized to the case of correlation. The proof presented above for the correlation part of the OEP (statement (ii) of the lemma) is valid for all correlation energy functionals leading to asymptotically bounded functions $u_{ci\sigma}(\mathbf{r})$. For asymptotically diverging $u_{ci\sigma}(\mathbf{r})$ the lemma might still be valid. In particular, if the divergence is the same as the one (Eq.(124)) found in the exchange case, the proof of statement (i) carries over. The lemma has a number of important consequences which will be discussed in the following two subsections.

2.3.2 Asymptotic form

In this section we shall investigate the asymptotic form of the exchange and correlation potentials. It will be shown that $V_{\mathrm{x}\sigma}(\mathbf{r})$ and $u_{\mathrm{x}N_\sigma\sigma}(\mathbf{r})$ approach each other exponentially fast for $r \to \infty$, and that the difference between $V_{\mathrm{c}\sigma}(\mathbf{r})$ and $u_{\mathrm{c}N_\sigma\sigma}(\mathbf{r})$ decays exponentially as well. Using the notation of the last section the detailed statements read as follows:

Theorem 1:

$$V_{\mathrm{x}\sigma}(\mathbf{r}) - u_{\mathrm{x}N_\sigma\sigma}(\mathbf{r}) \stackrel{r\to\infty}{\longrightarrow} r^{\left(\frac{1}{\beta_{(N_\sigma-1)\sigma}}-\frac{1}{\beta_{N_\sigma\sigma}}-m\right)} \mathrm{e}^{-(\beta_{(N_\sigma-1)\sigma}-\beta_{N_\sigma\sigma})r} \tag{132}$$

where m is an integer satisfying $m \geq 2$.

Theorem 2: *If the constant $C_{(N_\sigma-1)\sigma}$ defined by Eq. (88) does not vanish then*

$$V_{\mathrm{c}\sigma}(\mathbf{r}) - u_{\mathrm{c}N_\sigma\sigma}(\mathbf{r}) \stackrel{r\to\infty}{\longrightarrow} r^{\left(\frac{2}{\beta_{(N_\sigma-1)\sigma}}-\frac{2}{\beta_{N_\sigma\sigma}}+1\right)} \mathrm{e}^{-2(\beta_{(N_\sigma-1)\sigma}-\beta_{N_\sigma\sigma})r}. \tag{133}$$

If $C_{(N_\sigma-1)\sigma} = 0$ the right-hand side of (133) is an upper bound of $|V_{\mathrm{c}\sigma}(\mathbf{r}) - u_{\mathrm{c}N_\sigma\sigma}(\mathbf{r})|$ for $r \to \infty$, i.e. for $C_{(N_\sigma-1)\sigma} = 0$, $V_{\mathrm{c}\sigma}(\mathbf{r})$ and $u_{\mathrm{c}N_\sigma\sigma}(\mathbf{r})$ approach each other even faster than given by the right-hand side of Eq. (133).

To prove theorem 1 we write

$$\Psi_{N_\sigma\sigma}(r) = q(r)\frac{e^{-\beta_{N_\sigma\sigma}r}}{r} \quad . \tag{134}$$

Using the lemma of the last section ensuring that $C_{N_\sigma\sigma} = 0$, $q(r)$ must satisfy the following asymptotic differential equation:

$$-\frac{1}{2}r^{-\frac{1}{\beta_{N_\sigma\sigma}}}q''(r) + \beta_{N_\sigma\sigma}r^{-\frac{1}{\beta_{N_\sigma\sigma}}}q'(r) - r^{-\left(\frac{1}{\beta_{N_\sigma\sigma}}+1\right)}q(r) = V_{\mathrm{x}\sigma}(\mathbf{r}) - u_{\mathrm{x}N_\sigma\sigma}(\mathbf{r}) \quad . \tag{135}$$

This is readily verified by inserting (100), (102) and (134) in Eq. (125). By virtue of Eqs. (35) and (131) the sum

$$\sum_{i=1}^{N_\sigma-1}\psi^*_{i\sigma}(\mathbf{r})\varphi_{i\sigma}(\mathbf{r}) \tag{136}$$

must be asymptotically dominated by the $i = (N_\sigma - 1)$ term which decays as

$$\begin{aligned}&\psi^*_{(N_\sigma-1)\sigma}(\mathbf{r})\varphi_{(N_\sigma-1)\sigma}(\mathbf{r})\\ &\quad\overset{r\to\infty}{\longrightarrow}\frac{1}{\varepsilon_{N_\sigma\sigma}-\varepsilon_{(N_\sigma-1)\sigma}}r^{\left(\frac{1}{\beta_{N_\sigma\sigma}}+\frac{1}{\beta_{(N_\sigma-1)\sigma}}-2-m\right)}\mathrm{e}^{-(\beta_{N_\sigma\sigma}+\beta_{(N_\sigma-1)\sigma})r} \quad .\end{aligned} \tag{137}$$

This term cannot be canceled by any other term of the sum (136). Hence, for the OEP equation (55) to be asymptotically satisfied, the expression (137) must be canceled by the $i = N_\sigma$ term which behaves as

$$\psi^*_{N_\sigma\sigma}(\mathbf{r})\varphi_{N_\sigma\sigma}(\mathbf{r}) \overset{r\to\infty}{\longrightarrow} q(r)r^{\left(\frac{1}{\beta_{N_\sigma\sigma}}-2\right)}\mathrm{e}^{-2\beta_{N_\sigma\sigma}r} \quad . \tag{138}$$

Equating the right-hand side of Eqs. (137) and (138), the function $q(r)$ is readily determined to be

$$q(r) = \frac{1}{\varepsilon_{N_\sigma\sigma}-\varepsilon_{(N_\sigma-1)\sigma}}r^{\left(\frac{1}{\beta_{(N_\sigma-1)\sigma}}-m\right)}\mathrm{e}^{-(\beta_{(N_\sigma-1)\sigma}-\beta_{N_\sigma\sigma})r} \quad . \tag{139}$$

Finally, by inserting this result in the left-hand side of Eq. (135), we confirm that the right-hand side of this equation decays asymptotically as stated in theorem 1.

To prove theorem 2 we write for the correlation-only case

$$\Psi_{N_\sigma\sigma}(r) = p(r)\frac{\mathrm{e}^{-\beta_{N_\sigma\sigma}r}}{r} \quad . \tag{140}$$

Since $C_{N_\sigma\sigma} = 0$, $p(r)$ must satisfy the following asymptotic differential equation (cf. Eq. (109)):

$$-\frac{1}{2}r^{-\frac{1}{\beta_{N_\sigma\sigma}}}p''(r) + \beta_{N_\sigma\sigma}r^{-\frac{1}{\beta_{N_\sigma\sigma}}}p'(r) - r^{-\left(\frac{1}{\beta_{N_\sigma\sigma}}+1\right)}p(r) = V_{\mathrm{c}\sigma}(\mathbf{r}) - u_{\mathrm{c}N_\sigma\sigma}(\mathbf{r}) \quad . \tag{141}$$

If $C_{(N_\sigma-1)\sigma} \neq 0$, the sum

$$\sum_{i=1}^{N_\sigma-1}\psi^*_{i\sigma}(\mathbf{r})\varphi_{i\sigma}(\mathbf{r}) \tag{142}$$

is asymptotically dominated by the $i = (N_\sigma - 1)$ term which, according to Eqs. (115) and (116), decays as

$$\psi^*_{(N_\sigma-1)\sigma}(\mathbf{r})\varphi_{(N_\sigma-1)\sigma}(\mathbf{r}) \overset{r\to\infty}{\longrightarrow} r^{\left(\frac{2}{\beta_{(N_\sigma-1)\sigma}}-1\right)}\mathrm{e}^{-2\beta_{(N_\sigma-1)\sigma}r} \quad . \tag{143}$$

Once again this term cannot be canceled by any other term of the sum (142). Hence it must be canceled asymptotically by the $i = N_\sigma$ term which behaves as

$$\psi^*_{N_\sigma\sigma}(\mathbf{r})\varphi_{N_\sigma\sigma}(\mathbf{r}) \stackrel{r\to\infty}{\longrightarrow} p(r) r^{\left(\frac{1}{\beta_{N_\sigma\sigma}}-2\right)} \mathrm{e}^{-2\beta_{N_\sigma\sigma} r} \ . \tag{144}$$

Equating the right-hand sides of Eqs. (143) and (144) we can identify the asymptotic form of $p(r)$:

$$p(r) \propto r^{\left(\frac{2}{\beta_{(N_\sigma-1)\sigma}}-\frac{1}{\beta_{N_\sigma\sigma}}+1\right)} \mathrm{e}^{-2(\beta_{(N_\sigma-1)\sigma}-\beta_{N_\sigma\sigma})r} \ . \tag{145}$$

Insertion of this expression in the left-hand side of Eq. (141) proves Eq. (133) for the case $C_{(N_\sigma-1)\sigma} \neq 0$. If $C_{(N_\sigma-1)\sigma} = 0$ the asymptotic form of $V_{\mathrm{c}\sigma}(\mathbf{r}) - u_{\mathrm{c}N_\sigma\sigma}(\mathbf{r})$ cannot be stated explicitly. It is clear, however, that the $i = N_\sigma$ term (144) must be canceled asymptotically by some contribution to the sum (142). Since, by Eqs. (115) and (116), *all* contributions to the sum (142) fall off more rapidly than the right-hand side of (143), $p(r)$ must decay more rapidly than the right-hand side of (145). Hence, by Eq. (141), the right-hand side of (133) provides an upper bound of $|V_{\mathrm{c}\sigma}(\mathbf{r}) - u_{\mathrm{c}N_\sigma\sigma}(\mathbf{r})|$ for $r \to \infty$ if $C_{(N_\sigma-1)\sigma} = 0$. This completes the proof.

Since the asymptotic form of $u_{\mathrm{x}N_\sigma\sigma}(\mathbf{r})$, as derived in Eq. (123), is $-\frac{1}{r}$, theorem 1 immediately implies that

$$V_{\mathrm{x}\sigma}(\mathbf{r}) \stackrel{r\to\infty}{\longrightarrow} -\frac{1}{r} \ . \tag{146}$$

This is a well-known result that has been obtained in several different ways [13, 14, 16, 19, 47, 50, 51, 52]. The exact correlation potential of DFT is known [47] to fall off as $-\alpha/(2r^4)$ for atoms with spherical N and $(N-1)$-electron ground states, with α being the static polarizability of the $(N-1)$-electron ground state. Theorem 2 provides a simple way of checking how the OEP correlation-only potential $V_{\mathrm{c}\sigma}(\mathbf{r})$ falls off for a given approximate orbital functional $E_{\mathrm{c}}^{\mathrm{approx}}[\{\varphi_{i\sigma}\}]$: One only needs to determine the asymptotic decay of $u_{\mathrm{c}N_\sigma\sigma}(\mathbf{r})$.

We now turn to the discussion of the KLI potential. We shall demonstrate that the above rigorous properties of the full OEP are preserved by the KLI approximation. To this end we write the KLI approximation (76) separately for the exchange and correlation potentials:

$$\sum_{i=1}^{N_\sigma} |\varphi_{i\sigma}(\mathbf{r})|^2 \left(V^{\mathrm{KLI}}_{\mathrm{x}\sigma}(\mathbf{r}) - U_{\mathrm{x}i\sigma}(\mathbf{r}) - \left(\bar{V}^{\mathrm{KLI}}_{\mathrm{x}i\sigma} - \bar{U}_{\mathrm{x}i\sigma}\right)\right) = 0 \tag{147}$$

$$\sum_{i=1}^{N_\sigma} |\varphi_{i\sigma}(\mathbf{r})|^2 \left(V^{\mathrm{KLI}}_{\mathrm{c}\sigma}(\mathbf{r}) - U_{\mathrm{c}i\sigma}(\mathbf{r}) - \left(\bar{V}^{\mathrm{KLI}}_{\mathrm{c}i\sigma} - \bar{U}_{\mathrm{c}i\sigma}\right)\right) = 0 \ . \tag{148}$$

where, for convenience, we have introduced

$$U_{\mathrm{x}i\sigma}(\mathbf{r}) = \frac{1}{2}\left(u_{\mathrm{x}i\sigma}(\mathbf{r}) + u^*_{\mathrm{x}i\sigma}(\mathbf{r})\right) \tag{149}$$

and

$$U_{\mathrm{c}i\sigma}(\mathbf{r}) = \frac{1}{2}\left(u_{\mathrm{c}i\sigma}(\mathbf{r}) + u^*_{\mathrm{c}i\sigma}(\mathbf{r})\right) \tag{150}$$

in order to deal with real-valued quantities only. Following the argument given in the beginning of section 2.3.1 (Eqs. (89) - (97)) we can assume *without restriction* that

$$V^{\mathrm{KLI}}_{\mathrm{x}\sigma}(\mathbf{r}) \stackrel{r\to\infty}{\longrightarrow} 0 \tag{151}$$

$$V_{c\sigma}^{\rm KLI}(\mathbf{r}) \stackrel{r\to\infty}{\longrightarrow} 0 \tag{152}$$

$$U_{ci\sigma}(\mathbf{r}) \stackrel{r\to\infty}{\longrightarrow} 0\,. \tag{153}$$

This is because the structure of Eqs. (147) and (148) is again such that an additive constant in the potentials (151) - (153) cancels out. Of course, Eq. (153) is valid only for those approximate orbital functionals $E_{\rm c}[\{\varphi_{i\sigma}\}]$ leading to bounded functions $u_{ci\sigma}(\mathbf{r})$ for $r\to\infty$ (cf. condition (86)).

In order to determine the asymptotic form of the KLI-x-only potential $V_{{\rm x}\sigma}^{\rm KLI}(\mathbf{r})$, we first investigate the asymptotic behavior of the term $\sum_{i=1}^{N_\sigma}|\varphi_{i\sigma}(\mathbf{r})|^2 u_{{\rm x}i\sigma}(\mathbf{r})$ appearing in the KLI equation (147): By Eqs. (118) and (119) the expression

$$|\varphi_{N_\sigma\sigma}(\mathbf{r})|^2 u_{{\rm x}N_\sigma\sigma}(\mathbf{r}) + \sum_{i=1}^{N_\sigma-1}|\varphi_{i\sigma}(\mathbf{r})|^2 u_{{\rm x}i\sigma}(\mathbf{r})$$

can be written as

$$= |\varphi_{N_\sigma\sigma}(\mathbf{r})|^2 u_{{\rm x}N_\sigma\sigma}(\mathbf{r}) + \sum_{i=1}^{N_\sigma-1}\sum_{j=1}^{N_\sigma}\varphi_{i\sigma}(\mathbf{r})\varphi_{j\sigma}^*(\mathbf{r})K_{ji\sigma}(\mathbf{r})$$

$$= |\varphi_{N_\sigma\sigma}(\mathbf{r})|^2\left(u_{{\rm x}N_\sigma\sigma}(\mathbf{r}) + \sum_{i=1}^{N_\sigma-1}\sum_{j=1}^{N_\sigma}\left(\frac{\varphi_{i\sigma}(\mathbf{r})}{\varphi_{N_\sigma\sigma}(\mathbf{r})}\right)\left(\frac{\varphi_{j\sigma}^*(\mathbf{r})}{\varphi_{N_\sigma\sigma}^*(\mathbf{r})}\right)K_{ji\sigma}(\mathbf{r})\right)\,.$$

Since $K_{ji\sigma}(\mathbf{r})$ decays as an inverse power the double sum over i and j must be asymptotically dominated by the term with $i=N_\sigma-1$, $j=N_\sigma$ so that

$$\stackrel{r\to\infty}{\longrightarrow} |\varphi_{N_\sigma\sigma}(\mathbf{r})|^2\left(u_{{\rm x}N_\sigma\sigma}(\mathbf{r}) + \frac{\varphi_{(N\sigma-1)\sigma}(\mathbf{r})}{\varphi_{N_\sigma\sigma}(\mathbf{r})}K_{N_\sigma(N_\sigma-1)\sigma}(\mathbf{r})\right)\,.$$

The KLI equation (147) then yields

$$\begin{aligned}
&\sum_{i=1}^{N_\sigma}|\varphi_{i\sigma}(\mathbf{r})|^2\left[V_{{\rm x}\sigma}^{\rm KLI}(\mathbf{r}) - U_{{\rm x}i\sigma}(\mathbf{r}) - \left(\bar{V}_{{\rm x}i\sigma}^{\rm KLI} - \bar{U}_{{\rm x}i\sigma}\right)\right]\\
&\stackrel{r\to\infty}{\longrightarrow}\ |\varphi_{N_\sigma\sigma}(\mathbf{r})|^2\left[V_{{\rm x}\sigma}^{\rm KLI}(\mathbf{r}) - U_{{\rm x}N_\sigma\sigma}(\mathbf{r}) - \left(\bar{V}_{{\rm x}N_\sigma\sigma}^{\rm KLI} - \bar{U}_{{\rm x}N_\sigma\sigma}\right)\right.\\
&\qquad + \left(\frac{\varphi_{(N\sigma-1)\sigma}(\mathbf{r})}{\varphi_{N_\sigma\sigma}(\mathbf{r})}K_{N_\sigma(N_\sigma-1)\sigma}(\mathbf{r}) + \text{c.c.}\right)\\
&\qquad \left. + \sum_{i=1}^{N_\sigma-1}\frac{|\varphi_{i\sigma}(\mathbf{r})|^2}{|\varphi_{N_\sigma\sigma}(\mathbf{r})|^2}\left(V_{{\rm x}\sigma}^{\rm KLI}(\mathbf{r}) - U_{{\rm x}i\sigma}(\mathbf{r}) - \left(\bar{V}_{{\rm x}i\sigma}^{\rm KLI} - \bar{U}_{{\rm x}i\sigma}\right)\right)\right] \equiv 0\,.
\end{aligned} \tag{154}$$

Since the KLI equation must be satisfied in the asymptotic region, the expression in square brackets on the right-hand side of Eq. (154) must vanish identically for $r\to\infty$. The term involving $\varphi_{(N_\sigma-1)\sigma}(\mathbf{r})/\varphi_{N_\sigma\sigma}(\mathbf{r})$ cannot be canceled by any of the terms involving $|\varphi_{i\sigma}(\mathbf{r})|^2/|\varphi_{N_\sigma\sigma}(\mathbf{r})|^2$ because the latter decay more rapidly. From this we conclude that

$$\begin{aligned}
&V_{{\rm x}\sigma}^{\rm KLI}(\mathbf{r}) - U_{{\rm x}N_\sigma\sigma}(\mathbf{r}) - \left(\bar{V}_{{\rm x}N_\sigma\sigma}^{\rm KLI} - \bar{U}_{{\rm x}N_\sigma\sigma}\right)\\
&\stackrel{r\to\infty}{\longrightarrow}\ -\frac{\varphi_{(N\sigma-1)\sigma}(\mathbf{r})}{\varphi_{N_\sigma\sigma}(\mathbf{r})}K_{N_\sigma(N_\sigma-1)\sigma}(\mathbf{r}) + \text{c.c.}\\
&\stackrel{r\to\infty}{\longrightarrow}\ -r^{\left(\frac{1}{\beta_{(N_\sigma-1)\sigma}} - \frac{1}{\beta_{N_\sigma\sigma}} - m\right)}\mathrm{e}^{-(\beta_{(N_\sigma-1)\sigma}-\beta_{N_\sigma\sigma})r}
\end{aligned} \tag{155}$$

where, in the second step, we have used Eqs. (102) and (121). $U_{\mathrm{x}N_\sigma\sigma}(\mathbf{r})$ goes to zero asymptotically (cf. Eq. (123)) and the arbitrary additive constant in $V_{\mathrm{x}\sigma}^{\mathrm{KLI}}(\mathbf{r})$ had been fixed in such a way that $V_{\mathrm{x}\sigma}^{\mathrm{KLI}}(\mathbf{r})$ vanishes asymptotically (cf. Eq. (151)). Hence Eq. (155) immediately implies that [14, 16, 19]

$$\bar{V}_{\mathrm{x}N_\sigma\sigma}^{\mathrm{KLI}} = \bar{U}_{\mathrm{x}N_\sigma\sigma} \tag{156}$$

and thereby

$$V_{\mathrm{x}\sigma}^{\mathrm{KLI}}(\mathbf{r}) - U_{\mathrm{x}N_\sigma\sigma}(\mathbf{r}) \stackrel{r\to\infty}{\longrightarrow} -r^{\left(\frac{1}{\beta_{(N_\sigma-1)\sigma}}-\frac{1}{\beta_{N_\sigma\sigma}}-m\right)}\mathrm{e}^{-(\beta_{(N_\sigma-1)\sigma}-\beta_{N_\sigma\sigma})r} \ . \tag{157}$$

We thus conclude that both the lemma of section 2.3.1 and the theorem 1 are preserved in the KLI approximation. Once again, Eqs. (123) and (157) immediately imply that [14, 16, 19]

$$V_{\mathrm{x}\sigma}^{\mathrm{KLI}} \stackrel{r\to\infty}{\longrightarrow} -\frac{1}{r} \ . \tag{158}$$

For the correlation potential $V_{\mathrm{c}\sigma}^{\mathrm{KLI}}(\mathbf{r})$ the considerations are even simpler. Dividing the KLI equation by $|\varphi_{N_\sigma\sigma}(\mathbf{r})|^2$ we find:

$$0 \equiv V_{\mathrm{c}\sigma}^{\mathrm{KLI}}(\mathbf{r}) - U_{\mathrm{c}N_\sigma\sigma}(\mathbf{r}) - C_{N_\sigma\sigma} + \sum_{i=1}^{N_\sigma-1}\frac{|\varphi_{i\sigma}(\mathbf{r})|^2}{|\varphi_{N_\sigma\sigma}(\mathbf{r})|^2}\left(V_{\mathrm{c}\sigma}^{\mathrm{KLI}}(\mathbf{r}) - U_{\mathrm{c}i\sigma}(\mathbf{r}) - C_{i\sigma}\right) \tag{159}$$

where

$$C_{i\sigma} := \bar{V}_{\mathrm{c}i\sigma}^{\mathrm{KLI}} - \bar{U}_{\mathrm{c}i\sigma} \ . \tag{160}$$

By Eqs. (102), (152) and (153) all the r-dependent functions in (159) vanish asymptotically. Since the KLI equation (159) must be satisfied for $r \to \infty$ as well we readily conclude that

$$C_{N_\sigma\sigma} = 0 \tag{161}$$

so that

$$V_{\mathrm{c}\sigma}^{\mathrm{KLI}}(\mathbf{r}) - U_{\mathrm{c}N_\sigma\sigma}(\mathbf{r}) = \sum_{i=1}^{N_\sigma-1}\frac{|\varphi_{i\sigma}(\mathbf{r})|^2}{|\varphi_{N_\sigma\sigma}(\mathbf{r})|^2}\left(C_{i\sigma} - V_{\mathrm{c}\sigma}(\mathbf{r}) + U_{\mathrm{c}i\sigma}^{\mathrm{KLI}}(\mathbf{r})\right) \ . \tag{162}$$

If $C_{(N_\sigma-1)\sigma} \neq 0$, the right-hand side of (162) is asymptotically dominated by the $i = (N_\sigma-1)$ term and we obtain

$$V_{\mathrm{c}\sigma}^{\mathrm{KLI}}(\mathbf{r}) - U_{\mathrm{c}N_\sigma\sigma}(\mathbf{r}) \stackrel{r\to\infty}{\longrightarrow} r^{\left(\frac{2}{\beta_{(N_\sigma-1)\sigma}}-\frac{2}{\beta_{N_\sigma\sigma}}\right)}\mathrm{e}^{-2(\beta_{(N_\sigma-1)\sigma}-\beta_{N_\sigma\sigma})r} \tag{163}$$

If $C_{(N_\sigma-1)\sigma} = 0$, the right-hand side of (163) is an upper bound of $|V_{\mathrm{c}\sigma}^{\mathrm{KLI}}(\mathbf{r}) - U_{\mathrm{c}N_\sigma\sigma}(\mathbf{r})|$ for $r \to \infty$. We note that $V_{\mathrm{c}\sigma}^{\mathrm{KLI}}(\mathbf{r})$ and $U_{\mathrm{c}N_\sigma\sigma}(\mathbf{r})$ approach each other exponentially fast for $r \to \infty$ with the same exponential function as theorem 2 predicts for the full OEP. However, the power of r multiplying the exponential function in (163) differs by 1 from the power in theorem 2.

2.3.3 Derivative discontinuities

In the early eighties an unexpected property of the exact xc potential was discovered [53, 54, 55]: Writing the density $\rho(\mathbf{r}) = M\ \xi(\mathbf{r})$ with a shape function $\xi(\mathbf{r})$ integrating to 1 and allowing for arbitrary (fractional) particle numbers M, the exact xc potential

$V_{\rm xc}[M\xi](\mathbf{r})$ is a discontinuous function of M. None of the standard density functionals such as the LDA, gradient expansions or GGAs show these discontinuities. Once again KLI were the first to point out [16, 19, 17] that the OEP correctly reproduces the required discontinuities, as will be discussed below.

DFT is readily extended to systems where the density ρ integrates to a non-integer particle number

$$M = N + \omega = \int d^3r\ \rho(\mathbf{r}) \quad \text{with } N \in \mathbf{N},\ \ 0 \le \omega \le 1 \tag{164}$$

(see [2] for a detailed description). In this generalization, a system with fractional particle number $N+\omega$ is described by an ensemble consisting of the N and $N+1$ particle systems. Specifically, the ensemble density $\rho_{N+\omega}$ of the system with non-integer particle number $N+\omega$ is given by

$$\rho_{N+\omega}(\mathbf{r}) = (1-\omega)\,\rho_N(\mathbf{r}) + \omega\rho_{N+1}(\mathbf{r}) \tag{165}$$

where ρ_N and ρ_{N+1} are the ground-state densities of the N and $N+1$ particle systems, respectively. The ensemble energy is given by

$$E_{N+\omega} = (1-\omega)\,E_N + \omega E_{N+1}\,, \tag{166}$$

i.e., the energy for fractional particle number is obtained by connecting the ground-state energies of integer particle numbers by straight lines. As a consequence,

$$\mu(M) = \frac{\partial E_M}{\partial M}\,, M \in \mathbf{R}, \tag{167}$$

jumps discontinuously if M passes through an integer. From (166) one obtains

$$\mu(M) = \begin{cases} -I(Z): & Z-1 < M < Z \\ -A(Z): & Z < M < Z+1 \end{cases} \tag{168}$$

where $I(Z)$ is the first ionization potential

$$I(Z) = E_{Z-1}(Z) - E_Z(Z) \tag{169}$$

and $A(Z)$ the electron affinity

$$A(Z) = E_Z(Z) - E_{Z+1}(Z) \tag{170}$$

of a system with nuclear charge Z, electron number M and energy $E_M(Z)$. Using the HK variational equation

$$\left.\frac{\delta E[\rho]}{\delta\rho(\mathbf{r})}\right|_M = \mu(M) \tag{171}$$

we can express the derivative discontinuity of the total-energy functional

$$\Delta := \lim_{\omega\to 0}\left\{\left.\frac{\delta E[\rho]}{\delta\rho(\mathbf{r})}\right|_{N+\omega} - \left.\frac{\delta E[\rho]}{\delta\rho(\mathbf{r})}\right|_{N-\omega}\right\}_{\rho_N} \tag{172}$$

in terms of the chemical potential

$$= \lim_{\omega\to 0}\left\{\mu(N+\omega) - \mu(N-\omega)\right\}\,. \tag{173}$$

By virtue of Eq. (168) we obtain

$$\Delta = I(N) - A(N) \,. \tag{174}$$

This fundamental equation shows that the derivative discontinuity of the total-energy functional is identical with the *band gap* of an infinite insulator and, in the case of finite species, with twice the chemical *hardness*. A glance at the expression for the total energy (16) shows that only two terms may contribute to the derivative discontinuity, namely $T_{\rm S}$ and $E_{\rm xc}$. In order to further evaluate the derivative discontinuity of the interacting system, we first observe that for a system of N non-interacting particles the derivative discontinuity $\Delta_{\rm nonint}$ of the total energy

$$\begin{aligned} \Delta_{\rm nonint} &= \lim_{\omega\to 0} \left\{ \left.\frac{\delta E[\rho]}{\delta\rho(\mathbf{r})}\right|_{N+\omega} - \left.\frac{\delta E[\rho]}{\delta\rho(\mathbf{r})}\right|_{N-\omega} \right\} \\ &= \lim_{\omega\to 0} \left\{ \left.\frac{\delta T_{\rm S}[\rho]}{\delta\rho(\mathbf{r})}\right|_{N+\omega} - \left.\frac{\delta T_{\rm S}[\rho]}{\delta\rho(\mathbf{r})}\right|_{N-\omega} \right\} \end{aligned} \tag{175}$$

is given by

$$\Delta_{\rm nonint} = I_{\rm nonint} - A_{\rm nonint} = \varepsilon_{N+1}(N) - \varepsilon_N(N) \tag{176}$$

where $\varepsilon_m(M)$ denotes the m-th single particle orbital of the M-particle system. If the right-hand side of Eq. (175) is evaluated at the ground-state density ρ_N of the interacting N-particle system, the non-interacting system leading to this density is the KS system and the resulting discontinuity is

$$\Delta^{\rm KS}_{\rm nonint} = \varepsilon^{\rm KS}_{N+1}(N) - \varepsilon^{\rm KS}_N(N) \,. \tag{177}$$

Hence the total discontinuity of the interacting system

$$\begin{aligned} \Delta &= \lim_{\omega\to 0} \left\{ \left.\frac{\delta E[\rho]}{\delta\rho(\mathbf{r})}\right|_{N+\omega} - \left.\frac{\delta E[\rho]}{\delta\rho(\mathbf{r})}\right|_{N-\omega} \right\}_{\rho_N} \\ &= \lim_{\omega\to 0} \left\{ \left.\frac{\delta T_{\rm S}[\rho]}{\delta\rho(\mathbf{r})}\right|_{N+\omega} - \left.\frac{\delta T_{\rm S}[\rho]}{\delta\rho(\mathbf{r})}\right|_{N-\omega} \right\}_{\rho_N} \\ &+ \lim_{\omega\to 0} \left\{ \left.\frac{\delta E_{\rm xc}[\rho]}{\delta\rho(\mathbf{r})}\right|_{N+\omega} - \left.\frac{\delta E_{\rm xc}[\rho]}{\delta\rho(\mathbf{r})}\right|_{N-\omega} \right\}_{\rho_N} \end{aligned} \tag{178}$$

can be written as

$$\Delta = \Delta^{\rm KS}_{\rm nonint} + \Delta_{\rm xc} \tag{179}$$

where

$$\Delta_{\rm xc} = \lim_{\omega\to 0} \left\{ \left.\frac{\delta E_{\rm xc}[\rho]}{\delta\rho(\mathbf{r})}\right|_{N+\omega} - \left.\frac{\delta E_{\rm xc}[\rho]}{\delta\rho(\mathbf{r})}\right|_{N-\omega} \right\}_{\rho_N} . \tag{180}$$

As it is known [47] that

$$I = -\varepsilon^{\rm KS}_N(N) \tag{181}$$

and

$$A = -\varepsilon^{\rm KS}_{N+1}(N+1) \tag{182}$$

it follows from Eqs. (174), (177) and (179) that

$$\Delta_{\rm xc} = \varepsilon^{\rm KS}_{N+1}(N+1) - \varepsilon^{\rm KS}_{N+1}(N). \tag{183}$$

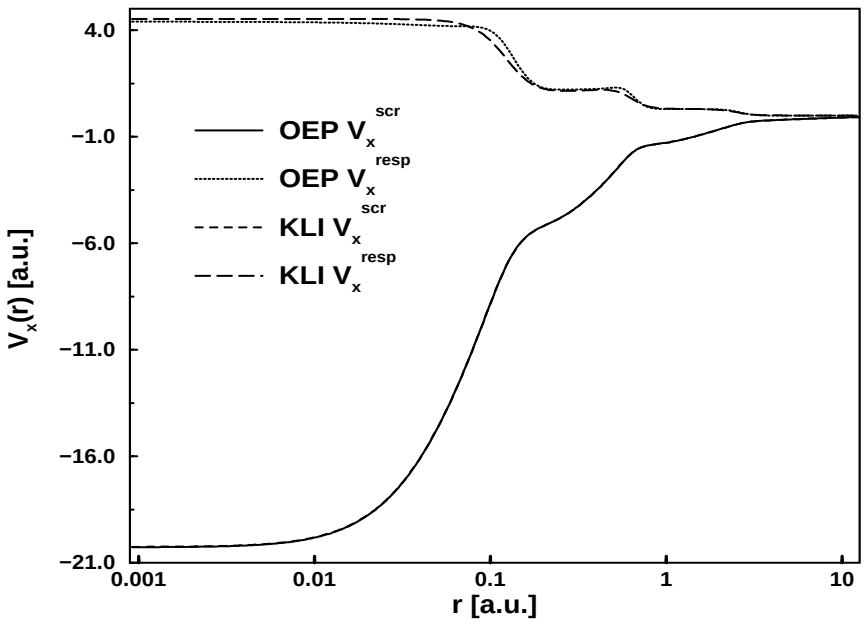

Figure 1: *Screening and screening response potentials* $V_{\rm x}^{\rm scr}(\mathbf{r})$ *and* $V_{\rm x}^{\rm resp}(\mathbf{r})$ *for Ca from the OEP and KLI method.*

We will now investigate the xc-potential. First we observe that the exact xc-energy functional may be written in terms of the (coupling-constant averaged) pair-correlation function $g_{\sigma\sigma'}[\rho](\mathbf{r},\mathbf{r}')$ as

$$E_{\rm xc}[\rho] = \frac{1}{2}\sum_{\sigma\sigma'}\int\int\ d^3r\ d^3r'\ \frac{\rho_\sigma(\mathbf{r})\rho_{\sigma'}(\mathbf{r}')}{|\mathbf{r}-\mathbf{r}'|}\left(g_{\sigma\sigma'}[\rho](\mathbf{r},\mathbf{r}')-1\right). \tag{184}$$

Following van Leeuwen, Gritsenko and Baerends [56], the xc-potential may be split up in the following manner:

$$V_{{\rm xc}\sigma}(\mathbf{r}) = V_{{\rm xc}\sigma}^{\rm scr}(\mathbf{r}) + V_{{\rm xc}\sigma}^{\rm resp}(\mathbf{r}) \tag{185}$$

where the screening potential is defined as

$$V_{{\rm xc}\sigma}^{\rm scr}(\mathbf{r}) = \sum_{\sigma'}\int d^3r'\ \frac{\rho_{\sigma'}(\mathbf{r}')}{|\mathbf{r}-\mathbf{r}'|}\left(g_{\sigma\sigma'}[\rho](\mathbf{r},\mathbf{r}')-1\right) \tag{186}$$

and the screening response potential as

$$V_{{\rm xc}\sigma}^{\rm resp}(\mathbf{r}) = \frac{1}{2}\sum_{\sigma'\sigma''}\int\int d^3r'\ d^3r''\ \frac{\rho_{\sigma'}(\mathbf{r}')\rho_{\sigma'}((\mathbf{r})r'')}{|\mathbf{r}'-\mathbf{r}''|}\frac{\delta g_{\sigma'\sigma''}[\rho](\mathbf{r}',\mathbf{r}'')}{\delta\rho_\sigma(\mathbf{r})}. \tag{187}$$

As the xc-energy may be written as

$$E_{\rm xc}[\rho] = \frac{1}{2}\sum_{\sigma}\int d^3r\ \rho_\sigma(\mathbf{r})V_{{\rm xc}\sigma}^{\rm scr}(\mathbf{r}) \tag{188}$$

it is obvious that the discontinuity of the xc-potential will only show up in the screening response potential and not in the screening potential, as the xc-energy itself must be continuous as a function of particle number.

In the x-only limit, the pair-correlation function is given by

$$g_{\mathrm{x}\,\sigma\sigma'}[\rho](\mathbf{r},\mathbf{r}') = \left(1 - \frac{\sum_{i,j=1}^{N_\sigma} \omega_{i\sigma}\omega_{j\sigma}\varphi_{i\sigma}(\mathbf{r})\varphi^*_{i\sigma}(\mathbf{r}')\varphi_{j\sigma}(\mathbf{r}')\varphi^*_{j\sigma}(\mathbf{r})}{\rho_\sigma(\mathbf{r})\rho_\sigma(\mathbf{r}')}\right)\delta_{\sigma\sigma'} \tag{189}$$

where $\omega_{i\sigma}$ denotes the possibly fractional occupation number of the orbital $i\sigma$. Substitution into (186) gives for the exchange part of the screening potential

$$V^{\mathrm{scr}}_{\mathrm{x}\sigma}(\mathbf{r}) = \frac{1}{\rho_\sigma(\mathbf{r})}\sum_{i=1}^{N_\sigma} u_{\mathrm{x}i\sigma}(\mathbf{r})|\varphi_{i\sigma}(\mathbf{r})|^2 \tag{190}$$

which is responsible for the $1/r$ behavior of $V_{\mathrm{x}\sigma}$ for large r. By comparison with the exact potential in the form of Eq. (70) the exchange part of the screening response potential is identified as

$$V^{\mathrm{resp}}_{\mathrm{x}\sigma}(\mathbf{r}) = \frac{1}{\rho_\sigma(\mathbf{r})}\sum_{i=1}^{N_\sigma}\left[\left(\bar{V}_{\mathrm{x}i\sigma} - \bar{u}_{\mathrm{x}i\sigma}\right)|\varphi_{i\sigma}(\mathbf{r})|^2 + \nabla\left(\psi_{i\sigma}(\mathbf{r})\nabla\varphi_{i\sigma}(\mathbf{r})\right)\right]. \tag{191}$$

The last term in the above expression is the one omitted in KLI approximation and therefore known to be small. The first term, on the other hand, shows a clear step structure. It is almost constant within the atomic shells where the orbitals vary little and changes rapidly

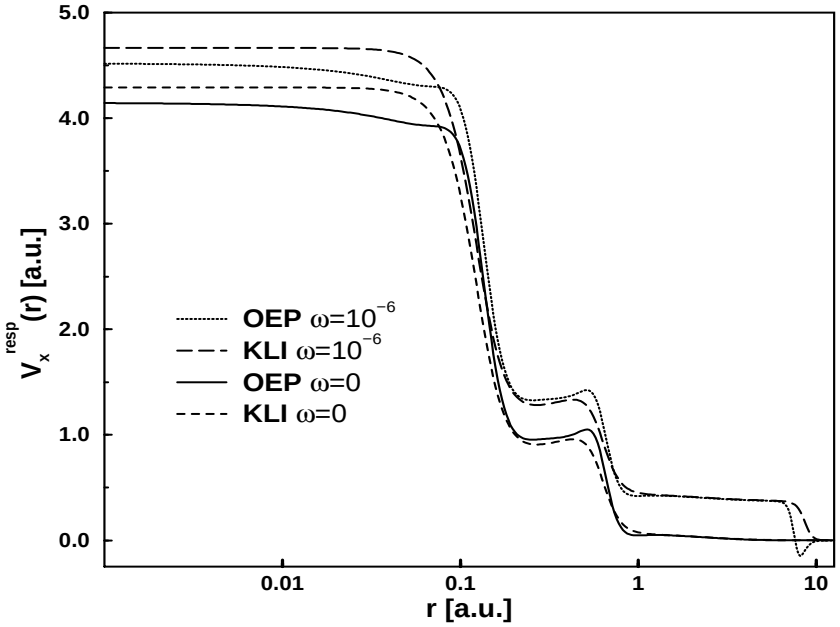

Figure 2: *Derivative discontinuities in the screening response potential* $V^{\mathrm{resp}}_{\mathrm{x}\uparrow}(\mathbf{r})$ *for* Ca^+ *for* $N_\uparrow = 9 + \omega$ *electrons from the x-only OEP and KLI method.*

at the atomic shell boundaries, where the orbitals decay. This is clearly visible in Figure 1 where the screening and screening-response potentials from the OEP and KLI method are plotted for the Calcium atom. The step structure, first discovered by van Leeuwen et. al. [56], is responsible for the discontinuity of the total exchange potential as a function of particle number. As the particle number changes through an integer N to $N+\omega$ with $\omega << 1$ and a new outer shell is started to be filled, a new step is added to $V_{\mathrm{x}\sigma}^{\mathrm{resp}}(\mathbf{r})$, shifting the total potential by a constant, i.e. by Δ_{x}. In Figure 2 this discontinuity is plotted for the Calcium ion. Clearly, the OEP and KLI methods give very similar results. This constant shift has no effect on the KS orbitals in the limit of vanishing ω as the KS equation (33) is invariant under additive constants to the KS potential. This is consistent with the fact that the density, being just the sum of the absolute squares of the occupied orbitals, is a continuous function of the particle number.

2.4 Hartree-Fock versus x-only OEP, a comparison

In this section we compare the x-only OEP scheme with the Hartree-Fock (HF) method. Both approaches are based on the same total-energy functional:

$$\begin{aligned} E_{\mathrm{tot}}\left[\{\varphi_{j\tau}\}\right] &= \sum_{\sigma=\uparrow,\downarrow}\sum_{i=1}^{N_\sigma}\int d^3r\;\varphi_{i\sigma}^*(\mathbf{r})\left(-\frac{1}{2}\nabla^2\right)\varphi_{i\sigma}(\mathbf{r}) \\ &\quad + \int d^3r\; v_{\mathrm{ext}}(\mathbf{r})\rho(\mathbf{r}) + \frac{1}{2}\int d^3r\int d^3r'\;\frac{\rho(\mathbf{r})\rho(\mathbf{r}')}{|\mathbf{r}-\mathbf{r}'|} \\ &\quad - \frac{1}{2}\sum_{\sigma=\uparrow,\downarrow}\int d^3r\int d^3r'\;\frac{\rho_\sigma(\mathbf{r},\mathbf{r}')\rho_\sigma(\mathbf{r}',\mathbf{r})}{|\mathbf{r}-\mathbf{r}'|} \end{aligned} \tag{192}$$

where

$$\rho_\sigma(\mathbf{r},\mathbf{r}') = \sum_{i=1}^{N_\sigma}\varphi_{i\sigma}^*(\mathbf{r}')\varphi_{i\sigma}(\mathbf{r})\;. \tag{193}$$

In HF, this total energy functional is minimized without restriction (except for orthonormality of the orbitals), leading to the variational equation

$$\left(-\frac{\nabla^2}{2} + v_{\mathrm{ext}}(\mathbf{r}) + \int d^3r\,\frac{\rho(\mathbf{r}')}{|\mathbf{r}-\mathbf{r}'|}\right)\varphi_{i\sigma}^{\mathrm{HF}}(\mathbf{r}) - \int d^3r'\;\frac{\rho_\sigma^{\mathrm{HF}}(\mathbf{r},\mathbf{r}')}{|\mathbf{r}-\mathbf{r}'|}\varphi_{i\sigma}^{\mathrm{HF}}(\mathbf{r}') = \varepsilon_{i\sigma}^{\mathrm{HF}}\varphi_{i\sigma}^{\mathrm{HF}}(\mathbf{r})\,. \tag{194}$$

This single-particle Schrödinger equation features a non-local effective potential. By contrast, in the OEP method the total-energy functional (192) is minimized under the subsidiary condition that the orbitals come from a *local* potential, i.e.,

$$\left(-\frac{\nabla^2}{2} + v_{\mathrm{ext}}(\mathbf{r}) + \int d^3r\,\frac{\rho(\mathbf{r}')}{|\mathbf{r}-\mathbf{r}'|} + V_{\mathrm{x}\sigma}^{\mathrm{OEP}}(\mathbf{r})\right)\varphi_{i\sigma}^{\mathrm{KS}}(\mathbf{r}) = \varepsilon_{i\sigma}^{\mathrm{KS}}\varphi_{i\sigma}^{\mathrm{KS}}(\mathbf{r})\;, \tag{195}$$

where $V_{\mathrm{x}\sigma}^{\mathrm{OEP}}(\mathbf{r})$ is determined by the integral equation (82). Since the self-consistent HF solutions of Eq. (194) yield the lowest possible value of (192) the energy obtained from the self-consistent OEP scheme is necessarily higher:

$$E_{\mathrm{tot}}^{\mathrm{HF}} \le E_{\mathrm{tot}}^{\mathrm{OEP}}\;. \tag{196}$$

The difference between the two, however, turns out to be very small as we shall see in section 4.

A well-known consequence [48] of the non-locality of the HF potential is the fact that the *occupied* HF orbitals all have the *same* exponential decay:

$$\varphi_{i\sigma}^{\mathrm{HF}}(r) \stackrel{r\to\infty}{\longrightarrow} \mathrm{e}^{-\beta_{N_\sigma\sigma} r} \qquad \text{for all } i \leq N_\sigma \,. \tag{197}$$

The orbitals resulting form the OEP, on the other hand, fall off each with its own orbital energy

$$\varphi_{i\sigma}^{\mathrm{KS}}(r) \stackrel{r\to\infty}{\longrightarrow} \mathrm{e}^{-\beta_{i\sigma} r} \qquad \text{for all } i \,. \tag{198}$$

In HF, the effective potential acting on an unoccupied orbital $\varphi_{u\sigma}^{\mathrm{HF}}(\mathbf{r})$ falls off exponentially. This is most easily seen by rewriting the exchange term as

$$\begin{aligned} \left(\hat{v}_{\mathrm{x}\sigma}^{\mathrm{HF}} \varphi_{u\sigma}^{\mathrm{HF}}\right)(\mathbf{r}) &= -\int d^3r' \, \frac{\rho_\sigma^{\mathrm{HF}}(\mathbf{r},\mathbf{r}')}{|\mathbf{r}-\mathbf{r}'|} \varphi_{u\sigma}^{\mathrm{HF}}(\mathbf{r}') \\ &= \left\{ -\sum_{i=1}^{N_\sigma} \frac{\varphi_{i\sigma}^{\mathrm{HF}}(\mathbf{r})}{\varphi_{u\sigma}^{\mathrm{HF}}(\mathbf{r})} K_{iu\sigma}^{\mathrm{HF}}(\mathbf{r}) \right\} \varphi_{u\sigma}^{\mathrm{HF}}(\mathbf{r}) \end{aligned} \tag{199}$$

where

$$K_{iu\sigma}^{\mathrm{HF}}(\mathbf{r}) = \int d^3r' \, \frac{\varphi_{i\sigma}^{*\mathrm{HF}}(\mathbf{r}') \varphi_{u\sigma}^{\mathrm{HF}}(\mathbf{r}')}{|\mathbf{r}-\mathbf{r}'|} \,. \tag{200}$$

The term in curly brackets can be interpreted as a local exchange potential (which depends on the orbital it acts on). Since $K_{iu\sigma}^{\mathrm{HF}}$ falls off with a power law (cf. Eq. (121)) the local exchange potential in curly brackets falls off exponentionally if $\varphi_{u\sigma}^{\mathrm{HF}}(\mathbf{r})$ is a virtual orbital, and hence the total HF potential falls off exponentially as well. As a consequence the HF potential can support very few (if any) unoccupied bound states which are a very poor starting point if used as a lowest-order approximation for excited states. By contrast, the x-only OEP falls off as $-1/r$ (cf. Eq. (146)) for *all* orbitals, including the unoccupied ones. In recent calculations of excitation energies, the unoccupied OEP eigenvalues were found to be an excellent starting point [25, 26, 27, 57, 58]. Likewise, the band gap of semiconductors and insulators is much too large in HF while the x-only OEP yields band gaps rather close to experiment (see also section 4.4).

3 Relativistic generalization of the OEP and KLI methods

In the previous section the use of orbital-dependent xc-functionals was discussed within the context of nonrelativistic DFT. Relativistic effects were completely neglected. However, if heavier elements come into play, relativistic contributions become more and more important: For example, the ground-state energies of high-Z atoms or the bond lengths of molecules are changed considerably [59]. Also, the importance of relativistic effects in solids was recognized long ago [60].

In this section, we present the generalization of the OEP and KLI methods to the realm of relativistic systems. Before doing so, we first briefly outline the fundamental ideas of relativistic DFT (RDFT).

Similar to non-relativistic DFT, a HK theorem can be proven which can be summarized as follows [61]: The renormalized ground-state four current $j^\nu(\mathbf{r})$ of an interacting system of Dirac particles uniquely determines – up to within a gauge transformation – the external static four potential $A_{\mathrm{ext}}^\mu[j^\nu]$ as well as the ground-state wave function $\Psi[j^\nu]$. As

a consequence, any observable of the relativistic many-body system under consideration is a unique functional of the ground-state four current. (For a more detailed discussion of RDFT, also including questions of renormalization, the reader is referred to recent reviews [62, 63].) As usual, the exact four current of the interacting system can in principle be obtained from an auxiliary non-interacting system – the relativistic Kohn-Sham (RKS) system [62, 64, 65, 66]:

$$j^\nu(\mathbf{r}) = \sum_{-c^2<\varepsilon_k\leq\varepsilon_N} \bar{\varphi}_k(\mathbf{r})\gamma^\nu\varphi_k(\mathbf{r}) \tag{201}$$

Here and in the following, we assume that vacuum contributions can be neglected. This means that we restrict ourselves to the calculation of relativistic effects and ignore radiative corrections. Since we aim at electronic structure calculations for atoms, molecules and solids, the neglected terms are expected to be small.

The four-component spinors $\varphi_k(\mathbf{r})$ are obtained from the single-particle Dirac equation

$$\gamma_0\left(-ic\boldsymbol{\gamma}\cdot\nabla + c^2 + \gamma_\mu A_S^\mu[j^\nu](\mathbf{r})\right)\varphi_k(\mathbf{r}) = \varepsilon_k\varphi_k(\mathbf{r}) \tag{202}$$

(for notational and metric conventions cf. [67]). The local effective potential $A_S^\mu[j^\nu](\mathbf{r})$ is given by

$$A_S^\mu[j^\nu](\mathbf{r}) = A_0^\mu(\mathbf{r}) + \int d^3r' \frac{j^\mu(\mathbf{r}')}{|\mathbf{r}-\mathbf{r}'|} + A_{\rm xc}^\mu[j^\nu](\mathbf{r})\,, \tag{203}$$

where the first term is the static external potential, for example the potential of the nuclei assumed at rest. The second term represents the Hartree potential, whereas the last term denotes the xc four potential defined by

$$A_{\rm xc}^\mu[j^\nu](\mathbf{r}) := \frac{\delta E_{\rm xc}[j^\nu]}{\delta j_\mu(\mathbf{r})}\,, \tag{204}$$

with the relativistic xc energy functional $E_{\rm xc}[j^\nu]$ now being a functional of the four current j^ν. Eqs. (201)-(204) represent the relativistic KS (RKS) scheme which has to be solved self-consistently.

3.1 Relativistic optimized effective potential method

Similar to the nonrelativistic case, the HK theorem, applied to the non-interacting system, guarantees that the RKS spinors are unique functionals of the ground state four current. Therefore, every relativistic xc functional

$$E_{\rm xc} = E_{\rm xc}[\{\varphi_j\}] \tag{205}$$

depending *explicitly* on the set of single-particle spinors $\{\varphi_j\}$ is an *implicit* functional of j^ν. To calculate the corresponding xc four potential $A_{\rm xc}^\mu(\mathbf{r})$, one has to resort to the optimized potential method, now generalized to the realm of relativistic systems subject to static but otherwise arbitrary external four potentials [68].

The relativistic OEP (ROEP) integral equation can be derived in close analogy to its nonrelativistic counterpart: We again start out from the very definition of the xc four potential, Eq. (204). By applying the chain rule for functional derivatives, one obtains

$$A_{\mathrm{xc}\mu}^{\mathrm{ROEP}}(\mathbf{r}) = \frac{\delta E_{\mathrm{xc}}^{\mathrm{ROEP}}[\{\varphi_j\}]}{\delta j^{\mu}(\mathbf{r})}$$
$$= \sum_{-c^2<\varepsilon_k\leq\varepsilon_N} \int d^3r' \int d^3r'' \left(\frac{\delta E_{\mathrm{xc}}^{\mathrm{ROEP}}[\{\varphi_j\}]}{\delta\varphi_k(\mathbf{r}')} \frac{\delta\varphi_k(\mathbf{r}')}{\delta A_{S\nu}(\mathbf{r}'')} + \mathrm{c.c.} \right) \frac{\delta A_{S\nu}(\mathbf{r}'')}{\delta j^{\mu}(\mathbf{r})} \quad (206)$$

As in the non-relativistic expression (41), the first functional derivative is readily calculated once an approximation for $E_{\mathrm{xc}}[\{\varphi_j\}]$ is given. The last functional derivative in Eq. (206) is identified with the inverse of the static response function of a system of non-interacting Dirac particles, defined as

$$\chi_S^{\mu\nu}(\mathbf{r},\mathbf{r}') := \frac{\delta j^{\mu}(\mathbf{r})}{\delta A_{S\nu}(\mathbf{r}')} \quad (207)$$

such that Eq. (206) can be rewritten as

$$A_{\mathrm{xc}\mu}^{\mathrm{ROEP}}(\mathbf{r}) = \sum_{-c^2<\varepsilon_k\leq\varepsilon_N} \int d^3r' \int d^3r'' \left(\frac{\delta E_{\mathrm{xc}}^{\mathrm{ROEP}}[\{\varphi_j\}]}{\delta\varphi_k(\mathbf{r}')} \frac{\delta\varphi_k(\mathbf{r}')}{\delta A_{S\nu}(\mathbf{r}'')} + \mathrm{c.c.} \right) \chi_{S\nu\mu}^{-1}(\mathbf{r}'',\mathbf{r}) \,. \quad (208)$$

Acting with the response operator (207) on both sides of Eq. (208) and using the identity

$$\int d^3r \; \chi_{S\nu\mu}^{-1}(\mathbf{r}'',\mathbf{r}) \; \chi_S^{\mu\sigma}(\mathbf{r},\mathbf{r}') = \delta_{\nu}^{\;\sigma} \; \delta(\mathbf{r}''-\mathbf{r}') \quad (209)$$

leads (after rearranging the indices) to

$$\int d^3r' \, A_{\mathrm{xc}\nu}^{\mathrm{ROEP}}(\mathbf{r}') \, \chi_S^{\nu\mu}(\mathbf{r}',\mathbf{r}) = \sum_{-c^2<\varepsilon_k\leq\varepsilon_N} \int d^3r' \, \frac{\delta E_{\mathrm{xc}}^{\mathrm{ROEP}}[\{\varphi_j\}]}{\delta\varphi_k(\mathbf{r}')} \frac{\delta\varphi_k(\mathbf{r}')}{\delta A_{S\mu}(\mathbf{r})} + \mathrm{c.c.} \quad (210)$$

The remaining functional derivative $\delta\varphi_k/\delta A_{S\nu}$ can be calculated by using first-order perturbation theory, yielding

$$\frac{\delta\varphi_k(\mathbf{r}')}{\delta A_{S\mu}(\mathbf{r})} = \sum_{\substack{\varepsilon_l \\ l\neq k}} \frac{\varphi_l(\mathbf{r}')}{\varepsilon_k-\varepsilon_l} \bar{\varphi}_l(\mathbf{r})\gamma^{\mu}\varphi_k(\mathbf{r}) \,. \quad (211)$$

Once again, this expression can be used to express the response function

$$\chi_S^{\mu\nu}(\mathbf{r},\mathbf{r}') := \frac{\delta}{\delta A_{S\nu}(\mathbf{r}')} \left(\sum_{-c^2<\varepsilon_k\leq\varepsilon_N} \bar{\varphi}_k(\mathbf{r})\gamma^{\mu}\varphi_k(\mathbf{r}) \right) \quad (212)$$

in terms of the RKS spinors:

$$\chi_S^{\mu\nu}(\mathbf{r}',\mathbf{r}) = \sum_{-c^2<\varepsilon_k\leq\varepsilon_N} \sum_{\substack{\varepsilon_l \\ l\neq k}} \frac{\bar{\varphi}_k(\mathbf{r}')\gamma^{\mu}\varphi_l(\mathbf{r}') \; \bar{\varphi}_l(\mathbf{r})\gamma^{\nu}\varphi_k(\mathbf{r})}{\varepsilon_k-\varepsilon_l} + \mathrm{c.c.} \quad (213)$$

Finally, putting Eqs. (210), (211) and (213) together leads to the relativistic generalization of the OEP integral equation:

$$\sum_{-c^2<\varepsilon_k\leq\varepsilon_N} \int d^3r' \left(\bar{\varphi}_k(\mathbf{r}')\gamma^{\nu} A_{\mathrm{xc}\nu}^{\mathrm{ROEP}}(\mathbf{r}') - \frac{\delta E_{\mathrm{xc}}^{\mathrm{ROEP}}[\{\varphi_j\}]}{\delta\varphi_k(\mathbf{r}')} \right) G_{Sk}(\mathbf{r}',\mathbf{r}) \, \gamma^0\gamma^{\mu}\varphi_k(\mathbf{r}) + \mathrm{c.c.} = 0$$
$$\mu = 0,1,2,3 \quad (214)$$

where

$$G_{Sk}(\mathbf{r}',\mathbf{r}) := \sum_{\substack{\varepsilon_l \\ l\neq k}} \frac{\varphi_l(\mathbf{r}')\varphi_l^\dagger(\mathbf{r})}{\varepsilon_k - \varepsilon_l} \,. \tag{215}$$

These four integral equations determine the local xc four potential $A^\mu_{\rm xc}(\mathbf{r})$ – up to an arbitrary constant which can be specified by requiring $A^{\rm ROEP}_{{\rm xc}\mu}(\mathbf{r})$ to vanish asymptotically (for finite systems) – and have to be solved self-consistently with the RKS equation (202).

3.2 Relativistic KLI approximation

In close analogy to the nonrelativistic situation, one has to deal with the ROEP integral equations numerically. Owing to the four-component structure of Eq. (214) and to the fact that four integral equations have to be solved, considerably more effort is needed to determine the xc four potential $A^\mu_{\rm xc}(\mathbf{r})$ as compared to the nonrelativistic case. Therefore, a simplified scheme for the calculation of $A^\mu_{\rm xc}(\mathbf{r})$, leading to the relativistic generalization of the KLI approximation discussed in section 2.2, is presented in the following [68].

By defining

$$\psi_k^\dagger(\mathbf{r}) := \int d^3r' \left(\bar\varphi_k(\mathbf{r}')\gamma^\nu A^{\rm ROEP}_{{\rm xc}\nu}(\mathbf{r}') - \frac{\delta E^{\rm ROEP}_{\rm xc}}{\delta\varphi_k(\mathbf{r}')} \right) G_{Sk}(\mathbf{r}',\mathbf{r}) \tag{216}$$

one can rewrite the ROEP integral equation as

$$\sum_{-c^2<\varepsilon_k\leq\varepsilon_N} \bar\psi_k(\mathbf{r})\gamma^\mu\varphi_k(\mathbf{r}) + \text{c.c.} = 0 \,, \tag{217}$$

where the adjoint spinor $\bar\psi_k(\mathbf{r})$ is defined in the usual way, i.e.

$$\bar\psi_k(\mathbf{r}) := \psi_k^\dagger(\mathbf{r})\gamma^0 \,. \tag{218}$$

The quantity $\psi_k^\dagger(\mathbf{r})$, although being a four-component object, closely resembles its namesake introduced in Eq. (54): One readily proves the orthogonality relation

$$\int d^3r\, \psi_k^\dagger(\mathbf{r})\varphi_k(\mathbf{r}) = 0 \,. \tag{219}$$

Furthermore, its physical interpretation discussed in section 2.2 remains valid in the relativistic domain. Again, a differential equation that uniquely determines $\psi_k^\dagger(\mathbf{r})$ can be derived again. To demonstrate this, we use the defining property of $G_{Sk}(\mathbf{r}',\mathbf{r})$

$$G_{Sk}(\mathbf{r}',\mathbf{r}) \left(\hat h_{\rm D}^\dagger - \varepsilon_k \right) = - \left(\delta(\mathbf{r}'-\mathbf{r}) - \varphi_k(\mathbf{r}')\varphi_k^\dagger(\mathbf{r}) \right) \tag{220}$$

where the operator $\hat h_{\rm D}^\dagger$ denotes the hermitian conjugate of the RKS Hamiltonian, i.e.

$$\hat h_{\rm D}^\dagger := \gamma^0 \left(ic\boldsymbol{\gamma}\cdot \overleftarrow{\nabla} + c^2 + \gamma^\nu A_{S\nu}(\mathbf{r}) \right) \,, \tag{221}$$

acting from the right on the unprimed variable of $G_{Sk}(\mathbf{r}',\mathbf{r})$ (the arrow on top of the gradient indicates the direction in which the derivative has to be taken). Using Eq. (220),

we can act with the operator $(\hat{h}_{\rm D}^{\dagger} - \varepsilon_k)$ on Eq. (216), leading to the differential equation determining $\psi_k^{\dagger}(\mathbf{r})$:

$$\begin{aligned}
&\psi_k^{\dagger}(\mathbf{r}) \left(\hat{h}_{\rm D}^{\dagger} - \varepsilon_k\right) \\
&= -\int d^3r' \left(\bar{\varphi}_k(\mathbf{r}')\gamma_\nu A_{\rm xc}^{\nu}(\mathbf{r}') - \frac{\delta E_{\rm xc}^{\rm ROEP}}{\delta\varphi_k(\mathbf{r}')}\right) G_{Sk}(\mathbf{r}',\mathbf{r}) \left(\hat{h}_{\rm D}^{\dagger} - \varepsilon_k\right) \\
&= -\left(\bar{\varphi}_k(\mathbf{r})\gamma_\nu A_{\rm xc}^{\nu}(\mathbf{r}) - \frac{\delta E_{\rm xc}^{\rm ROEP}}{\delta\varphi_k(\mathbf{r})}\right) + \left(\bar{A}_{{\rm xc}k}^{\rm ROEP} - \bar{u}_{{\rm xc}k}\right)\varphi_k^{\dagger}(\mathbf{r})\,, \qquad (222)
\end{aligned}$$

with the constants $\bar{A}_{{\rm xc}k}^{\rm ROEP}$ and $\bar{u}_{{\rm xc}k}$ introduced in accordance to Eq. (60), i.e.

$$\bar{A}_{{\rm xc}k}^{\rm ROEP} := \int d^3r\, \bar{\varphi}_k(\mathbf{r})\gamma^\nu A_{{\rm xc}\nu}^{\rm ROEP}(\mathbf{r})\varphi_k(\mathbf{r}) \qquad (223)$$

and

$$\bar{u}_{{\rm xc}k} := \int d^3r\, \frac{\delta E_{\rm xc}^{\rm ROEP}}{\delta\varphi_k(\mathbf{r}')}\varphi_k(\mathbf{r})\,. \qquad (224)$$

Eq. (222) can now be used to further transform the ROEP integral equation (217). We therefore multiply Eq. (217) by $A_S^0(\mathbf{r})$:

$$\sum_{-c^2<\varepsilon_k\le\varepsilon_N} A_S^0(\mathbf{r})\bar{\psi}_k(\mathbf{r})\gamma^\mu\varphi_k(\mathbf{r}) + \text{c.c.} = 0 \qquad (225)$$

and employ Eq. (222), solved for $A_S^0(\mathbf{r})\psi_k^{\dagger}(\mathbf{r})$, to obtain

$$\begin{aligned}
\sum_{-c^2<\varepsilon_k\le\varepsilon_N} &\left(\bar{\varphi}_k(\mathbf{r})\gamma^\nu A_{{\rm xc}\nu}^{\rm ROEP}(\mathbf{r}) - \frac{\delta E_{\rm xc}^{\rm ROEP}}{\delta\varphi_k(\mathbf{r})} - \left(\bar{A}_{{\rm xc}k}^{\rm ROEP} - \bar{u}_{{\rm xc}k}\right)\varphi_k^{\dagger}(\mathbf{r})\right. \\
&\left. + \bar{\psi}_k(\mathbf{r})\left(ic\boldsymbol{\gamma}\cdot\overleftarrow{\nabla} + c^2 - \boldsymbol{\gamma}\cdot\mathbf{A}_S(\mathbf{r}) - \gamma^0\varepsilon_k\right)\right)\gamma^0\gamma^\mu\varphi_k(\mathbf{r}) + \text{c.c.} = 0\,. \qquad (226)
\end{aligned}$$

Defining the 4x4-matrix

$$\mathcal{J}^{\mu\nu}(\mathbf{r}) := \frac{1}{2}\sum_{-c^2<\varepsilon_k\le\varepsilon_N}\left(\bar{\varphi}_k(\mathbf{r})\gamma^\nu\gamma^0\gamma^\mu\varphi_k(\mathbf{r}) + \text{c.c.}\right) \qquad (227)$$

we rewrite Eq. (226) as

$$\mathcal{J}^{\mu\nu}(\mathbf{r})A_{{\rm xc}\nu}^{\rm ROEP}(\mathbf{r}) = \frac{1}{2}\sum_{-c^2<\varepsilon_k\le\varepsilon_N}\left(a_{{\rm xc}k}^{\mu}(\mathbf{r}) + \bar{\varphi}_k(\mathbf{r})\gamma^\mu\varphi_k(\mathbf{r})\left(\bar{A}_{{\rm xc}k}^{\rm ROEP} - \bar{u}_{{\rm xc}k}\right)\right) + \text{c.c.}\,, \qquad (228)$$

where $a_{{\rm xc}k}^{\mu}(\mathbf{r})$ is a shorthand notation for

$$a_{{\rm xc}k}^{\mu}(\mathbf{r}) := \frac{\delta E_{\rm xc}^{\rm ROEP}}{\delta\varphi_k(\mathbf{r})}\gamma^0\gamma^\mu\varphi_k(\mathbf{r}) - \bar{\psi}_k(\mathbf{r})\left(ic\boldsymbol{\gamma}\cdot\overleftarrow{\nabla} + c^2 - \boldsymbol{\gamma}\cdot\mathbf{A}_S(\mathbf{r}) - \gamma^0\varepsilon_k\right)\gamma^0\gamma^\mu\varphi_k(\mathbf{r}) \qquad (229)$$

In order to solve Eq. (228) for $A_{{\rm xc}\mu}^{\rm ROEP}(\mathbf{r})$, we first have to demonstrate that the 4x4-matrix $\mathcal{J}(\mathbf{r})$ defined by Eq. (227) is nonsingular, i.e. that the inverse $\mathcal{J}^{-1}(\mathbf{r})$ exists. Using the commutator algebra of the γ-matrices

$$\{\gamma^\nu,\gamma^\mu\} = 2\,g^{\nu\mu}\,, \qquad (230)$$

where $g^{\nu\mu}$ denotes the metric tensor and the fact that the hermitian conjugate of γ^ν is given by

$$\gamma^{\nu^\dagger} = \gamma^0 \gamma^\nu \gamma^0 \,, \tag{231}$$

$\mathcal{J}^{\mu\nu}(\mathbf{r})$ can be rewritten as

$$\mathcal{J}^{\mu\nu}(\mathbf{r}) = j^\mu(\mathbf{r})\, g^{\nu 0} - j^0(\mathbf{r})\, g^{\nu\mu} + j^\nu(\mathbf{r})\, g^{\mu 0} \,. \tag{232}$$

From this equation the determinant of $\mathcal{J}(\mathbf{r})$ is easily calculated:

$$\det\,(\mathcal{J}(\mathbf{r})) = \begin{vmatrix} j^0(\mathbf{r}) & j^1(\mathbf{r}) & j^2(\mathbf{r}) & j^3(\mathbf{r}) \\ j^1(\mathbf{r}) & j^0(\mathbf{r}) & & \\ j^2(\mathbf{r}) & & j^0(\mathbf{r}) & \\ j^3(\mathbf{r}) & & & j^0(\mathbf{r}) \end{vmatrix} = \rho^4(\mathbf{r}) \left(1 - \frac{\mathbf{j}^2(\mathbf{r})}{c^2 \rho^2(\mathbf{r})} \right) \tag{233}$$

where, in the last step, the four current was decomposed into the density and the spatial component of the current according to

$$j^\mu(\mathbf{r}) = \left(\rho(\mathbf{r}), \frac{1}{c}\mathbf{j}(\mathbf{r}) \right) \,. \tag{234}$$

Since $\rho(\mathbf{r}) > 0$ and $\mathbf{j}(\mathbf{r})/c\rho(\mathbf{r})$ represent the velocity field $v(\mathbf{r}) < 1$ of the system, one obtains

$$\det\,(\mathcal{J}(\mathbf{r})) > 0 \tag{235}$$

proving that the inverse $\mathcal{J}^{-1}(\mathbf{r})$ exists.

Therefore, Eq. (228) can be solved for the xc four potential:

$$A^{\mathrm{ROEP}}_{\mathrm{xc}\mu}(\mathbf{r}) = \frac{1}{2}\, \mathcal{J}^{-1}_{\mu\nu}(\mathbf{r}) \sum_{-c^2 < \varepsilon_k \leq \varepsilon_N} \left(a^\nu_{\mathrm{xc}k}(\mathbf{r}) + \bar{\varphi}_k(\mathbf{r}) \gamma^\nu \varphi_k(\mathbf{r}) \left(\bar{A}^{\mathrm{ROEP}}_{\mathrm{xc}k} - \bar{u}_{\mathrm{xc}k} \right) \right) + \mathrm{c.c.} \tag{236}$$

This equation represents an exact transformation of the ROEP integral equation (214). In particular, due to the appearance of the quantity $\psi^\dagger_k(\mathbf{r})$ in $a^\nu_{\mathrm{xc}k}(\mathbf{r})$, Eq. (236) is still an integral equation. Similar to its nonrelativistic counterpart, Eq. (70), a simple approximation is obtained by completely neglecting all terms involving $\psi^\dagger_k(\mathbf{r})$ in Eq. (229). The resulting equation representing the relativistic generalization of the KLI approximation is then given by

$$A^{\mathrm{RKLI}}_{\mathrm{xc}\mu}(\mathbf{r}) = \frac{1}{2}\, \mathcal{J}^{-1}_{\mu\nu}(\mathbf{r}) \sum_{-c^2 < \varepsilon_k \leq \varepsilon_N} \left(\frac{\delta E^{\mathrm{ROEP}}_{\mathrm{xc}}}{\delta \varphi_k(\mathbf{r})} \gamma^0 \gamma^\nu \varphi_k(\mathbf{r}) + j^\nu_k(\mathbf{r}) \left(\bar{A}^{\mathrm{RKLI}}_{\mathrm{xc}k} - \bar{u}_{\mathrm{xc}k} \right) \right) + \mathrm{c.c.} \tag{237}$$

where the orbital current is defined as

$$j^\nu_k(\mathbf{r}) := \bar{\varphi}_k(\mathbf{r})\, \gamma^\nu\, \varphi_k(\mathbf{r}) \tag{238}$$

Although still being an integral equation, this RKLI equation can be solved explicitly in terms of the RKS spinors. This can be seen by multiplying Eq. (237) by $j^\mu_l(\mathbf{r})$, summing over all μ and integrating over space, yielding

$$\bar{A}^{\mathrm{RKLI}}_{\mathrm{xc}l} = \bar{A}^S_{\mathrm{xc}l} + \sum_{-c^2 < \varepsilon_k \leq \varepsilon_N} M_{lk} \left(\bar{A}^{\mathrm{RKLI}}_{\mathrm{xc}k} - \frac{1}{2} \left(\bar{u}_{\mathrm{xc}k} - \bar{u}^*_{\mathrm{xc}k} \right) \right) \tag{239}$$

where

$$\bar{A}^S_{\mathrm{xc}l} := \frac{1}{2}\int d^3r\, j^\mu_l(\mathbf{r})\mathcal{J}^{-1}_{\mu\nu}(\mathbf{r}) \sum_{-c^2<\varepsilon_k\leq\varepsilon_N} \left(\frac{\delta E^{\mathrm{ROEP}}_{\mathrm{xc}}}{\delta\varphi_k(\mathbf{r})}\gamma^0\gamma^\nu\varphi_k(\mathbf{r}) + \mathrm{c.c.}\right) \tag{240}$$

and

$$M_{lk} := \int d^3r\, j^\mu_l(\mathbf{r})\mathcal{J}^{-1}_{\mu\nu}(\mathbf{r}) j^\nu_k(\mathbf{r})\,. \tag{241}$$

The unknown coefficients $(\bar{A}^{\mathrm{RKLI}}_{\mathrm{xc}k} - \frac{1}{2}(\bar{u}_{\mathrm{xc}k} - \bar{u}^*_{\mathrm{xc}k}))$ are then determined by the set of linear equations

$$\sum_{-c^2<\varepsilon_k\leq\varepsilon_N} \left(\frac{1}{2}\delta_{lk} - M_{lk}\right)\left(\bar{A}^{\mathrm{RKLI}}_{\mathrm{xc}k} - \frac{1}{2}(\bar{u}_{\mathrm{xc}k} - \bar{u}^*_{\mathrm{xc}k})\right) = \left(\bar{A}^S_{\mathrm{xc}l} - \frac{1}{2}(\bar{u}_{\mathrm{xc}l} - \bar{u}^*_{\mathrm{xc}l})\right) \tag{242}$$

Inserting the result in Eq. (237) we finally obtain an expression for the xc four potential $A^{\mathrm{RKLI}}_{\mathrm{xc}\mu}(\mathbf{r})$ that depends explicitly on the set of single-particle spinors $\{\varphi_j\}$.

3.3 Relativistic OEP in the electrostatic case

In the previous section, we discussed the extension of the OEP method to relativistic systems subject to static but otherwise arbitrary external fields. In particular, the ROEP method allows one to deal with external magnetic fields of arbitrary strength. In electronic structure calculations for atoms, molecules and solids, however, we most commonly encounter situations where no magnetic fields are present (in a suitable Lorentz frame, typically the rest frame of the nuclei). In this so-called "electrostatic case", the general approach presented above can be considerably simplified.

We consider the situation where the spatial components of the external four potential vanish, i.e. $\mathbf{A}_{\mathrm{ext}}(\mathbf{r}) = 0$. (This also includes a partial fixing of the gauge.) Then, one can derive a simplified Hohenberg-Kohn-Sham scheme [63, 64, 69] stating that the zeroth component $\rho(\mathbf{r}) = j^0(\mathbf{r})$ of the ground-state current density alone uniquely determines the scalar external potential $V = V[\rho]$ as well as the ground-state wave function $\Psi[\rho]$. Consequently, only the scalar effective potential $V_S(\mathbf{r})$, given by

$$V_S[\rho](\mathbf{r}) := V_{\mathrm{ext}}(\mathbf{r}) + \int d^3r\, \frac{\rho(\mathbf{r})}{|\mathbf{r}-\mathbf{r}'|} + V_{\mathrm{xc}}[\rho](\mathbf{r})\,, \tag{243}$$

with

$$V_{\mathrm{xc}}[\rho](\mathbf{r}) := \frac{\delta E_{\mathrm{xc}}[\rho]}{\delta\rho(\mathbf{r})}\,, \tag{244}$$

is present in the RKS equation (202). By applying the definition for $V_{\mathrm{xc}}(\mathbf{r})$ to the case of explicitly orbital-dependent xc functionals $E_{\mathrm{xc}}[\{\varphi_j[\rho]\}]$, we obtain the ROEP integral equation for the "electrostatic case":

$$\sum_{-c^2<\varepsilon_k\leq\varepsilon_N} \int d^3r' \left(\varphi^\dagger_k(\mathbf{r}')V^{\mathrm{ROEP}}_{\mathrm{xc}}(\mathbf{r}') - \frac{\delta E^{\mathrm{ROEP}}_{\mathrm{xc}}}{\delta\varphi_k(\mathbf{r}')}\right) G_{Sk}(\mathbf{r}',\mathbf{r})\,\varphi_k(\mathbf{r}) + \mathrm{c.c.} = 0\,. \tag{245}$$

Although this equation, first derived in the x-only limit by Shadwick, Talman and Norman [69], is considerably simpler than the ROEP integral equation (214), its numerical solution is still a very demanding task and has been achieved so far only for spherical atoms [63, 64, 69, 70].

In order to avoid a full numerical treatment of Eq. (245), one can again derive an RKLI approximation. Following the arguments in section 3.2, the RKLI equation for the "electrostatic case" is:

$$V_{\rm xc}^{\rm RKLI}(\mathbf{r}) = \frac{1}{2\rho(\mathbf{r})} \sum_{-c^2<\varepsilon_k\leq\varepsilon_N} \left(\frac{\delta E_{\rm xc}^{\rm ROEP}}{\delta\varphi_k(\mathbf{r})}\varphi_k(\mathbf{r}) + \rho_k(\mathbf{r}) \left(\bar{V}_{{\rm xc}k}^{\rm RKLI} - \bar{u}_{{\rm xc}k} \right) \right) + \text{c.c.}\,, \qquad (246)$$

with $\bar{V}_{{\rm xc}k}^{\rm RKLI}$ defined similar to Eq. (223). As in the nonrelativistic case, this equation can be understood as a mean-field-type approximation to the full ROEP integral equation (245) [68]. Furthermore, the RKLI equation (246) closely resembles its nonrelativistic counterpart, Eq. (76). In section 4.2, we will show that the RKLI approximation (246) is highly accurate when applied to the calculation of relativistic effects in high-Z atoms.

To conclude this section, we emphasize that the results of this section can *not* be obtained as a well-defined limit of the results of the sections 3.1 and 3.2 but must be derived separately within the framework of RDFT in the "electrostatic case" [63, 64]. This is because the basic variables of the underlying HK theorems are different: In the "electrostatic case", the density $\rho(\mathbf{r})$ alone is sufficient to determine all ground-state properties of the relativistic, interacting many-body system, whereas the four current $j^\mu(\mathbf{r})$ must be used when arbitrary external four potentials are considered. This does not mean that the spatial components $\mathbf{j}(\mathbf{r})$ of the four current vanish in this case; they are simply functionals $\mathbf{j}[\rho](\mathbf{r})$ of the density.

4 Numerical results

4.1 Exchange-only calculations for nonrelativistic systems

4.1.1 Atomic systems

The x-only limit of the xc energy functional is given by the exact Fock term, Eq. (27). As explained in the preceding section, the OEP method then provides the corresponding exchange potential $V_{\rm x}^{\rm exact}(\mathbf{r})$ and therefore represents the exact implementation of x-only DFT. Consequently it provides a benchmark for testing approximate exchange energy functionals employed within the Kohn-Sham scheme. In this section, we will review selected results of fully self-consistent x-only calculations performed with the OEP method and the KLI approximation to it [13, 14, 16, 17, 18, 19, 20, 21, 22, 33, 36, 37, 38, 42, 44, 52, 71, 72, 73, 74] as described in section 2. For comparison, we list the results from traditional KS calculations using the x-only LDA (xLDA), where the exchange energy is given by

$$E_{\rm x}^{\rm LDA}[\rho] = -\frac{3}{2}\left(\frac{3}{4\pi}\right)^{\frac{1}{3}} \sum_{\sigma=\uparrow,\downarrow} \int d^3r \rho_\sigma^{\frac{4}{3}}(\mathbf{r}), \qquad (247)$$

the generalized gradient approximation (GGA) due to Becke (B88) [75],

$$E_{\rm x}^{\rm B88}[\rho] = E_{\rm x}^{\rm LDA}[\rho] - \beta \sum_{\sigma=\uparrow,\downarrow} \int d^3r \rho_\sigma^{\frac{4}{3}}(\mathbf{r}) \frac{x_\sigma^2(\mathbf{r})}{\left(1 + 6\beta x_\sigma(\mathbf{r}) \sinh^{-1} x_\sigma(\mathbf{r})\right)} \qquad (248)$$

where

$$x_\sigma(\mathbf{r}) := \frac{|\nabla\rho_\sigma(\mathbf{r})|}{\rho_\sigma^{\frac{4}{3}}(\mathbf{r})} \qquad (249)$$

and $\beta = 0.0042$, and the GGA due to Perdew and Wang (xPW91) [76, 77, 78], which may be written as

$$E_{\rm x}^{\rm PW91}[\rho] = -\frac{3}{2}\left(\frac{3}{4\pi}\right)^{\frac{1}{3}} \sum_{\sigma=\uparrow,\downarrow} \int d^3r \rho_\sigma^{\frac{4}{3}}(\mathbf{r}) F\left(s_\sigma(\mathbf{r})\right) \tag{250}$$

with

$$F(s) = \frac{1 + 0.19645 s \sinh^{-1}(7.7956 s) + \left(0.2743 - 0.1508 \exp(-100 s^2)\right) s^2}{\left(1 + 0.19645 s \sinh^{-1}(7.7956 s) + 0.004 s^4\right)} \tag{251}$$

and

$$s_\sigma(\mathbf{r}) = \frac{|\nabla \rho_\sigma(\mathbf{r})|}{(6\pi^2)^{\frac{1}{3}} \rho_\sigma^{\frac{4}{3}}(\mathbf{r})}. \tag{252}$$

We will also give results obtained with the xLDA-SIC functional

$$\begin{aligned} E_{\rm x}^{\rm LDA-SIC}[\{\varphi_{j\sigma}\}] &= E_{\rm x}^{\rm LDA}[\rho_\uparrow, \rho\downarrow] - \sum_{\sigma=\uparrow,\downarrow} \sum_{i=1}^{N_\sigma} E_{\rm x}^{\rm LDA}[|\varphi_{i\sigma}|^2, 0] \\ &\quad -\frac{1}{2} \sum_{\sigma=\uparrow,\downarrow} \sum_{i=1}^{N_\sigma} \int d^3r \int d^3r' \, \frac{|\varphi_{i\sigma}(\mathbf{r})|^2 |\varphi_{i\sigma}(\mathbf{r}')|^2}{|\mathbf{r} - \mathbf{r}'|} \end{aligned} \tag{253}$$

$$\tag{254}$$

employed within the KLI scheme for comparison. We will refer to this method as xLDA-SICKLI, respectively. As it has been found [43] that the exact OEP for the xLDA-SIC functional yields results which differ only marginally from the ones obtained with the KLI approximation, we will not list them here. In addition, we include the results of spin-unrestricted HF (SUHF) calculations, taken from [15].

For the OEP, KLI, B88, PW91 and xLDA calculations we have used a numerical code which solves the radial part of the Schrödinger equation (33) on a logarithmic mesh by the Numerov method as described in [79]. For non-spherical open-shell systems angular averaging was used in order to calculate the density and the exchange energy according to the Fock expression (27), for the latter in the form suggested by Slater [80]. Therefore, an analytical treatment of the angular parts was possible for all systems. The SIC-LDA energy functional was evaluated using spherically averaged total and orbital densities, as it was found [43] that the use of the exact nonspherical densities results only in minor changes of a few tenths of a percent. The OEP integral equation (48) for the radial variable r,

$$\int_0^\infty dr' K_\sigma(r, r') V_{{\rm x}\sigma}(r') = I_\sigma(r) \tag{255}$$

with

$$K_\sigma(r, r') = \sum_{i=1}^{N_\sigma} \int \frac{r^2 d\Omega}{4\pi} \int r'^2 d\Omega' \; \varphi_{i\sigma}^*(\mathbf{r}') G_{{\rm s}i\sigma}(\mathbf{r}, \mathbf{r}') \varphi_{i\sigma}(\mathbf{r}) \tag{256}$$

and

$$I_\sigma(r) = \sum_{i=1}^{N_\sigma} \int \frac{r^2 d\Omega}{4\pi} \int r'^2 dr' d\Omega' \; \varphi_{i\sigma}^*(\mathbf{r}') u_{{\rm x}i\sigma}(\mathbf{r}') G_{{\rm s}i\sigma}(\mathbf{r}, \mathbf{r}') \varphi_{i\sigma}(\mathbf{r}) \tag{257}$$

was solved on the same mesh as the radial Schrödinger equation by numerical quadrature. The radial parts of the functions $G_{{\rm s}i\sigma}(\mathbf{r}, \mathbf{r}')$ were obtained from the radial parts of the

Table 1: *Absolute total ground-state energies for H through Ar calculated self-consistently employing various x-only approximations. SUHF results have been taken from [15]. All numbers in atomic units.*

	SUHF	OEP	KLI	B88	PW91	xLDA	xLDA-SICKLI
H	0.5000	0.5000	0.5000	0.4979	0.4953	0.4571	0.5000
He	2.8617	2.8617	2.8617	2.8634	2.8552	2.7236	2.8617
Li	7.4328	7.4325	7.4324	7.4288	7.4172	7.1934	7.4342
Be	14.5730	14.5724	14.5723	14.5664	14.5543	14.2233	14.5784
B	24.5293	24.5283	24.5281	24.5173	24.5035	24.0636	24.5490
C	37.6900	37.6889	37.6887	37.6819	37.6658	37.1119	37.7450
N	54.4046	54.4034	54.4030	54.4009	54.3824	53.7093	54.5064
O	74.8136	74.8121	74.8117	74.8148	74.7964	73.9919	74.9624
F	99.4108	99.4092	99.4087	99.4326	99.4130	98.4740	99.6351
Ne	128.5471	128.5454	128.5448	128.5901	128.5689	127.4907	128.8586
Na	161.8590	161.8566	161.8559	161.8834	161.8613	160.6443	162.2170
Mg	199.6146	199.6116	199.6107	199.6320	199.6120	198.2488	200.0273
Al	241.8768	241.8733	241.8723	241.8829	241.8617	240.3561	242.3409
Si	288.8545	288.8507	288.8495	288.8551	288.8320	287.1820	289.3775
P	340.7193	340.7150	340.7137	340.7107	340.6857	338.8885	341.2989
S	397.5063	397.5016	397.5002	397.4921	397.4665	395.5190	398.1483
Cl	459.4826	459.4776	459.4760	459.4697	459.4426	457.3435	460.1966
Ar	526.8175	526.8122	526.8105	526.7998	526.7710	524.5174	527.5994

orbitals $\varphi_{i\sigma}(\mathbf{r})$ and the corresponding complementary solutions of the radial part of the Schrödinger equation (33). A more detailed description may be found in [13, 72, 37].

In Tables 1, 2 and 3 we show the total ground-state energies obtained with the x-only DFT methods mentioned above and the SUHF scheme for neutral atoms with nuclear charge Z from 1 to 54. The OEP ground-state configurations used for the transition elements are listed in Table 4.

Comparing the first two columns of Tables 1, 2 and 3, it is evident that the SUHF and OEP results are very close to each other [9]. For some transition elements marked with an asterisk in Tables 2 and 3 the SUHF results have been obtained as expectation value of the Hamiltonian with respect to a linear combination of *two or more* Slater determinants in order to ensure a wave function exhibiting the appropriate symmetry, whereas the OEP and the other DFT calculations have been performed with a *single-determinant wave function.* This is the reason why for these systems the difference between the two values is larger. OEP and KLI results using more than a single Slater determinant have been performed by Li et. al. [15].

Table 2: *Absolute total ground-state energies for K through Kr calculated self-consistently employing various x-only approximations. For elements denoted with an asterisk the SUHF results have been obtained by using wave-functions consisting of more than one Slater determinant, whereas the DFT results are obtained with a single-determinant wave function. SUHF results have been taken from [15]. All numbers in atomic units.*

	SUHF	OEP	KLI	B88	xPW91	xLDA
K	599.1649	599.1591	599.1571	599.1483	599.1194	596.7115
Ca	676.7582	676.7519	676.7497	676.7529	676.7262	674.1601
Sc	759.7359	759.7277	759.7249	759.7567	759.7294	757.0083
Ti*	848.4066	848.3802	848.3772	848.4360	848.4078	845.5307
V*	942.8856	942.8569	942.8539	942.9369	942.9078	939.8733
Cr	1043.3568	1043.3457	1043.3422	1043.4917	1043.4564	1040.2732
Mn	1149.8698	1149.8600	1149.8569	1149.9671	1149.9360	1146.5831
Fe	1262.4500	1262.4380	1262.4344	1262.5851	1262.5543	1259.0385
Co*	1381.4186	1381.3818	1381.3781	1381.5710	1381.5400	1377.8606
Ni*	1506.8303	1506.8340	1506.8303	1507.0634	1507.0321	1503.1881
Cu	1638.9642	1638.9523	1638.9481	1639.2804	1639.2473	1635.2392
Zn	1777.8481	1777.8344	1777.8307	1778.1196	1778.0870	1773.9099
Ga	1923.2612	1923.2487	1923.2454	1923.4735	1923.4402	1919.0951
Ge	2075.3603	2075.3483	2075.3453	2075.5287	2075.4937	2070.9811
As	2234.2399	2234.2281	2234.2251	2234.3657	2234.3291	2229.6475
Se	2399.8691	2399.8573	2399.8543	2399.9654	2399.9289	2395.0759
Br	2572.4418	2572.4300	2572.4269	2572.5159	2572.4780	2567.4546
Kr	2752.0550	2752.0430	2752.0398	2752.1006	2752.0613	2746.8661

As, by construction, the SUHF scheme gives the variationally best, i.e. lowest total energy, the x-only OEP solutions are always somewhat higher in energy, with the exception of one and two electron systems where the two methods coincide. The largest difference occurs for Be where the ground-state energies differ by 41 ppm. The disagreement decreases with increasing atomic number to about 2 ppm for Xe. We point out that these differences are due to the different nature of the HF and DFT approach and are resolved by the correlation contributions, which are defined differently for each scheme [81]. Therefore, the quality of the approximate x-only DFT approaches has to be judged by comparison with OEP rather than HF results [9].

To assess the quality of the KLI approximation, we have plotted on the left-hand side of Figure 3 the deviation of the KLI from the exact OEP results as a function of atomic number. As both methods use the same total energy functional but the KLI scheme yields an approximate one-particle potential, the inequality $E^{\mathrm{OEP}} \leq E^{\mathrm{KLI}}$ [16] is always satisfied.

Table 3: *Absolute total ground-state energies for Rb through Xe calculated self-consistently employing various x-only approximations. For elements denoted with an asterisk the SUHF results have been obtained by using wave functions consisting of more than one Slater determinant, whereas the DFT results are obtained with a single-determinant wave function. SUHF results have been taken from [15]. All numbers in atomic units.*

	SUHF	OEP	KLI	B88	xPW91	xLDA
Rb	2938.3576	2938.3455	2938.3421	2938.3909	2938.3517	2932.9835
Sr	3131.5457	3131.5334	3131.5299	3131.5791	3131.5422	3125.9981
Y	3331.6846	3331.6710	3331.6670	3331.7256	3331.6880	3325.9712
Zr*	3539.0117	3538.9700	3538.9656	3539.0327	3538.9941	3533.1035
Nb	3753.6006	3753.5855	3753.5807	3753.6672	3753.6223	3747.5635
Mo	3975.5530	3975.5371	3975.5320	3975.6140	3975.5678	3969.3323
Tc	4204.7949	4204.7793	4204.7741	4204.8362	4204.7943	4198.3724
Ru*	4441.5409	4441.5088	4441.5032	4441.5925	4441.5498	4434.9512
Rh*	4685.8822	4685.8485	4685.8429	4685.9394	4685.8959	4679.1175
Pd	4937.9210	4937.9060	4937.9016	4938.0157	4937.9712	4931.0100
Ag	5197.6989	5197.6815	5197.6758	5197.7652	5197.7196	5190.5783
Cd	5465.1331	5465.1144	5465.1084	5465.1907	5465.1463	5457.8218
In	5740.1694	5740.1514	5740.1455	5740.1999	5740.1550	5732.6492
Sn	6022.9325	6022.9149	6022.9091	6022.9450	6022.8985	6015.2128
Sb	6313.4870	6313.4697	6313.4639	6313.4799	6313.4318	6305.5658
Te	6611.7856	6611.7683	6611.7625	6611.7725	6611.7246	6603.6768
I	6917.9814	6917.9642	6917.9582	6917.9671	6917.9181	6909.6900
Xe	7232.1384	7232.1210	7232.1150	7232.1165	7232.0662	7223.6572

The results differ only slightly [15, 16, 19], the difference being largest for Li with 13 ppm and dropping to 0.8 ppm for Xe. For one and two-particle systems the KLI approximation is exact and thus gives total energies identical to the exact OEP solutions. The mean absolute deviation from the exact DFT values provided by the exact OEP scheme for all atoms displayed in Tables 1, 2 and 3 is only 3.1 mH.

Turning to the conventional approximations, i.e. to explicit density functionals, the high accuracy of the KLI approximation becomes evident. In Figure 3, we have plotted the difference between the exact total x-only ground-state energies and the results of the two GGAs for the atoms listed in Tables 1, 2 and 3. Comparing the left with the right plot in Figure 3, the much larger error of the conventional density functionals is clearly visible. It is also apparent that the GGAs do not provide an upper bound for the total energy: For quite a few atoms the GGA results lie *below* the exact ones. For the B88 exchange functional, this is most pronounced for He, where the deviation is -594 ppm while the

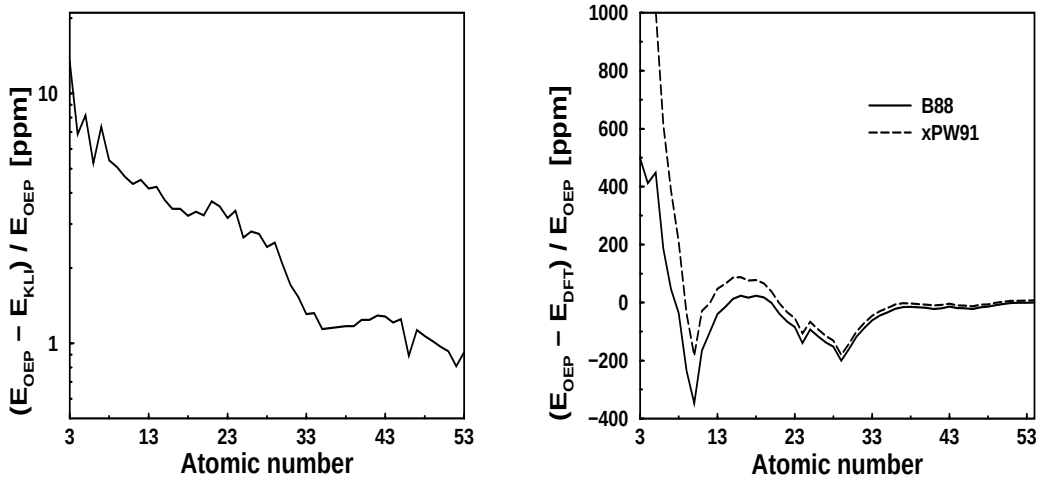

Figure 3: *Difference between the total energy from x-only OEP and KLI calculations (left) and between the total energy from x-only OEP and B88 and PW91 calculations (right) in ppm.*

xPW91 functional underestimates the exact value for Ne by −183 ppm. As for the KLI approximation, the absolute magnitude of the error of the GGAs decreases with increasing atomic number. For the B88 functional, the error drops from 4200 ppm for the Hydrogen atom to 0.6 ppm for Xe, whereas the xPW91 functional yields errors of 9400 ppm and 7.6 ppm for the same atoms, respectively. The mean absolute deviation is 66 mH for the B88 and 53 mH for the xPW91 energy functional.

A glance at the xLDA results for the total energy displayed in Tables 1, 2 and 3 shows that these results differ considerably from the exact OEP ones. The error introduced by this

Table 4: *OEP ground-state configurations of the transition elements.*

Atom	Configuration	Atom	Configuration
Sc	$3d^1 4s^2$	Y	$4d^1 5s^2$
Ti	$3d^2 4s^2$	Zr	$4d^3 5s^1$
V	$3d^3 4s^2$	Nb	$4d^4 5s^1$
Cr	$3d^5 4s^1$	Mo	$4d^5 5s^1$
Mn	$3d^5 4s^2$	Tc	$4d^5 5s^2$
Fe	$3d^6 4s^2$	Ru	$4d^7 5s^1$
Co	$3d^7 4s^2$	Rh	$4d^8 5s^1$
Ni	$3d^8 4s^2$	Pd	$4d^{10} 5s^0$
Cu	$3d^{10} 4s^1$	Ag	$4d^{10} 5s^1$
Zn	$3d^{10} 4s^2$	Cd	$4d^{10} 5s^2$

Table 5: *Absolute eigenvalues of Ar obtained from various self-consistent x-only calculations. SUHF values have been taken from [82]. All values in atomic units.*

	SUHF	OEP	KLI	B88	xPW91	xLDA	xLDA-SICKLI
1s	118.6104	114.4524	114.42789	114.1890	114.1887	113.7159	114.3650
2s	12.3222	11.1534	11.1820	10.7911	10.7932	10.7299	10.9804
2p	9.5715	8.7339	8.7911	8.4107	8.4141	8.3782	8.6191
3s	1.2774	1.0993	1.0942	0.8459	0.8481	0.8328	1.0497
3p	0.5910	0.5908	0.5893	0.3418	0.3441	0.3338	0.5493

approximation is clearly the largest of all the approximate x-only functionals considered here. It drops from 85800 ppm for Hydrogen to 1170 ppm for Xe, yielding a mean absolute deviation of 156.7 mH.

xLDA-SICKLI results for atoms H through Ar are given in Table 1. As for the KLI calculations employing the exact exchange energy functional, the method yields exact results for one and spin-unpolarized two electron systems. For atoms with more electrons, the xLDA results are considerably improved by the SIC scheme but for heavier atoms the resulting total energies are still worse than the ones obtained from the two GGA approaches. The mean absolute deviation for the atoms H through Ar is 299 mH.

Table 6: *Absolute eigenvalues of Cu obtained from various self-consistent x-only calculations. SUHF values have been taken from [37]. All values in atomic units.*

	SUHF	OEP	KLI	B88	xPW91	xLDA	xLDA-SICKLI
1s↑	328.7940	321.5109	321.3829	321.4929	321.4910	320.7080	321.4691
2s↑	40.8187	38.2779	38.2515	38.1898	38.1923	38.0830	38.2498
2p↑	35.6168	33.5336	33.5481	33.4859	33.5336	33.4214	33.5755
3s↑	5.0124	4.2328	4.1868	4.0360	4.0387	4.0054	4.1463
3p↑	3.3222	2.7535	2.7191	2.5751	2.5782	2.5577	2.6973
3d↑	0.4891	0.3046	0.2854	0.1616	0.1648	0.1575	0.2923
4s↑	0.2396	0.2405	0.2440	0.1625	0.1639	0.1588	0.2693
1s↓	328.7921	321.7166	321.5309	321.4919	321.4900	320.7069	321.6692
2s↓	40.8195	38.4734	38.4660	38.1925	38.1946	38.0860	38.4544
2p↓	35.6193	33.7275	33.7608	33.4877	33.4913	33.4235	33.7789
3s↓	5.0116	4.4212	4.4131	4.0399	4.0419	4.0093	4.3469
3p↓	3.3274	2.9410	2.9443	2.5782	2.5807	2.5609	2.8968
3d↓	0.4933	0.4893	0.4984	0.1558	0.1587	0.1512	0.4801

Table 7: *Absolute eigenvalues of the highest occupied orbital for atoms of the nitrogen group obtained from various self-consistent x-only calculations. SUHF and OEP values have been taken from [15]. All values in atomic units.*

		SUHF	OEP	KLI	B88	xPW91	xLDA	xLDA-SICKLI
N	2p↑	0.5709	0.5712	0.5705	0.2846	0.2867	0.2763	0.5363
	2s↓	0.7258	0.7258	0.7245	0.5036	0.5059	0.4820	0.7247
P	3p↑	0.3921	0.3916	0.3905	0.2100	0.2113	0.2033	0.3582
	3s↓	0.5562	0.5562	0.5554	0.3921	0.3944	0.3840	0.5690
As	4p↑	0.3702	0.3691	0.3678	0.1975	0.1988	0.1929	0.3356
	4s↓	0.5561	0.5562	0.5559	0.4145	0.4174	0.4106	0.5896
Sb	5p↑	0.3358	0.3347	0.3336	0.1819	0.1832	0.1785	0.3032
	5s↓	0.4689	0.4693	0.4696	0.3491	0.3520	0.3478	0.5032

The trends found for the total ground-state energies remain valid for most quantities of interest: The HF and OEP results differ very little, the KLI scheme provides the best approximation to the exact DFT results, the GGAs are (sometimes only slighty) worse while the xLDA is by far the least accurate approximation. However, the xLDA-SICKLI results are often of higher quality than those obtained from any of the GGAs.

For example, in Tables 5 and 6 we have listed the eigenvalues $\varepsilon_{i\sigma}$ corresponding to the occupied orbitals of Ar and Cu, respectively, as obtained with the various methods. In DFT, the energy eigenvalues have no physical interpretation except for the highest occupied one which – in the exact theory including all correlation effects – is equal to the ionization potential of the system [47]. However, the eigenvalues of the inner orbitals may indicate the quality of the exchange potential $V_{\rm x}(\mathbf{r})$. While the highest occupied eigenvalues obtained within the exact x-only OEP scheme are very close to the SUHF values, the inner eigenvalues differ more, illustrating their auxiliary nature within DFT calculations. The KLI approximation yields results very close to the exact OEP values, indicating the high quality of the KLI exchange potential. Most notable is the agreement of the highest occupied eigenvalues. As a typical example, we have listed the highest occupied eigenvalues for the atoms of the nitrogen group in Table 7. Both the GGA and the xLDA calculations are seriously in error, yielding results which are too small by roughly a factor of two. For Cu, the two outermost majority-spin eigenvalues are incorrectly ordered if the B88 or xLDA functionals are used. These errors in the outermost orbitals are due to the incorrect asymptotic behavior of the approximate potentials. The inner orbitals are usually in better agreement with the exact results. The xLDA-SICKLI results are clearly much better than the results from any of the explicitly density-dependent functionals. In particular, the improvement over the xLDA results is very remarkable. This demonstrates the great importance of the self-interaction correction part of the exchange functional, which is responsible for the correct $-1/r$ decay of the xLDA-SICKLI exchange potential.

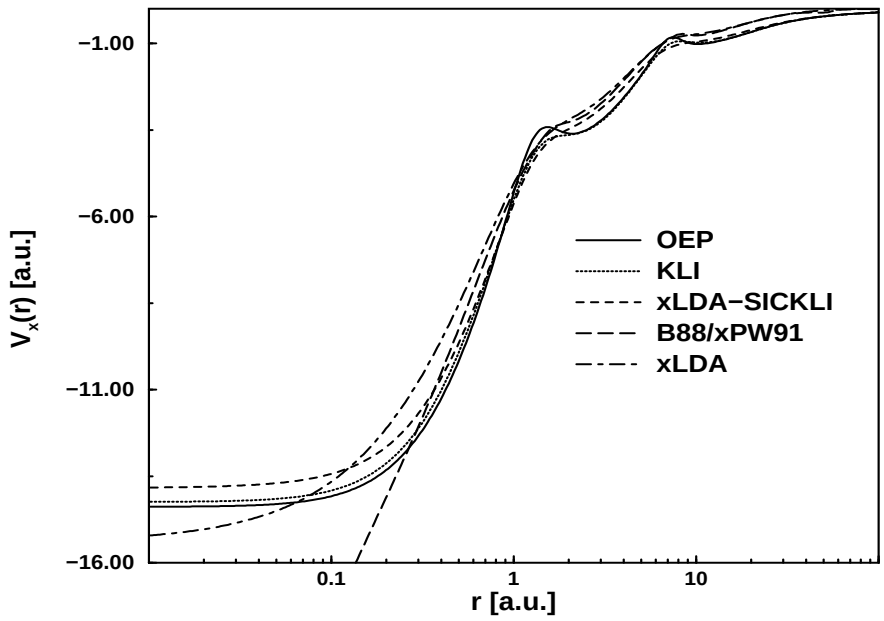

Figure 4: *Exchange potentials $V_x(\mathbf{r})$ for Ar from various self-consistent x-only calculations.*

The xLDA-SICKLI description even corrects the wrong ordering found in xLDA for the two outermost majority-spin eigenvalues in Cu.

In Figures 4 and 5 we have plotted $V_{\mathrm{x}}(\mathbf{r})$ resulting from various x-only schemes for the Ar atom. Figure 5 shows the asymptotic region in greater detail. As expected, the KLI potential closely follows the exact OEP curve, the two being indistinguishable in the asymptotic region where they both decay like $-1/r$, as was shown in section 2.3.2. For the xLDA-SICKLI potential, the same holds true. However, the exact OEP and the xLDA-SICKLI potential agree less closely in the inner regions as compared to the KLI potential. The exchange potentials corresponding to all of the conventional functionals decay too rapidly, the one obtained from the xPW91 functional even introduces a spurious dip in this region. The B88 potential is known [37] to decay like $-1/r^2$. The so called *intershell peaks* , i.e. the maxima of the potential occuring in the intershell regions, clearly visible in the OEP and KLI potentials, are not properly reproduced in the conventional DFT approximations. This is also the case for the xLDA-SICKLI potential, which exhibits no outer peak at all. Despite the rather close agreement of the innermost orbital energies, both of the GGA potentials exhibit an unphysical divergence at the position of the nucleus which may be traced back to the density gradients in the expressions for the exchange energy, cf. Eqs. (248) and (250). In Figure 6 we have plotted the difference between the spin-up and spin-down exchange potentials for Cu, which is a measure for the tendency of the atom to favour spin-polarization. While the KLI and xLDA-SICKLI approximations roughly follow the overall shape of the exact result but miss most of the finer structure, both of the GGAs and the xLDA give very different results. Most strikingly, they fail to

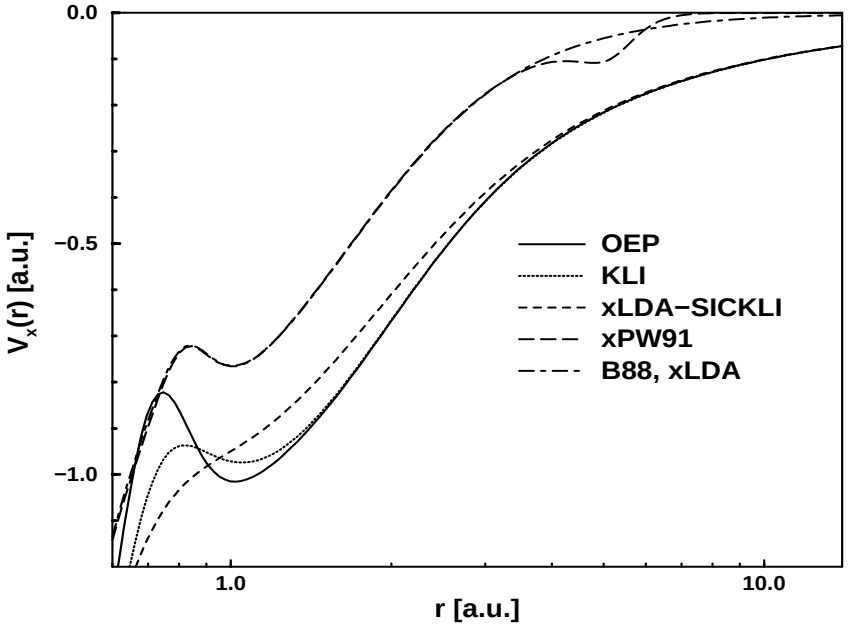

Figure 5: *Exchange potentials $V_x(\mathbf{r})$ for Ar from various self-consistent x-only calculations in the valence region. In this region, the xLDA potential is identical to the B88 one.*

Table 8: *Expectation values of r^2 for some noble gases. SUHF and OEP values from [15]. All numbers in atomic units.*

	SUHF	OEP	KLI	B88	xPW91	xLDA	xLDA-SICKLI
He	1.1848	1.1848	1.1848	1.2644	1.2805	1.3275	1.1848
Ne	0.9372	0.9372	0.9367	0.9952	1.0015	1.0036	0.9524
Ar	1.4464	1.4465	1.4467	1.4791	1.4876	1.4889	1.4699
Kr	1.0981	1.0980	1.0985	1.1176	1.1232	1.1803	1.1124
Xe	1.1602	1.1600	1.1607	1.1716	1.1768	1.1716	1.1695

reproduce the constant shift between $V_{\mathrm{x}\uparrow}(\mathbf{r})$ and $V_{\mathrm{x}\downarrow}(\mathbf{r})$ in the inner region of the atom. This is, to a lesser extent, also true for other atoms [37].

The accuracy of the calculated electron densities may be assessed by comparing various r^n expectation values. In Table 8 we list the r^2 expectation values for the noble gas atoms He through Xe as calculated with the various schemes. This quantity puts a strong weight on the electron density of the outer shells and therefore represents a measure of its quality in that region. The SUHF and OEP values are almost identical, while the KLI approximation introduces only a small error. The errors introduced by the conventional DFT methods are about two orders of magnitude larger, while the xLDA-SICKLI results lie somewhere in

Table 9: *Expectation values of r^{-1} for some earthalkali metals. SUHF and OEP values from [15]. All numbers in atomic units.*

	SUHF	OEP	KLI	B88	xPW91	xLDA	xLDA-SICKLI
Be	2.1022	2.1022	2.1039	2.1017	2.1008	2.0766	2.0934
Mg	3.3267	3.3267	3.3258	3.3261	3.3259	3.3147	3.3256
Ca	4.0080	4.0080	4.0086	4.0085	4.0084	4.0010	4.0050
Sr	5.1729	5.1729	5.1723	5.1729	5.1728	5.1685	5.1712

between, which is largely due to the correct asymptotic form of the potential. Again, the remarkable improvement over the LDA due to the inclusion of the self-interaction correction part is noteworthy.

The density in the inner region of the atom heavily contributes to the $1/r$-expectation value, which we show for the four lightest alkaline earths in Table 9. While the SUHF and OEP values are identical to all given digits and the xLDA gives the worst results, the comparison of the KLI and GGA results shows an unexpected feature as the latter are always better than the former. This is somewhat surprising as the GGA exchange potentials show an unphysical singularity for $r \to 0$ as discussed above.

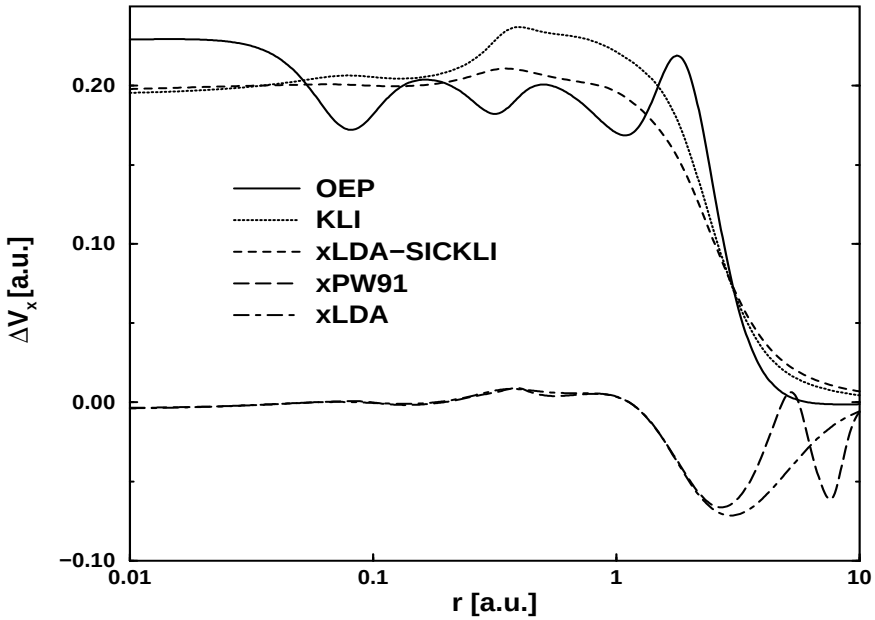

Figure 6: *Difference between spin-up and spin-down exchange potentials, $\Delta V_{\mathrm{x}}(\mathbf{r})$, for Cu from various self-consistent x-only calculations*

Table 10: *Magnetization density* $\zeta(0) = (\rho_\uparrow(0) - \rho_\downarrow(0))/(\rho_\uparrow(0) + \rho_\downarrow(0))$ *at the position of the nucleus for atoms of the nitrogen group from various self-consistent calculations. SUHF, OEP, and KLI values have been calculated from the results given in [15]. All values in units of* 10^{-6}.

	SUHF	OEP	KLI	B88	xPW91	xLDA	xLDA-SICKLI
N	910.8	921.5	-1623	125.0	195.7	-255.3	-98.2
P	-63.8	-72.1	-97.5	-116.9	-115.6	-129.4	-199.4
As	-24.2	-27.1	-26.3	-39.2	-36.4	-40.5	-46.8
Sb	-9.0	-10.4	-9.6	-15.1	-13.7	-16.0	-15.4

The magnetization density $\zeta(0) = (\rho_\uparrow(0) - \rho_\downarrow(0))/(\rho_\uparrow(0) + \rho_\downarrow(0))$ at the nucleus provides a very sensitive test for the quality of the spin densities. In Table 10 this quantity is shown for the four lightest atoms of the nitrogen group. The relatively large difference between the SUHF and OEP results underlines the sensitivity of this quantity. For the nitrogen atom the KLI approximation leads to a completely worthless result as the sign is reversed compared to the OEP value. For this atom, the GGAs give the right sign but only one tenth of the correct number. For P, As and Sb the KLI scheme provides the best approximation,

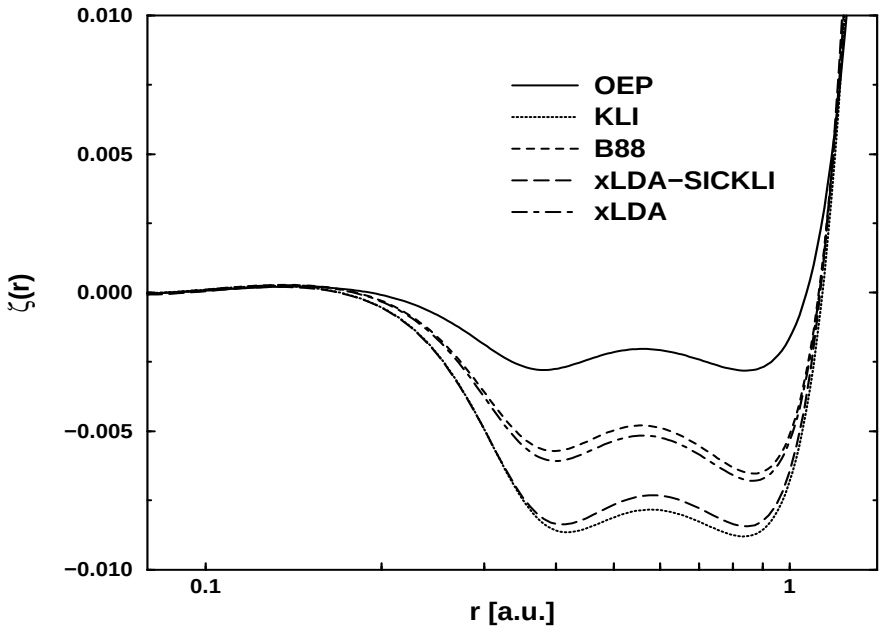

Figure 7: *Magnetization density* $\zeta = (\rho_\uparrow - \rho_\downarrow)/(\rho_\uparrow + \rho_\downarrow)$ *for Cu from various self-consistent x-only calculations. The result from the PW91 functional is very similar to the one from the B88 one.*

whereas the xLDA is worst. The pattern apparent from these few systems is by no means special but rather typical throughout the periodic table [15]. We conclude that no current approximations yield even moderate accuracy for the magnetization density at the nucleus.

Another failure of the KLI and xLDA-SICKLI approximations is apparent from Figure 7, where we have plotted the magnetization density for Cu. Clearly, the KLI results are twice as far off the exact curve as the GGA and xLDA approximations. For most systems, however, the differences are not as dramatic as for Cu.

4.1.2 Diatomic molecules

In order to demonstrate the validity of the KLI approach for more complex systems, we have performed KLI calculations for diatomic molecules employing the exact exchange energy functional as defined by equation (27). Our calculations have been performed with a fully numerical basis-set-free code, developed from the Xα program written by Laaksonen, Sundholm and Pyykkö [83, 84, 85]. The code solves the one-particle Schrödinger equation for diatomic molecules

$$\left(-\frac{\nabla^2}{2} - \frac{Z_1}{|\mathbf{R}_1 - \mathbf{r}|} - \frac{Z_2}{|\mathbf{R}_2 - \mathbf{r}|} + V_{\mathrm{H}}(\mathbf{r}) + V_{\mathrm{x}\sigma}^{\mathrm{KLI}}(\mathbf{r})\right) \varphi_{j\sigma}(\mathbf{r}) = \varepsilon_{j\sigma}\varphi_{j\sigma}(\mathbf{r}), \tag{258}$$

where $\mathbf{R_i}$ denotes the location and Z_i the nuclear charge of the i-th nucleus in the molecule. This partial differential equation is solved in prolate spheroidal coordinates on a two-dimensional mesh by a relaxation method. The third variable, the azimuthal angle, is treated analytically. The Hartree potential

$$V_{\mathrm{H}}(\mathbf{r}) = \int d^3r' \, \frac{\rho(\mathbf{r}')}{|\mathbf{r} - \mathbf{r}'|} \tag{259}$$

and the functions

$$u_{\mathrm{x}i\sigma}(\mathbf{r}) = -\frac{1}{\varphi_{i\sigma}^*(\mathbf{r})} \sum_{k=1}^{N_\sigma} \varphi_{k\sigma}^*(\mathbf{r}) \int d^3r' \, \frac{\varphi_{i\sigma}^*(\mathbf{r}')\varphi_{k\sigma}(\mathbf{r}')}{|\mathbf{r} - \mathbf{r}'|} \tag{260}$$

needed for the calculation of the exchange potential $V_{\mathrm{x}\sigma}^{\mathrm{KLI}}(\mathbf{r})$ (cf. Eq. (76)) are calculated as solutions of a Poisson and Poisson-like equation, respectively. In this step, the same relaxation technique as for the solution of the Schrödinger equation (258) is employed. Starting with an initial guess for the wave functions $\varphi_{i\sigma}(\mathbf{r})$, equations (258), (259), (260) together with (76) are iterated until self-consistency is achieved. A detailed description of the code is given in [86].

For comparison, we have performed additional x-only calculations with two other approximations of $V_{x\sigma}(\mathbf{r})$ and E_x, respectively. The first one of these, denoted by *Slater* in the following, employs – like the HF and x-only KLI methods – the exact representation (27) of E_x but uses the averaged exchange potential due to Slater [87] given by

$$V_{x\sigma}^S(\mathbf{r}) = -\frac{1}{\rho_\sigma(\mathbf{r})} \sum_{i,j=1}^{N_\sigma} \varphi_{j\sigma}^*(\mathbf{r})\varphi_{i\sigma}(\mathbf{r}) \int d^3r' \, \frac{\varphi_{i\sigma}^*(\mathbf{r}')\varphi_{j\sigma}(\mathbf{r}')}{|\mathbf{r} - \mathbf{r}'|} \, . \tag{261}$$

This expression can also be obtained from (76) by setting the constants $\bar{V}_{\mathrm{xc}i\sigma} - \bar{u}_{\mathrm{xc}i\sigma}$ equal to zero for all i. The other is the well known x-only local density approximation (xLDA)

Table 11: *X-only results for LiH. HF values for bond length of 3.015 a.u. from [86]. Present calculations performed on a* 153×193 *grid with bond length of 3.015 a.u. All numbers in atomic units. Taken from [88].*

	HF	KLI	Slater	xLDA
E_{TOT}	-7.9874	-7.9868	-7.9811	-7.7043
$\varepsilon_{1\sigma}$	-2.4452	-2.0786	-2.3977	-1.7786
$\varepsilon_{2\sigma}$	-0.3017	-0.3011	-0.3150	-0.1284
Q_1^e	0.6531	0.6440	0.8614	0.8679
Q_2^e	7.1282	7.1365	6.9657	6.7717
Q_3^e	2.9096	2.9293	3.0799	2.6924
Q_4^e	16.0276	16.1311	15.5881	15.0789

Table 12: *X-only results for BH. HF values for bond length of 2.336 a.u. from [86]. Present calculations performed on a* 193×265 *grid with bond length of 2.336 a.u. All numbers in atomic units. Taken from [88].*

	HF	KLI	Slater	xLDA
E_{TOT}	-25.1316	-25.1290	-25.1072	-24.6299
$\varepsilon_{1\sigma}$	-7.6863	-6.8624	-7.4837	-6.4715
$\varepsilon_{2\sigma}$	-0.6482	-0.5856	-0.6358	-0.3956
$\varepsilon_{3\sigma}$	-0.3484	-0.3462	-0.3721	-0.1626
Q_1^e	5.3525	5.3498	5.2991	5.3154
Q_2^e	12.1862	12.1416	11.4720	11.9542
Q_3^e	15.6411	15.5618	14.3328	14.0904
Q_4^e	25.8492	25.4188	25.2152	21.9134

of conventional DFT, where the exchange energy is given by Eq. (247). As for the KLI calculations, we have successfully tested our implementations on atomic systems.

Results are given in Tables 11 through 18 for LiH, BH, FH, He_2, Li_2, Be_2, N_2 and OH^-. For each system we show the total ground state energy E_{TOT}, the various orbital energies ε and the nonzero electronic contributions to the dipole, quadrupole, octopole and hexadecapole moments denoted by Q_1^e, Q_2^e, Q_3^e and Q_4^e, calculated from the geometrical center of the respective molecule. For FH, N_2 and OH^- we give the total moments Q_L^{tot} (including nuclear contributions), calculated from the center of mass of the respective molecule. For these three molecules we also present the expectation values of $1/r$, denoted by $< 1/r >$, calculated at the nuclei.

Table 13: *X-only results for FH. HF values for bond length of 1.7328 a.u. from [86]. Present calculations performed on a* 161×321 *grid with bond length of 1.7328 a.u. All numbers in atomic units. Taken from [88].*

	HF	KLI	Slater	xLDA
E_{TOT}	-100.0708	-100.0675	-100.0225	-99.1512
$\varepsilon_{1\sigma}$	-26.2946	-24.5116	-25.6625	-24.0209
$\varepsilon_{2\sigma}$	-1.6010	-1.3994	-1.4327	-1.0448
$\varepsilon_{3\sigma}$	-0.7682	-0.7772	-0.8167	-0.4483
$\varepsilon_{1\pi}$	-0.6504	-0.6453	-0.6897	-0.3109
Q_1^{tot}	-0.7561	-0.8217	-0.8502	-0.6962
Q_2^{tot}	1.7321	1.8012	1.8472	1.7124
Q_3^{tot}	-2.5924	-2.7222	-2.8781	-2.4662
Q_4^{tot}	5.0188	5.1825	5.3720	4.7068
$< 1/r >_H$	6.1130	6.0878	6.0909	6.0901
$< 1/r >_F$	27.1682	27.1622	27.6049	27.0289

Table 14: *X-only results for* He_2*. HF values for bond length of 5.6 a.u. from [86]. Present calculations performed on a* 209×225 *grid with bond length of 5.6 a.u. All numbers in atomic units. Taken from [88].*

	HF	KLI	Slater	xLDA
E_{TOT}	-5.72333	-5.72332	-5.72332	-5.44740
$\varepsilon_{1\sigma g}$	-0.92017	-0.91929	-0.91977	-0.51970
$\varepsilon_{1\sigma u}$	-0.91570	-0.91566	-0.91614	-0.51452
Q_2^e	31.36165	31.35931	31.35907	31.35507
Q_4^e	245.8779	245.8643	245.8615	245.8255

For the quantities of physical interest, i.e. for E_{tot}, the energies ε_{HOMO} of the highest occupied orbitals and the multipole moments, the x-only KLI and HF results differ only slightly, typically by a few hundredths of a percent for the total energies, a few tenths of a percent for ε_{HOMO} and a few percent for the multipole moments. The largest difference for ε_{HOMO} is found for Be_2, where the results differ by 3%. For N_2, the energetic order of the $1\pi_u$ and $3\sigma_g$ orbitals obtained with the HF method is reversed in all DFT approaches, which reproduce the experimentally observed order of the outer valence ionization potentials [89]. As far as the multipole moments are concerned, the largest discrepancy between the x-only

Table 15: *X-only results for Li_2. HF values for bond length of 5.051 a.u. from [86]. Present calculations performed on a 209×225 grid with bond length of 5.051 a.u. All numbers in atomic units. Taken from [88].*

	HF	KLI	Slater	xLDA
E_{TOT}	-14.8716	-14.8706	-14.8544	-14.3970
$\varepsilon_{1\sigma g}$	-2.4531	-2.0276	-2.3875	-1.7869
$\varepsilon_{1\sigma u}$	-2.4528	-2.0272	-2.3873	-1.7864
$\varepsilon_{2\sigma g}$	-0.1820	-0.1813	-0.1989	-0.0922
Q_2^e	27.6362	27.4993	29.0014	29.4401
Q_4^e	159.9924	159.6809	169.1300	172.8505

Table 16: *X-only results for Be_2. HF values for bond length of 4.6 a.u. from [86]. Present calculations performed on a 209×225 grid with bond length of 4.6 a.u. All numbers in atomic units. Taken from [88].*

	HF	KLI	Slater	xLDA
E_{TOT}	-29.1337	-29.1274	-29.0939	-28.4612
$\varepsilon_{1\sigma g}$	-4.73150	-4.09876	-4.60353	-3.78576
$\varepsilon_{1\sigma u}$	-4.73147	-4.09872	-4.60351	-3.87571
$\varepsilon_{2\sigma g}$	-0.39727	-0.33452	-0.37659	-0.23067
$\varepsilon_{2\sigma u}$	-0.24209	-0.23489	-0.26524	-0.13163
Q_2^e	46.0878	46.2475	43.4833	46.2501
Q_4^e	261.774	277.365	249.135	281.950

KLI and HF approach occurs for the total hexadecapole moment of OH^-, where the results differ by 11.9%. The $1/r$-expectation values obtained with the HF and x-only KLI methods are almost identical, differing by only a few hundredths of a precent with the exception of the ones for the hydrogen nuclei in FH and OH^-, where the difference is an order of magnitude larger. In these cases, the Slater and for FH also the xLDA approximation give values closer to the HF results.

Except for the cases mentioned above, the Slater method gives values for E_{TOT}, ε_{HOMO}, the multipole moments and $1/r$-expectation values which differ to a larger extent from both the KLI and HF results than the latter from each other. From the energy eigenvalues of the inner orbitals it is obvious that the Slater exchange potential $V_{x\sigma}^S(\mathbf{r})$ is deeper than the one obtained in the KLI method which therefore yields results closer to the HF ones.

Table 17: *X-only results for N_2. HF values for bond length of 2.07 a.u. from [86]. Present calculations performed on a 209×225 grid with bond length of 2.07 a.u. All numbers in atomic units. Taken from [88].*

	HF	KLI	Slater	xLDA
E_{TOT}	-108.9936	-108.9856	-108.9109	-107.7560
$\varepsilon_{1\sigma g}$	-15.6822	-14.3722	-15.2692	-13.8950
$\varepsilon_{1\sigma u}$	-15.6787	-14.3709	-15.2682	-13.8936
$\varepsilon_{2\sigma g}$	-1.4726	-1.3076	-1.3316	-0.9875
$\varepsilon_{2\sigma u}$	-0.7784	-0.7452	-0.7473	-0.4434
$\varepsilon_{3\sigma g}$	-0.6347	-0.6305	-0.6521	-0.3335
$\varepsilon_{1\pi u}$	-0.6152	-0.6818	-0.6960	-0.3887
Q_2^{tot}	-0.9372	-0.9489	-1.1757	-1.1643
Q_4^{tot}	-7.3978	-6.7481	-7.1272	-6.2553
$< 1/r >_N$	21.6543	21.6439	21.9749	21.5820

Finally, the xLDA results differ strongly from the other methods, yielding much higher total energies. Especially prominent are the values for ε_{HOMO}, which are roughly twice as large as the ones from any of the other methods. Once again, this is due to the wrong exponential decay of $V_{x\sigma}^{LDA}(\mathbf{r})$ for large r. For the negatively charged molecule OH^- there is no convergence of the self-consistency cycle if the xLDA approximation is used.

We expect that the bulk part of the differences between the x-only KLI and the HF results is not caused by the KLI approximation, but is rooted in the different nature of the HF and the DFT approaches. This was found for atomic systems as discussed in the previous subsection and we see no reason why this should not be the case for molecular systems as well.

However, the x-only KLI approach is also prone to reproduce some failures of HF theory. For example, the dissociation energy of Be_2 is found to be -12.3 mH in the HF and -17.2mH in the x-only KLI scheme, i.e. the molecule is predicted to be unstable by both methods. The xLDA, on the other hand, gives 14.6 mH for the dissociation energy, which is still far from the exact value of 3.8mH (calculated from the results given in [90] and [91]) but at least leads to a stable molecule. This effect is also present for other systems and has to be corrected by properly chosen correlation functionals. Calculations on diatomic molecules using the LDA-SIC functional in KLI approximation have been reported by Krieger et. al. [92, 93].

Table 18: *X-only results for OH^-. HF values for bond length of 1.835 a.u. from [86]. Present calculations performed on a 105×145 grid with bond length of 1.835 a.u. All numbers in atomic units.*

	HF	KLI	Slater
E_{TOT}	-75.4180	-75.4145	-75.3681
$\varepsilon_{1\sigma}$	-20.1858	-18.5775	-19.6091
$\varepsilon_{2\sigma}$	-0.9009	-0.7062	-0.7316
$\varepsilon_{3\sigma}$	-0.2508	-0.2363	-0.2668
$\varepsilon_{1\pi}$	-0.1097	-0.1066	-0.1355
Q_1^{tot}	0.4855	0.5792	0.5941
Q_2^{tot}	-1.8314	-1.9808	-1.7975
Q_3^{tot}	1.4003	1.7646	1.9280
Q_4^{tot}	-4.0346	-4.5159	-4.6758
$< 1/r >_H$	5.7355	5.7061	5.7399
$< 1/r >_O$	23.2588	23.2524	23.6925

4.2 Comparison of nonrelativistic with relativistic results

The discussions in the preceding section were solely based on nonrelativistic DFT. In order to investigate the influence of relativistic effects, we present, in this section, results of fully relativistic calculations on closed-shell atoms.

Since we are not concerned with any magnetic fields in our calculations, the following analysis is done in the framework of the "electrostatic case", discussed in section 3.3. First of all, a brief remark concerning the nature of relativistic interactions has to be made: In QED, the electron-electron interaction, mediated by the exchange of photons, is properly described by the (free) photon propagator $D^0_{\mu\nu}(x-y)$. It can be decomposed into an instantaneous (longitudinal) Coulomb part and a transversal contribution that contains all retardation effects [94]:

$$D^0_{\mu\nu}(x-y) = i g_{0\mu} g_{0\nu} \frac{\delta(x^0 - y^0)}{|\mathbf{x}-\mathbf{y}|} + D^{0,\mathrm{T}}_{\mu\nu}(x-y)\,. \tag{262}$$

Based on this decomposition, we may split $E_{\mathrm{H}}[\rho]$ as well as $E_{\mathrm{xc}}[\rho]$ into their longitudinal and transverse contributions, i.e.

$$E_{\mathrm{H}}[\rho] = E^{\mathrm{L}}_{\mathrm{H}}[\rho] + E^{\mathrm{T}}_{\mathrm{H}}[\rho] \tag{263}$$

$$E_{\mathrm{xc}}[\rho] = E^{\mathrm{L}}_{\mathrm{xc}}[\rho] + E^{\mathrm{T}}_{\mathrm{xc}}[\rho]\,. \tag{264}$$

Aiming at calculations for atomic systems, we can expect the interaction to be dominated by the familiar Coulomb term. Therefore, as a starting point, it seems plausible to neglect all transverse contributions. This approach represents the RDFT analogue of the standard relativistic many-body treatment employing the Dirac-Coulomb Hamiltonian.

Restricting ourselves to the longitudinal (Coulomb) interactions, we have performed self-consistent calculations in the x-only limit of RDFT. In analogy to the nonrelativistic case, the x-only limit of the xc energy functional is defined by using the exact expression for the exchange energy functional, i.e. the relativistic Fock term

$$E_{\rm x}^{\rm L,exact}[\rho] = -\frac{1}{2} \sum_{-c^2<\varepsilon_j,\varepsilon_k<e_F} \int d^3r \int d^3r' \, \frac{\varphi_j^\dagger(\mathbf{r})\varphi_k(\mathbf{r})\varphi_k^\dagger(\mathbf{r}')\varphi_j(\mathbf{r}')}{|\mathbf{r}-\mathbf{r}'|} \, . \tag{265}$$

in the case of longitudinal interactions only. As discussed in section 3.3, the exact longitudinal exchange potential $V_{\rm x}^{\rm L}(\mathbf{r})$ can be obtained by solving the full ROEP integral equation (214) with $E_{\rm xc}$ replaced by $E_{\rm x}^{\rm L,exact}$. Simultaneous solution of the ROEP integral equation and the RKS equation (202) therefore represents the exact implementation of the longitudinal x-only limit of RDFT. It is compared to the RKLI method, which employs the same exact expression (265) for the exchange energy and only approximates the local exchange potential $V_{\rm x}^{\rm L}(\mathbf{r})$ by means of Eq. (246).

Besides, we list results of traditional x-only RKS schemes obtained from the longitudinal x-only LDA (xRLDA), given by

$$E_{\rm x}^{\rm L,RLDA}[\rho] = \int d^3r e_{\rm x}^{\rm NRLDA}(\rho)\Phi_0^{\rm L}(\beta) \, , \tag{266}$$

with the nonrelativistic energy density

$$e_{\rm x}^{\rm NRLDA}(\rho) = -\frac{3}{4}\left(\frac{3}{\pi}\right)^{\frac{1}{3}} \rho^{\frac{4}{3}}(\mathbf{r}) \tag{267}$$

and the relativistic correction

$$\Phi_0^{\rm L}(\beta) := \frac{5}{6} + \frac{1}{3\beta^2} + \frac{2\eta}{3\beta}\,{\rm arsinh}\,\beta - \frac{2\eta^4}{3\beta^4}\ln\eta - \frac{1}{2}\left(\frac{\eta}{\beta} - \frac{{\rm arsinh}\,\beta}{\beta^2}\right)^2 \tag{268}$$

with

$$\beta(\mathbf{r}) := \frac{1}{c}\Big(3\pi^2\rho(\mathbf{r})\Big)^{\frac{1}{3}} \tag{269}$$

and

$$\eta(\mathbf{r}) := \Big(1+\beta(\mathbf{r})^2\Big)^{\frac{1}{2}} \, . \tag{270}$$

Furthermore, we performed calculations with two recently introduced relativistic GGAs (RGGAs) [70, 95]. The first one is given by the functional

$$E_{\rm x}^{\rm L,RGGA}[\rho] = \int d^3r e_{\rm x}^{\rm NRLDA}(\rho)\left(\Phi_0^{\rm L}(\beta) + g(\xi)\Phi_2^{\rm L}(\beta)\right) \, , \tag{271}$$

with the quantity $g(\xi)$ proposed by Becke (RB88)

$$g_{B88}(\xi) = \frac{d\xi}{1 + 9d\xi^{1/2}{\rm arcsinh}\left[2\left(6\pi^2\right)^{1/3}\xi^{1/2}\right]/(4\pi)} \tag{272}$$

(d=0.2743). The second one is a [2/2]-Padé approximant (RECMV92) [52]

$$g_{ECMV92}(\xi) = \frac{A_1\xi + A_2\xi^2}{1 + B_1\xi + B_2\xi^2} \tag{273}$$

Table 19: *Parameters for the longitudinal correction factor (275). Taken from [70]*

	RECMV92	RB88
a1	2.21259	2.20848
a2	0.669152	0.668684
b1	1.32998	1.33075
b2	0.794803	0.795105

$(A_1 = 0.3402, A_2 = 5.9955, B_1 = 27.5026, B_2 = 5.7728)$, where

$$\xi(\mathbf{r}) = \left(\frac{\nabla\rho(\mathbf{r})}{2(3\pi^2\rho(\mathbf{r}))^{1/3}\rho(\mathbf{r})} \right)^2 . \tag{274}$$

The relativistic effects are accounted for via the function $\Phi_2^{\mathrm{L}}(\beta)$, which is also given by a [2/2]-Padé approximant

$$\Phi_2^{\mathrm{L}}(\beta) = \frac{1 + a_1\beta^2 + a_2\beta^4}{1 + b_1\beta^2 + b_2\beta^4} \tag{275}$$

with the constants given in Table 19.

These various approaches are analyzed for spherical (closed-shell) atoms. To this end, the spin-angular part of the wave function is treated analytically and the remaining radial part of the Dirac equation is solved numerically on a logarithmic mesh employing an Adams-Bashforth-Moulton predictor-corrector scheme [64]. We also note, that for these closed-shell atoms the transverse Hartree energy vanishes, i.e. $E_{\mathrm{H}}^{\mathrm{T}} = 0$. In all our calculations we use finite nuclei modeled by a homogeneously charged sphere with the radii given by

$$R_{\mathrm{nucl}} = 1.0793\ A^{1/3} + 0.73587\ \mathrm{fm} \tag{276}$$

and A being the atomic mass taken from [96]. We mention in passing that employing finite nuclei is not necessary to ensure convergent results as, for example, in the relativistic Thomas-Fermi model. We incorporate finite nuclei because they represent the physically correct approach.

In Table 20, we show the longitudinal ground-state energy $E_{\mathrm{tot}}^{\mathrm{L}}$ obtained from the various self-consistent x-only RDFT approaches and, in addition, from relativistic Hartree-Fock (RHF) calculations. Furthermore, since we are interested in the effects induced by relativity, we calculated the relativistic contribution to $E_{\mathrm{tot}}^{\mathrm{L}}$, defined by

$$\Delta E_{\mathrm{tot}} := E_{\mathrm{tot}}^{\mathrm{L}}[\rho^{\mathrm{R}}] - E_{\mathrm{tot}}^{\mathrm{NR}}[\rho^{\mathrm{NR}}] , \tag{277}$$

which is listed in Table 21. We note that the nonrelativistic total ground-state energies $E_{\mathrm{tot}}^{\mathrm{NR}}[\rho^{\mathrm{NR}}]$ are *not* those of section 4.1, but have also been calculated employing finite nuclei. From Table 21, we realize that the inclusion of relativistic effects leads to drastic corrections especially for high-Z atoms. For example, Table 21 shows that the relativistic correction of Hg amounts for about 6.7% of the total energy thus demonstrating the need for a fully relativistic treatment. Comparing the different approaches, we basically find the same trends as in the nonrelativistic context: The RHF and ROEP data agree closely with each

Table 20: *Longitudinal ground-state energy* $-E_{\rm tot}^{L}$ *from various self-consistent x-only and RHF calculations.* $\bar{\triangle}$ *denotes the mean absolute deviation and* $\bar{\delta}$ *the average relative deviation (in 0.1 percent) from the exact ROEP values. All numbers in atomic units. Taken from [68].*

	RHF	ROEP	RKLI	RB88	RECMV92	xRLDA
He	2.862	2.862	2.862	2.864	2.864	2.724
Be	14.576	14.575	14.575	14.569	14.577	14.226
Ne	128.692	128.690	128.690	128.735	128.747	127.628
Mg	199.935	199.932	199.931	199.952	199.970	198.556
Ar	528.684	528.678	528.677	528.666	528.678	526.337
Ca	679.710	679.704	679.702	679.704	679.719	677.047
Zn	1794.613	1794.598	1794.595	1794.892	1794.880	1790.458
Kr	2788.861	2788.848	2788.845	2788.907	2788.876	2783.282
Sr	3178.080	3178.067	3178.063	3178.111	3178.079	3172.071
Pd	5044.400	5044.384	5044.380	5044.494	5044.442	5036.677
Cd	5593.319	5593.299	5593.292	5593.375	5593.319	5585.086
Xe	7446.895	7446.876	7446.869	7446.838	7446.761	7437.076
Ba	8135.644	8135.625	8135.618	8135.612	8135.532	8125.336
Yb	14067.669	14067.621	14067.609	14068.569	14068.452	14054.349
Hg	19648.865	19648.826	19648.815	19649.141	19649.004	19631.622
Rn	23602.005	23601.969	23601.959	23602.038	23601.892	23582.293
Ra	25028.061	25028.027	25028.017	25028.105	25027.962	25007.568
No	36740.682	36740.625	36740.609	36741.900	36741.783	36714.839
$\bar{\triangle}$			0.006	0.189	0.168	8.668
$\bar{\delta}$			0.002	0.103	0.108	6.20

other, the small differences resulting again from the different nature of the two approaches which correspond to different definitions of the respective correlation energies. Since with increasing atomic number, the inner orbitals, contributing most to the total energy, become more and more localized, the differences between the non-local RHF potential and the local ROEP decrease. In fact, we see from Table 20 that the smallest deviations are found for No. Comparing the second and third columns of Table 20, it is obvious that the RKLI method yields results in very close agreement with the exact ROEP ones. The mean absolute deviation from the exact ROEP data of the 18 neutral atoms listed in Table 20 is only 5 mH. Hence it is of the same order of magnitude as the corresponding mean absolute deviation in the nonrelativistic case as discussed in the preceding section. Moreover, when looking at Table 21, we realize that the relativistic contributions to $E_{\rm tot}^{\rm L}$ are reproduced

Table 21: Relativistic Contribution $-\Delta E_{\mathrm{tot}}^{\mathrm{L}}$ from various self-consistent x-only and RHF calculations. $\bar{\triangle}$ denotes the mean absolute deviation and $\bar{\delta}$ the average relative deviation (in 0.1 percent) from the exact ROEP values. All numbers in atomic units. Taken from [68].

	RHF	ROEP	RKLI	RB88	RECMV92	xRLDA
He	0.000	0.000	0.000	0.000	0.000	0.000
Be	0.003	0.003	0.003	0.003	0.003	0.002
Ne	0.145	0.145	0.145	0.145	0.145	0.138
Mg	0.320	0.320	0.320	0.321	0.321	0.308
Ar	1.867	1.867	1.867	1.867	1.867	1.821
Ca	2.953	2.953	2.953	2.952	2.953	2.888
Zn	16.771	16.770	16.770	16.779	16.779	16.555
Kr	36.821	36.820	36.820	36.822	36.821	36.432
Sr	46.554	46.553	46.553	46.552	46.551	46.092
Pd	106.527	106.526	106.526	106.526	106.525	105.715
Cd	128.245	128.243	128.243	128.243	128.241	127.323
Xe	214.860	214.858	214.858	214.825	214.822	213.522
Ba	252.223	252.222	252.221	252.176	252.173	250.725
Yb	676.559	676.551	676.549	676.590	676.588	673.785
Hg	1240.521	1240.513	1240.511	1240.543	1240.538	1236.349
Rn	1736.153	1736.144	1736.142	1736.151	1736.151	1730.890
Ra	1934.777	1934.770	1934.768	1934.781	1934.783	1929.116
No	3953.172	3953.155	3953.151	3953.979	3954.015	3944.569
$\bar{\triangle}$			0.001	0.056	0.058	1.788
$\bar{\delta}$			0.009	1.14	1.35	33.7

almost perfectly within the RKLI scheme. In other words, almost no additional deviations are introduced by the relativistic treatment of the KLI scheme, so that the high quality of the nonrelativistic KLI approximation is maintained in the relativistic domain. Turning towards the conventional x-only schemes, the conclusions drawn in section 4.1 can be repeated: The RGGAs, although clearly improving over the xRLDA, are worse by more than one order of magnitude when compared to the RKLI, whereas the xRLDA yields the least accurate results.

These trends also remain valid when other quantities of interest are considered. For example, in Table 22 we have listed the relativistic contributions to the longitudinal exchange energy, defined analogously to Eq. (277). Again, only small deviations between the ROEP and RKLI results are found. From the third and fourth columns of Table 22 we notice

Table 22: Relativistic Contribution $-\Delta E_{\mathrm{x}}$ to the exchange energy from various self-consistent x-only calculations. $\bar{\triangle}$ denotes the mean absolute deviation and $\bar{\delta}$ the average relative deviation (in percent) from the exact ROEP values. All energies in atomic units. Taken from [68].

	ROEP	RKLI	RB88	RECMV92	xRLDA
He	0.000	0.000	0.000	0.000	0.000
Be	0.001	0.001	0.001	0.001	0.000
Ne	0.015	0.015	0.015	0.015	0.007
Mg	0.029	0.029	0.029	0.029	0.015
Ar	0.118	0.118	0.117	0.118	0.069
Ca	0.172	0.172	0.171	0.171	0.104
Zn	0.627	0.626	0.632	0.632	0.402
Kr	1.215	1.214	1.212	1.211	0.814
Sr	1.478	1.477	1.473	1.472	1.005
Pd	2.785	2.787	2.782	2.780	1.958
Cd	3.264	3.264	3.255	3.252	2.322
Xe	5.021	5.020	4.977	4.974	3.657
Ba	5.739	5.736	5.684	5.680	4.215
Yb	12.043	12.024	12.027	12.024	9.194
Hg	19.963	19.956	19.965	19.957	15.734
Rn	26.637	26.620	26.612	26.610	21.307
Ra	29.241	29.218	29.225	29.224	23.513
No	52.403	52.402	53.168	53.205	43.683
$\bar{\triangle}$		0.004	0.053	0.056	1.819
$\bar{\delta}$		0.079	1.03	0.857	35.9

that the results of the RGGA functionals – with the exception of No – are also in excellent agreement with the exact data. However, since the RGGAs are optimized for exactly these quantities [70], this might not come as a surprise. Again, the RLDA is the least accurate approximation. It is worthwhile noting that the exchange energy $E_{\mathrm{x}}^{\mathrm{L}}$ is influenced quite substantially by relativistic effects, too. Taking again Hg as an example, we realize that the 5.8%-contribution to $E_{\mathrm{x}}^{\mathrm{L}}$ is of the same order as for the total energy. Furthermore, even for lighter atoms such as Mg, the relativistic corrections to $E_{\mathrm{x}}^{\mathrm{L}}$ are comparable or even larger than the differences between the currently best nonrelativistic exchange-energy functionals as might be seen by comparing the results to the ones of section 4.1. As a consequence, a relativistic treatment is indispensable for the ultimate comparison with experiments [64].

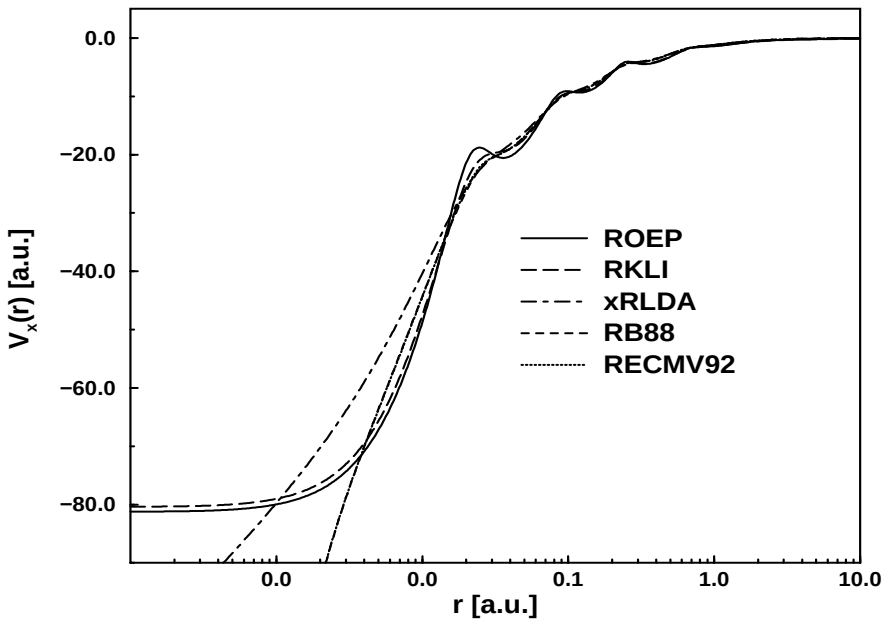

Figure 8: *Longitudinal exchange potential* $V_{\rm x}^{\rm L}(r)$ *for Hg from various self-consistent x-only calculations. Taken from [68].*

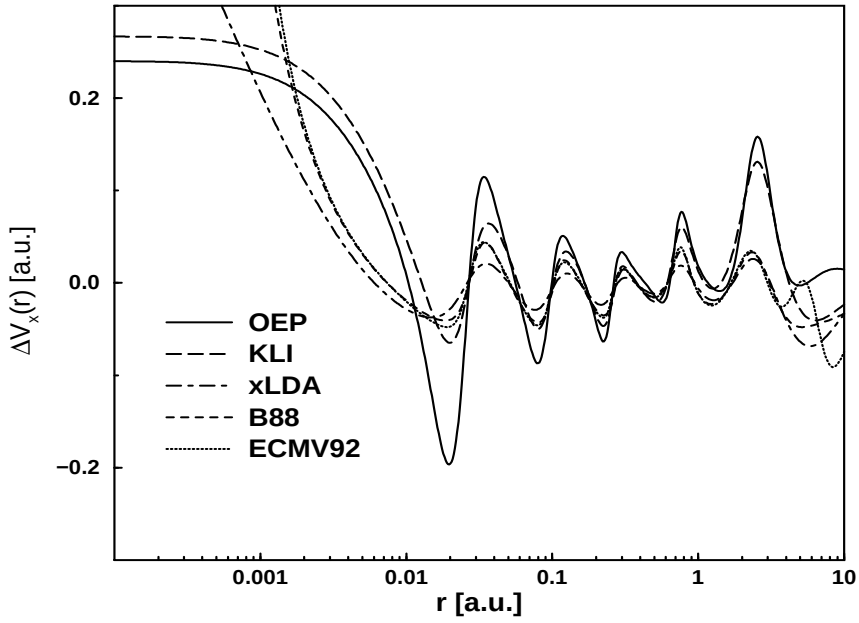

Figure 9: *Relativistic contribution to the exchange potential* $\Delta V_{\rm x}(r)$*, Eq. (278), for Hg from various self-consistent x-only calculations. Taken from [68].*

Table 23: Single particle energies ($-\epsilon_{nlj}$) for Hg from various self-consistent x-only calculations. All numbers in atomic units.

	ROEP	NROEP	RKLI	RB88	RECMV92	xRLDA
1S1/2	3047.430	2756.925	3047.764	3047.706	3047.644	3044.410
2S1/2	540.056	461.647	539.821	539.782	539.788	539.250
2P1/2	518.061	444.015	517.964	518.080	518.049	517.746
2P3/2	446.682	444.015	446.543	446.616	446.599	446.399
3S1/2	128.272	108.762	128.187	128.054	128.058	127.905
3P1/2	118.350	100.430	118.333	118.238	118.233	118.148
3P3/2	102.537	100.430	102.507	102.407	102.404	102.346
3D3/2	86.201	84.914	86.193	86.093	86.095	86.060
3D5/2	82.807	84.914	82.802	82.699	82.700	82.668
4S1/2	28.427	23.522	28.360	28.112	28.114	28.046
4P1/2	24.161	19.895	24.125	23.896	23.895	23.854
4P3/2	20.363	19.895	20.312	20.072	20.072	20.030
4D3/2	13.411	13.222	13.386	13.166	13.166	13.146
4D5/2	12.700	13.222	12.674	12.452	12.453	12.432
4F5/2	3.756	4.250	3.755	3.561	3.561	3.559
4F7/2	3.602	4.250	3.601	3.407	3.407	3.404
5S1/2	4.403	3.501	4.407	4.289	4.289	4.286
5P1/2	3.012	2.344	3.015	2.896	2.896	2.896
5P3/2	2.363	2.344	2.353	2.224	2.225	2.218
5D3/2	0.505	0.538	0.496	0.366	0.367	0.363
5D5/2	0.439	0.538	0.429	0.299	0.300	0.296
6S1/2	0.329	0.262	0.332	0.223	0.222	0.222

Next, we turn our attention to local properties such as the exchange potential $V_{\mathrm{x}}^{\mathrm{L}}(r)$. In Fig. 8, the exchange potential is plotted for the case of Hg. As expected, the RKLI potential follows the exact curve most closely, although the strong intershell peaks of the ROEP curve are not fully reproduced. However, it again improves significantly over the conventional RDFT results, where this structure is smeared out or even absent. In addition, large errors are introduced within the conventional RDFT schemes in the asymptotic regions near as well as far off the nucleus. Since these observations closely resemble the ones made in the analysis of nonrelativistic systems in section 4.1, we consider the relativistic contribution separately. The relativistic contribution to the exchange potential, given by

$$\Delta V_{\mathrm{x}}(r) := \frac{V_{\mathrm{x}}^{\mathrm{L}}[\rho^{\mathrm{R}}](r) - V_{\mathrm{x}}^{\mathrm{NR}}[\rho^{\mathrm{NR}}](r)}{V_{\mathrm{x}}^{\mathrm{NROEP}}[\rho^{\mathrm{NR}}](r)}\,, \tag{278}$$

is plotted in Fig. 9. We first observe strong oscillations between 0.1 a.u. and 5 a.u. These oscillations are introduced by the displacement of the density due to relativistic effects and thus represent a direct consequence of the atomic shell structure. As the shell structure of the exchange potential is not fully reproduced within the RKLI approach, the amplitudes of the oscillations are somewhat smaller compared to $\Delta V_{\rm x}^{\rm OEP}(r)$. While these deviations are clearly visible, the RKLI curve is still closest to the exact one, especially in the region near the nucleus and in the valence region, where large deviations occur for the conventional RDFT methods.

As a consequence of the failures of the conventional RDFT schemes in the asymptotic region, large deviations are found for the energies of the outermost orbitals. This observation – well-known from nonrelativistic calculations – is also found in fully relativistic treatments as shown in Table 23, where the single-particle energies of Hg are listed. In contrast, the RKLI approximation, yielding the correct $-1/r$-behavior of the potential as $r \to \infty$, produces results very similar to the exact ROEP data. Apart from the fact that the single-particle energies are only auxiliary quantities and do not possess any actual physical meaning, the influence of relativity is seen very clearly in Table 23. As could be expected, the effects are strongest for the innermost orbitals whose energies are considerably lowered. However, due to the requirements of orthogonality this also largely influences the outer orbitals which, for example, causes the energy of the $6s1/2$ state of Hg to decrease by about 25%. Furthermore, due to the contraction of the s- and p-orbitals, the nucleus is screened more efficiently, leading to more weakly bound d- and f-levels as can be seen in Table 23. Finally, we clearly recognize the influence of spin-orbit coupling, removing the degeneracy in the angular momentum quantum number l when relativistic effects come into play.

4.3 Inclusion of correlation contributions for nonrelativistic systems

The inclusion of correlation effects into the OEP scheme is straightforward, as indicated by the subscripts xc in section 2. As we will demonstrate in this section, the correlation-energy functional developed by Colle and Salvetti [97, 98] is well suited for atomic systems.

This functional has been obtained via a Jastrow-type ansatz for the correlated total wavefunction through a series of approximations. It may be written in spinpolarized form as [99]

$$\begin{aligned} E_{\rm c}^{\rm CS}[\{\varphi_{j\tau}\}] &= -ab\int d^3r\ \gamma(\mathbf{r})\xi(\mathbf{r})\Bigg[\sum_\sigma \rho_\sigma(\mathbf{r})\sum_i |\nabla\varphi_{i\sigma}(\mathbf{r})|^2 - \frac{1}{4}|\nabla\rho(\mathbf{r})|^2 \\ &\qquad - \frac{1}{4}\sum_\sigma \rho_\sigma(\mathbf{r})\triangle\rho_\sigma(\mathbf{r}) + \frac{1}{4}\rho(\mathbf{r})\triangle\rho(\mathbf{r})\Bigg] \\ &\quad -a\int d^3r\ \gamma(\mathbf{r})\frac{\rho(\mathbf{r})}{\eta(\mathbf{r})}, \end{aligned} \tag{279}$$

where

$$\gamma(\mathbf{r}) = 4\,\frac{\rho_\uparrow(\mathbf{r})\rho_\downarrow(\mathbf{r})}{\rho(\mathbf{r})^2}, \tag{280}$$

$$\eta(\mathbf{r}) = 1 + d\rho(\mathbf{r})^{-\frac{1}{3}}, \tag{281}$$

$$\xi(\mathbf{r}) = \frac{\rho(\mathbf{r})^{-\frac{5}{3}}e^{-c\rho(\mathbf{r})^{-\frac{1}{3}}}}{\eta(\mathbf{r})}. \tag{282}$$

The constants a, b, c and d are given by

$$a = 0.04918, \qquad b = 0.132,$$
$$c = 0.2533, \qquad d = 0.349.$$

Performing the functional derivative with respect to the one-particle orbitals, one obtains for $u_{cj\sigma}(\mathbf{r})$[34]

$$\begin{aligned} u_{cj\sigma}(\mathbf{r}) &= -\frac{a}{\eta(\mathbf{r})}\left(\gamma(\mathbf{r}) + \rho(\mathbf{r})\frac{1}{\varphi^*_{j\sigma}(\mathbf{r})}\frac{\partial\gamma(\mathbf{r})}{\partial\varphi_{j\sigma}(\mathbf{r})}\right) - \frac{ad}{3}\gamma(\mathbf{r})\frac{\rho(\mathbf{r})^{-\frac{1}{3}}}{\eta(\mathbf{r})^2} \\ &\quad -\frac{ab}{4}\frac{1}{\varphi^*_{j\sigma}(\mathbf{r})}\left[\frac{\partial}{\partial\varphi_{j\sigma}(\mathbf{r})}\Big(\gamma(\mathbf{r})\xi(\mathbf{r})\Big)\right]\left[4\sum_{\sigma'}\rho_{\sigma'}(\mathbf{r})\sum_i |\nabla\varphi_{i\sigma'}(\mathbf{r})|^2\right. \\ &\qquad \left. -\Big(\nabla\rho(\mathbf{r})\Big)^2 + \Big(\rho_\uparrow(\mathbf{r})\triangle\rho_\downarrow(\mathbf{r}) + \rho_\downarrow(\mathbf{r})\triangle\rho_\uparrow(\mathbf{r})\Big)\right] \\ &\quad -\frac{ab}{2}\,\nabla\Big(\gamma(\mathbf{r})\xi(\mathbf{r})\Big)\Big(\nabla\rho(\mathbf{r}) + \nabla\rho_{\tilde\sigma}(\mathbf{r})\Big) \\ &\quad -\frac{ab}{4}\triangle\Big(\gamma(\mathbf{r})\xi(\mathbf{r})\Big)\rho_{\tilde\sigma}(\mathbf{r}) \\ &\quad -\,ab\;\gamma(\mathbf{r})\xi(\mathbf{r})\left[\sum_i |\nabla\varphi_{i\sigma}(\mathbf{r})|^2 + \frac{1}{2}\Big(\triangle\rho(\mathbf{r}) + \triangle\rho_{\tilde\sigma}(\mathbf{r})\Big)\right] \\ &\quad +\,ab\;\frac{\nabla\varphi^*_{j\sigma}(\mathbf{r})}{\varphi^*_{j\sigma}(\mathbf{r})}\nabla\Big(\gamma(\mathbf{r})\xi(\mathbf{r})\rho_\sigma(\mathbf{r})\Big) \\ &\quad +\,ab\;\frac{\triangle\varphi^*_{j\sigma}(\mathbf{r})}{\varphi^*_{j\sigma}(\mathbf{r})}\rho_\sigma(\mathbf{r})\gamma(\mathbf{r})\xi(\mathbf{r}) \end{aligned} \tag{283}$$

where $\tilde\sigma$ denotes the spin projection opposite to σ, i.e. $\tilde\sigma = \uparrow$ if $\sigma = \downarrow$ and vice versa. The KLI scheme obtained by combining the correlation-energy functional of Colle and Salvetti with the exact exchange-energy expression (27) will be denoted by KLICS.

For comparison, we have also performed calculations on atoms using the conventional Kohn-Sham method with two standard exchange-correlation energy functionals. The first one of these is the exchange-energy functional by Becke, c.f. Eq. (248), combined with the correlation-energy functional by Lee, Yang and Parr [99],

$$\begin{aligned} E_{\rm c}^{\rm LYP}[\rho_\uparrow,\rho_\downarrow] &= -ab\int d^3r\;\gamma(\mathbf{r})\xi(\mathbf{r})\left[2^{\frac{5}{3}}C_F\left(\sum_\sigma\rho_\sigma(\mathbf{r})^{\frac{8}{3}}\right) + \frac{1}{4}|\nabla\rho(\mathbf{r})|^2 - \frac{1}{4}\rho(\mathbf{r})\triangle\rho(\mathbf{r})\right. \\ &\qquad \left. -\frac{1}{36}\left(\sum_\sigma|\nabla\rho_\sigma(\mathbf{r})|^2\right) - \frac{1}{12}\left(\sum_\sigma\rho_\sigma(\mathbf{r})\triangle\rho_\sigma(\mathbf{r})\right)\right] \\ &\quad -a\int d^3r\;\gamma(\mathbf{r})\frac{\rho(\mathbf{r})}{\eta(\mathbf{r})} \end{aligned} \tag{284}$$

where

$$C_F = \frac{3}{10}\left(3\pi^2\right)^{2/3} \tag{285}$$

and $\gamma(\mathbf{r})$, $\eta(\mathbf{r})$ and $\xi(\mathbf{r})$ are given by Eqs. (280), (281) and (282), respectively. In the following, this procedure is referred to as BLYP. The other is the generalized gradient approximation by Perdew and Wang [77] referred to as PW91. Its exchange part is given by Eq. (250) and the correlation part by

$$E_{\rm c}^{\rm PW91}[\rho_\uparrow,\rho_\downarrow] = \int d^3r\rho(\mathbf{r})\left(\varepsilon_{\rm c}^{\rm LDA}[\rho_\uparrow,\rho_\downarrow](\mathbf{r}) + H_0(\mathbf{r}) + H_1(\mathbf{r})\right) \tag{286}$$

where

$$H_0(\mathbf{r}) = \phi^3(\mathbf{r})\frac{\beta^2}{2\alpha}\ln\left(1+\frac{2\alpha}{\beta}\frac{t^2(\mathbf{r})+A(\mathbf{r})t^4(\mathbf{r})}{1+A(\mathbf{r})t^2(\mathbf{r})+A^2(\mathbf{r})t^4(\mathbf{r})}\right), \tag{287}$$

$$H_1(\mathbf{r}) = 15.7559\,(C_c - 0.003521)\,\phi^3(\mathbf{r})t^2(\mathbf{r})\exp\left(-100\phi^4(\mathbf{r})\left(\frac{k_s^2(\mathbf{r})}{k_F^2(\mathbf{r})t^2(\mathbf{r})}\right)\right), \tag{288}$$

$$k_F(\mathbf{r}) = (3\pi\rho(\mathbf{r}))^{1/3}, \tag{289}$$

$$k_s(\mathbf{r}) = \left(\frac{4k_F}{\pi}\right)^{1/2}, \tag{290}$$

$$r_s(\mathbf{r}) = \left(\frac{3}{4\pi\rho(\mathbf{r})}\right)^{1/3}, \tag{291}$$

$$\zeta(\mathbf{r}) = \frac{\rho_\uparrow(\mathbf{r})-\rho_\downarrow(\mathbf{r})}{\rho(\mathbf{r})}, \tag{292}$$

$$\phi(\mathbf{r}) = \frac{1}{2}\left[(1+\zeta(\mathbf{r}))^{2/3}\,(1-\zeta(\mathbf{r}))^{2/3}\right], \tag{293}$$

$$t^2(\mathbf{r}) = \frac{(\nabla\rho(\mathbf{r}))^2}{4\phi(\mathbf{r})k_s^2(\mathbf{r})\rho^2(\mathbf{r})}, \tag{294}$$

$$A(\mathbf{r}) = \frac{2\alpha}{\beta}\left[\exp\left(\frac{2\alpha\varepsilon_{\rm c}^{\rm LDA}[\rho_\uparrow,\rho_\downarrow](\mathbf{r})}{\phi^3(\mathbf{r})\beta^2}\right)-1\right]^{-1}, \tag{295}$$

$$C_c(\mathbf{r}) = \frac{c_1+c_2r_s(\mathbf{r})+c_3r_s^2(\mathbf{r})}{1+c_4r_s(\mathbf{r})+c_5r_s^2(\mathbf{r})+c_6r_s^3(\mathbf{r})} - c_x \tag{296}$$

and $\alpha = 0.09$, $\beta = 15.7559\times 4.235\times 10^{-3}$,$c_x = -1.667212\times 10^{-3}$, $c_1 = 2.568\times 10^{-3}$, $c_2 = 2.3266\times 10^{-2}$, $c_3 = 7.389\times 10^{-6}$,$c_4 = 8.723$, $c_5 = 0.472$, $c_6 = 7.389\times 10^{-2}$. $\varepsilon_{\rm c}^{\rm LDA}$ is the correlation energy per particle of a homogeneous electron gas in the parameterization by Perdew and Wang [100] given by

$$\varepsilon_{\rm c}^{\rm LDA}[\rho_\uparrow,\rho_\downarrow](\mathbf{r}) = \varepsilon^{\rm U}(\mathbf{r})\left(1-f(\mathbf{r})\zeta^4(\mathbf{r})\right)+\varepsilon^{\rm P}(\mathbf{r})f(\mathbf{r})\zeta^4(\mathbf{r})+\alpha_{\rm c}(\mathbf{r})f(\mathbf{r})\left(1-f\zeta^4(\mathbf{r})\right)/d \tag{297}$$

where

$$f(\mathbf{r}) = \frac{1}{\gamma}\left[(1+\zeta(\mathbf{r}))^{(4/3)}+(1-\zeta(\mathbf{r}))^{(4/3)}-2\right], \tag{298}$$

$$\varepsilon^{\rm U}(\mathbf{r}) = -2a_{01}\,(1+a_{11}r_s(\mathbf{r}))\ln\left(1+\frac{1}{2a_{01}\,(b_{11}x(\mathbf{r})+b_{21}x^2(\mathbf{r})+b_{31}x^3(\mathbf{r})+b_{41}x^4(\mathbf{r}))}\right), \tag{299}$$

$$\varepsilon^{\rm P}(\mathbf{r}) = -2a_{02}\,(1+a_{12}r_s(\mathbf{r}))\ln\left(1+\frac{1}{2a_{02}\,(b_{12}x(\mathbf{r})+b_{22}x^2(\mathbf{r})+b_{32}x^3(\mathbf{r})+b_{42}x^4(\mathbf{r}))}\right), \tag{300}$$

$$\alpha_c(\mathbf{r}) = -2a_{03}\,(1+a_{13}r_s(\mathbf{r}))\ln\left(1+\frac{1}{2a_{03}\,(b_{13}x(\mathbf{r})+b_{23}x^2(\mathbf{r})+b_{33}x^3(\mathbf{r})+b_{43}x^4(\mathbf{r}))}\right), \tag{301}$$

and

$$x(\mathbf{r}) = r_s^{1/2}(\mathbf{r}). \tag{302}$$

$r_s(\mathbf{r})$ and $\zeta(\mathbf{r})$ are given by Eqs. (291) and (292), respectively and the constants are $\gamma = 0.5198421$, $d = 1.709921$, $a_{01} = 0.031097$, $a_{02} = 0.01554535$, $a_{03} = 0.0168869$, $a_{11} = 0.21370$, $a_{12} = 0.20548$, $a_{13} = 0.11125$, $b_{11} = 7.5957$, $b_{12} = 14.1189$, $b_{13} = 10.357$,

$b_{21} = 3.5876$, $b_{22} = 6.1977$, $b_{23} = 3.6231$, $b_{31} = 1.6382$, $b_{32} = 3.3662$, $b_{33} = 0.88026$, $b_{41} = 0.49294$, $b_{42} = 0.62517$, $b_{43} = 0.49671$.

As far as available, we will also list SIC results using the exchange-energy functional given by Eq. (253) and the correlation energy

$$E_{\rm c}^{\rm LDA-SIC}[\{\varphi_{i\sigma}\}] = \int d^3r\rho(\mathbf{r})\varepsilon_{\rm c}^{\rm LDA}[\rho_\uparrow,\rho_\downarrow](\mathbf{r}) - \sum_{\sigma=\uparrow,\downarrow}\sum_{i=1}^{N_\sigma}\int d^3r\rho(\mathbf{r})\varepsilon_{\rm c}^{\rm LDA}[|\varphi_{i\sigma}|^2,0](\mathbf{r}) \quad (303)$$

where $\varepsilon_{\rm c}^{\rm LDA}$ is given by Eq. (297). If the corresponding potential is calculated using the KLI approximation (76), we will denote it by LDA-SICKLI.

4.3.1 Atomic systems

Table 24 shows the total absolute ground-state energies of the first-row atoms. For these systems, there exist accurate estimates of the exact non-relativistic values obtained from experimental ionization energies and improved *ab initio* calculations by Davidson et al. [102]. It is evident from this table, that the density functional methods perform quite well. The mean absolute errors, denoted by $\bar{\triangle}$ and given in the last row of Table 24, clearly show that the KLICS approach is significantly more accurate than the LDA-SICKLI and the conventional Kohn-Sham methods and nearly as accurate as recent CI based quantum chemical results by Montgomery et al. [101]. The situation is similar for second-row atoms, as can be seen from Table 25. As relativistic effects for these atoms are more important and experiments increasingly difficult, the comparison of the calculated values with the Lamb-shift corrected experimental ones from [2] has to be done cautiously and is by no means as rigorous as for first-row atoms. Nevertheless, the values calculated with the KLICS approach mirror these experimental values more closely than the other approximations.

Table 24: *Total absolute ground-state energies for first-row atoms from various self-consistent calculations. Quantum chemistry (QC) values from [101]. $\bar{\triangle}$ denotes the mean absolute deviation from the exact nonrelativistic values [102]. All numbers in atomic units.*

	KLICS	LDA-SICKLI	BLYP	PW91	QC	exact
He	2.9033	2.9198	2.9071	2.9000	2.9049	2.9037
Li	7.4829	7.5058	7.4827	7.4742	7.4743	7.4781
Be	14.6651	14.6953	14.6615	14.6479	14.6657	14.6674
B	24.6564	24.7022	24.6458	24.6299	24.6515	24.6539
C	37.8490	37.9335	37.8430	37.8265	37.8421	37.8450
N	54.5905	54.7295	54.5932	54.5787	54.5854	54.5893
O	75.0717	75.2590	75.0786	75.0543	75.0613	75.067
F	99.7302	99.9995	99.7581	99.7316	99.7268	99.734
Ne	128.9202	129.2868	128.9730	128.9466	128.9277	128.939
$\bar{\triangle}$	0.0047	0.1282	0.0108	0.0114	0.0045	

Table 25: *Total absolute ground-state energies for second-row atoms from various self-consistent calculations.* $\bar{\triangle}$ *denotes the mean absolute deviation from Lamb-shift corrected experimental values, taken from [2]. All numbers in atomic units.*

	KLICS	LDA-SICKLI	BLYP	PW91	experiment
Na	162.256	162.672	162.293	162.265	162.257
Mg	200.062	200.536	200.093	200.060	200.059
Al	242.362	242.891	242.380	242.350	242.356
Si	289.375	289.969	289.388	289.363	289.374
P	341.272	341.930	341.278	341.261	341.272
S	398.128	398.852	398.128	398.107	398.139
Cl	460.164	460.967	460.165	460.147	460.196
Ar	527.553	528.432	527.551	527.539	527.604
$\bar{\triangle}$	0.013	0.624	0.026	0.023	

Table 26: *Absolute exchange energies from various approximations. All values in atomic units.*

	KLICS	LDA-SICKLI	BLYP	PW91
He	1.028	1.031	1.018	1.009
Li	1.784	1.781	1.771	1.758
Be	2.674	2.665	2.658	2.644
B	3.760	3.758	3.727	3.711
C	5.064	5.099	5.028	5.010
N	6.610	6.701	6.578	6.558
O	8.200	8.327	8.154	8.136
F	10.025	10.228	9.989	9.972
Ne	12.110	12.416	12.099	12.082
Na	14.017	14.371	14.006	13.985
Mg	15.997	16.401	15.986	15.967
Al	18.081	18.523	18.053	18.033
Si	20.295	20.787	20.260	20.238
P	22.649	23.196	22.609	22.587
S	25.021	25.618	24.967	24.944
Cl	27.530	28.195	27.476	27.453
Ar	30.192	30.928	30.139	30.116

Table 27: *Absolute correlation energies from various approximations. All values in atomic units.*

	KLICS	LDA-SICKLI	BLYP	PW91
He	0.0416	0.0582	0.0437	0.0450
Li	0.0509	0.0715	0.0541	0.0571
Be	0.0934	0.1169	0.0954	0.0942
B	0.1289	0.1532	0.1287	0.1270
C	0.1608	0.1886	0.1614	0.1614
N	0.1879	0.2232	0.1925	0.1968
O	0.2605	0.2967	0.2640	0.2587
F	0.3218	0.3645	0.3256	0.3193
Ne	0.3757	0.4283	0.3831	0.3784
Na	0.4005	0.4555	0.4097	0.4040
Mg	0.4523	0.5089	0.4611	0.4486
Al	0.4905	0.5502	0.4979	0.4891
Si	0.5265	0.5910	0.5334	0.5322
P	0.5594	0.6314	0.5676	0.5762
S	0.6287	0.7037	0.6358	0.6413
Cl	0.6890	0.7700	0.6955	0.7055
Ar	0.7435	0.8330	0.7515	0.7687

Despite the somewhat larger errors the SIC results constitute a significant improvement over the conventional LDA results which are not shown here. For the latter the mean absolute deviation from the exact data is 0.3813 Hartrees for the first-row atoms and 1.225 Hartrees for the second-row atoms.

For further analysis, we list, in Tables 26 and 27, the values of E_x and E_c separately. Ignoring the LDA-SICKLI results for a moment, the data show two main features: First, the results for E_x are lowest for the KLICS and highest for the PW91 method, while the BLYP-values lie somewhere in between. And second, for E_c, this trend is reversed, as now the KLICS results are highest and the ones from BLYP and PW91 are lower in nearly all cases. In Table 28 we show results of various *x-only* calculations performed with only the exchange-energy parts of the respective functionals. For the spherical atoms listed, there exist exact x-only OEP values [37, 52]. It is evident, that the KLI-approximation gives values much closer to the exact ones than the generalized gradient approximations. From this and from Tables 26 and 27 one may conclude that an error cancellation between exchange and correlation energies occurs in the BLYP and PW91 schemes which leads to rather good total energies. Exchange and correlation energies *separately*, however, are reproduced less accurately in the BLYP and PW91 approaches. In the KLICS scheme,

Table 28: *Total absolute exchange energies of spherical first and second-row atoms for various self-consistent* x-only *calculations. The exact OEP data are from [37, 52]. All values in atomic units.*

	KLI	xLDA-SICKLI	B88	PW91	OEP
He	1.026	1.026	1.016	1.005	1.026
Li	1.781	1.777	1.768	1.754	1.781
Be	2.667	2.658	2.652	2.638	2.666
N	6.603	6.691	6.569	6.547	6.604
Ne	12.099	12.398	12.086	12.061	12.105
Na	14.006	14.355	13.993	13.968	14.013
Mg	15.983	16.383	15.972	15.950	15.988
P	22.633	23.177	22.593	22.565	22.634
Ar	30.174	30.905	30.122	30.089	30.175

Table 29: *Ionization potentials calculated from ground-state-energy differences of first-row atoms. QC values are from [101].* $\bar{\triangle}$ *denotes the mean absolute deviation from the experimental values, taken from [103]. All values in atomic units.*

	KLICS	LDA-SICKLI	BLYP	PW91	QC	exp
He	0.903	0.920	0.912		0.905	0.903
Li	0.203	0.200	0.203	0.207	0.198	0.198
Be	0.330	0.335	0.330	0.333	0.344	0.343
B	0.314	0.327	0.309	0.314	0.304	0.305
C	0.414	0.445	0.425	0.432	0.413	0.414
N	0.527	0.565	0.542	0.551	0.534	0.534
O	0.495	0.520	0.508	0.505	0.499	0.500
F	0.621	0.673	0.656	0.660	0.639	0.640
Ne	0.767	0.825	0.808	0.812	0.792	0.792
$\bar{\triangle}$	0.009	0.022	0.010	0.014	0.001	

both exchange and correlation energies are of high quality. As far as the LDA-SICKLI approach is concerned, both exchange and correlation energies are too low. Therefore, no error cancellation occurs leading to rather large errors in the total energies.

Limitations of the DFT approaches become evident for ionization potentials and electron affinities. In Tables 29 and 30 we show ionization potentials calculated from ground-state-energy differences and QC values from [101] as well as experimental ones from [103].

Table 30: *Ionization potentials calculated from ground-state-energy differences of second-row atoms.* $\bar{\triangle}$ *denotes the mean absolute deviation from the experimental values, taken from [103]. All values in atomic units.*

	KLICS	LDA-SICKLI	BLYP	PW91	experiment
Na	0.191	0.195	0.197	0.198	0.189
Mg	0.275	0.284	0.280	0.281	0.281
Al	0.218	0.222	0.212	0.221	0.220
Si	0.294	0.307	0.294	0.305	0.300
P	0.379	0.392	0.376	0.389	0.385
S	0.380	0.394	0.379	0.379	0.381
Cl	0.471	0.495	0.476	0.482	0.477
Ar	0.575	0.595	0.576	0.583	0.579
$\bar{\triangle}$	0.004	0.009	0.005	0.004	

The performance of the KLICS, B88 and PW91 methods is similar, while the LDA-SICKLI scheme leads to results showing a mean absolute deviation from the experimental values which is roughly twice as large as for any of the other DFT methods. On the whole, QC calculations lead to clearly better results. Somewhat surprisingly, the DFT methods work better for the second-row than for the first-row atoms.

In *exact* DFT, the highest occupied orbital energy of the neutral atom is identical with the ionization potential, while for negative ions the highest occupied energy level coincides with the electron affinity of the neutral atom [47]. How well ionization potentials and electron affinities are reproduced by the highest occupied energy eigenvalues resulting from an *approximate* xc functional is therefore a measure of the quality of the xc potential. Table 31 shows the ionization energies obtained from the highest occupied single-particle-energy eigenvalue of the neutral atoms. For the BLYP and PW91 approaches the resulting values are much worse than the ones in Table 29 and 30. The deviation from experiment is around 100 percent for all atoms. This is due to the incorrect asymptotic behavior of the BLYP and PW91 potentials. The KLICS and LDA-SICKLI potentials, on the other hand, have the correct $-1/r$ behavior for large r and the resulting highest occupied orbital energies are much closer to the experimental ionization potentials. Nevertheless, the KLICS values obtained from ground-state-energy differences (see Tables 29 and 30) are considerably more accurate.

For electron affinities, the situation is much worse, as may be seen from Tables 32 and 33. First of all, because of the wrong asymptotic behavior of the xc potential for large r, there is no convergence for negative ions within the self-consistent BLYP and PW91 schemes. This is not the case for the KLICS and LDA-SICKLI approaches. However, the resulting electron affinities obtained either from ground-state-energy differences or from the highest orbital energies of negative ions are far less accurate than the ionization energies.

Table 31: *Ionization potentials from the highest occupied orbital energy of neutral atoms.* $\bar{\triangle}$ *denotes the mean absolute deviation from the experimental (exp) values, taken from [103]. All values in atomic units.*

	KLICS	LDA-SICKLI	BLYP	PW91	exp
He	0.945	0.948	0.585	0.583	0.903
Li	0.200	0.197	0.111	0.119	0.198
Be	0.329	0.329	0.201	0.207	0.343
B	0.328	0.306	0.143	0.149	0.305
C	0.448	0.427	0.218	0.226	0.414
N	0.579	0.550	0.297	0.308	0.534
O	0.559	0.527	0.266	0.267	0.500
F	0.714	0.686	0.376	0.379	0.640
Ne	0.884	0.843	0.491	0.494	0.792
Na	0.189	0.190	0.106	0.113	0.189
Mg	0.273	0.275	0.168	0.174	0.281
Al	0.222	0.205	0.102	0.112	0.220
Si	0.306	0.287	0.160	0.171	0.300
P	0.399	0.371	0.219	0.233	0.385
S	0.404	0.383	0.219	0.222	0.381
Cl	0.506	0.481	0.295	0.301	0.477
Ar	0.619	0.580	0.373	0.380	0.579
$\bar{\triangle}$	0.030	0.016	0.183	0.177	

The KLICS method even gives the wrong sign for the Boron atom if the electron affinity is calculated from the ground-state-energy differences. On average, the values obtained from ground-state-energy differences are more accurate than the results obtained from the highest occupied orbital energies. Comparing the KLICS with the LDA-SICKLI results, the latter are slightly better on average. The fact that the KLICS and LDA-SICKLI approaches allow for a fully self-consistent calculation of electron affinities is encouraging, but the poor accuracy of the results clearly shows that the xc potentials need further improvement. Here, quantum-chemical approaches are definitely superior.

Two-electron systems The CS and LDA-SIC correlation functionals may be studied more thoroughly in two-electron atoms. There are two reasons for this: First of all, as pointed out above, the solution of the full OEP integral equation for these systems is identical to the one obtained from the KLI-scheme. Furthermore, the exact exchange-energy functional (27) is identical with $E_{\rm x}^{\rm LDA-SIC}$ for spin-saturated two-electron systems,

Table 32: *Self-consistent electron affinities for first-row atoms. QC values are from [101] and experimental (exp) values from [103].* $\bar{\delta}$ *denotes the mean value of* $|A_{\mathrm{DFT}} - A_{\mathrm{exp}}|/|A_{\mathrm{exp}}|$. *All values in atomic units.*

	KLICS[a]	KLICS[b]	LDA-SICKLI[a]	LDA-SICKLI[b]	QC	exp
Li	0.016	0.024	0.021	0.025	0.023	0.023
B	-0.002	0.033	0.025	0.028	0.008	0.010
C	0.028	0.083	0.062	0.073	0.045	0.046
O	0.017	0.110	0.065	0.100	0.052	0.054
F	0.082	0.208	0.138	0.189	0.125	0.125
$\bar{\delta}$	50.5	97.0	44.8	76.8	5.2	

[a] *from ground-state-energy differences*
[b] *from the highest occupied orbital energies of the negative ions.*

Table 33: *Self-consistent electron affinities for second-row atoms. Experimental (exp) values are from [103].* $\bar{\delta}$ *denotes the mean value of* $|A_{\mathrm{DFT}} - A_{\mathrm{exp}}|/|A_{\mathrm{exp}}|$. *All values in atomic units.*

	KLICS[a]	KLICS[b]	LDA-SICKLI[a]	LDA-SICKLI[b]	exp
Na	0.015	0.022	0.021	0.024	0.020
Al	0.007	0.024	0.023	0.020	0.016
Si	0.040	0.065	0.058	0.054	0.051
P	0.022	0.048	0.038	0.041	0.027
S	0.065	0.106	0.092	0.095	0.076
Cl	0.122	0.174	0.147	0.151	0.133
$\bar{\delta}$	24.0	39.3	22.5	23.5	

[a] *from ground-state-energy differences*
[b] *from the highest occupied orbital energies of the negative ions.*

so that the only error made is due to the approximation for E_c. Secondly there exist practically exact solutions [7] of the two-particle Schrödinger equation. Hence the various DFT-related quantities of interest can be compared with exact results.

In Table 34 we show total absolute ground-state energies of the atoms isoelectronic with helium. The exact nonrelativistic results in the last column are taken from [102]. Note that there is no convergence for negative ions in the conventional Kohn Sham method. In Figure 10, we have plotted the errors $E_{\mathrm{tot}}^{\mathrm{DFT}} - E_{\mathrm{tot}}^{\mathrm{exact}}$ corresponding to the numbers in Table 34. It is obvious that the KLICS scheme gives superior results, the mean absolute

Table 34: *Total absolute ground-state energies for the Helium-isoelectronic series from various self-consistent calculations.* $\bar{\triangle}$ *denotes the mean absolute deviation from the exact values from [102] . All numbers in atomic units.*

	KLICS	LDA-SICKLI	BLYP	PW91	exact
H^-	0.5189	0.5263			0.5278
He	2.9033	2.9198	2.9071	2.9000	2.9037
Li^+	7.2803	7.3057	7.2794	7.2676	7.2799
Be^{2+}	13.6556	13.6886	13.6500	13.6340	13.6556
B^{3+}	22.0301	22.0698	22.0200	21.9996	22.0310
C^{4+}	32.4045	32.4499	32.3896	32.3649	32.4062
N^{5+}	44.7788	44.8293	44.7592	44.7299	44.7814
O^{6+}	59.1531	59.2081	59.1286	59.0948	59.1566
F^{7+}	75.5274	75.5864	75.4981	75.4595	75.5317
Ne^{8+}	93.9017	93.9644	93.8675	93.8241	93.9068
Na^{9+}	114.2761	114.3422	114.2369	114.1886	114.2819
Mg^{10+}	136.6505	136.7197	136.6064	136.5531	136.6569
Al^{11+}	161.0250	161.0970	160.9758	160.9175	161.0320
Si^{12+}	187.3995	187.4742	187.3453	187.2819	187.4070
P^{13+}	215.7740	215.8512	215.7147	215.6462	215.7821
S^{14+}	246.1485	246.2281	246.0842	246.0105	246.1571
Cl^{15+}	278.5231	278.6049	278.4536	278.3748	278.5322
Ar^{16+}	312.8977	312.9816	312.8231	312.7390	312.9072
K^{17+}	349.2723	349.3582	349.1926	349.1032	349.2822
Ca^{18+}	387.6470	387.7347	387.5620	387.4674	387.6572
$\bar{\triangle}$	0.0053	0.0533	0.0450	0.0943	

error $\bar{\triangle}$ being smaller by an order of magnitude compared to the LDA-SICKLI and the two conventional Kohn-Sham approaches.

In Table 35 we have listed the highest occupied orbital energies for the two-electron series as obtained from various *self-consistent* calculations. Comparing the results with the exact values it is obvious that the KLICS and LDA-SICKLI schemes perform much better than the conventional Kohn-Sham approaches. The difference is less pronounced for the highly charged ions as the nuclear potential becomes more and more dominant as Z increases. A glance at the second column, in which we give the corresponding values from an *x-only* KLI calculation employing the exact functional (27), shows that the superior quality is due to the inclusion of the exact exchange in the KLI scheme leading to the correct asymptotic behavior of the KS potential. In fact, adding the CS correlation potential

Table 35: *Absolute highest occupied orbital energies from various self consistent calculations. Exact values calculated from [102]. All values in atomic units.*

	KLI	KLICS	LDA-SICKLI	BLYP	PW91	exact
	x-only	xc	xc	xc		
He	0.9180	0.9446	0.9481	0.5849	0.5833	0.9037
Li^{+}	2.7924	2.8227	2.8293	2.2312	2.2269	2.7799
Be^{2+}	5.6671	5.6992	5.6556	4.8760	4.8701	5.6556
B^{3+}	9.5420	9.5751	9.5871	8.5201	8.5129	9.5310
C^{4+}	14.4169	14.4507	14.4648	13.1638	13.1554	14.4062
N^{5+}	20.2918	20.3261	20.3421	18.8072	18.7978	20.2814
O^{6+}	27.1668	27.2014	27.2191	25.4504	25.4401	27.1566
F^{7+}	35.0418	35.0766	35.0959	33.0935	33.0823	35.0317
Ne^{8+}	43.9167	43.9517	43.9725	41.7366	41.7245	43.9068
Na^{9+}	53.7917	53.8269	53.8489	51.3796	51.3666	53.7819
Mg^{10+}	64.6667	64.7020	64.7252	62.0225	62.0086	64.6569
Al^{11+}	76.5417	76.5770	76.6015	73.6654	73.6506	76.5320
Si^{12+}	89.4167	89.4521	89.4776	86.3083	86.2926	89.4071
P^{13+}	103.2917	103.3272	103.3536	99.9511	99.9345	103.2821
S^{14+}	118.1666	118.2022	118.2296	114.5939	114.5764	118.1571
Cl^{15+}	134.0416	134.0773	134.1055	130.2367	130.2183	134.0322
Ar^{16+}	150.9166	150.9523	150.9814	146.8795	146.8602	150.9072
K^{17+}	168.7916	168.8273	168.8572	164.5223	164.5021	168.7822
Ca^{18+}	187.6666	187.7024	187.7330	183.1650	183.1439	187.6572

worsens the results, as may be seen by comparing the second and third columns: The correlation contribution lowers the already too small values from the x-only calculations for the highest occupied orbital energy even more. This indicates that the CS correlation potential has the wrong sign in the physically relevant regions of space. As the x-only LDA-SICKLI is identical with the x-only KLI scheme for these systems, the same conclusion can be drawn for the LDA-SICKLI correlation potential.

These findings are confirmed by Figure 11 where we plot the exact [7] and various self-consistent correlation potentials. It is evident that the approximate potentials show very large deviations from the exact one. In the region where most of the charge density is located, the approximate correlation potentials have the wrong sign. Furthermore, the potentials obtained with the CS functional within the KLICS scheme and the two conventional Kohn-Sham approximations exhibit spurious divergences at the origin. These may be traced back to gradients of the density and of the one-particle orbitals occurring in these correlation energy functionals. As the LDA-SICKLI functional does not contain any den-

sity gradients, these divergences are not found for the LDA-SICKLI potential. The need for further improvement of the correlation energy functionals in these respects is obvious.

Beryllium and Neon isoelectronic series For further analysis we have calculated the total ground state energies of positive ions isoelectronic with Beryllium (shown in Table 36) and Neon (shown in Table 37). Again, we compare various self-consistent DFT methods with exact data from Ref. [91] and plot the errors in Figures 12 and 13, respectively. The data for both series show the same trends: The overall best results are obtained with the KLICS scheme, where the absolute total and relative mean deviations from the exact values are smallest. The BLYP scheme is only slightly worse, but the PW91 functional gives errors almost twice as large as the other DFT approaches. From the plots in Figures 12 and 13 it is obvious that these statements hold for most ions individually.

There are two other trends worth noting: (a) While the absolute errors rise within the isoelectronic series as the atomic number increases, the percentage errors remain almost constant. (b) The mean absolute error is smaller by almost an order of magnitude for the ten-electron series compared to the four-electron series.

The ionization potentials from the various approaches as calculated from the highest occupied orbital energies are shown in Tables 38 and 39 for the four- and ten-electron series, respectively. The exact nonrelativistic values have been calculated from the data given in [91]. Owing to the correct asymptotic behavior of the KLICS potential it comes as no surprise that the KLICS data are superior to the ones obtained from the conventional Kohn-Sham approaches. The effect of the correlation potential within the OEP scheme is – like in the two-electron case – a lowering of the energy eigenvalue of the highest occupied orbital. This is seen by comparing the second and third columns showing the OEP results in x-only approximation and with inclusion of CS correlation in the KLI scheme, respectively. In contrast to the Helium and Neon isoelectronic series, this effect improves the quality of the results in the Beryllium isoelectronic series. We mention that the ionization potentials are in much better agreement with the exact results when calculated as ground-state energy differences.

4.3.2 Diatomic molecules

To examine the effect of correlation contributions, we have implemented the CS correlation-energy functional (279) in our fully numerical basis-set-free code for diatomic molecules [104]. For comparison, we have also performed calculations employing the conventional LDA [100] and the PW91 functional for $E_{\rm xc}$.

To demonstrate the accuracy of our implementation, we compare results for the Neon atom obtained with our molecular code with the ones from our one-dimensional atomic structure program in table 40. The deviation from the exact results obtained with the atomic code is a few μHartrees at most.

Ground-state properties of the closed-shell-first-row dimers and hydrides were calculated using the approximations mentioned above in a fully self-consistent fashion. As our program uses no basis functions, the results are free of basis-set truncation and basis-set superposition errors. Where available, we have also included HF results obtained with conventional codes using basis-set expansions. Therefore, the comparisons between DFT and HF results in Tables 41, 43 and 44 have to be interpreted with due care.

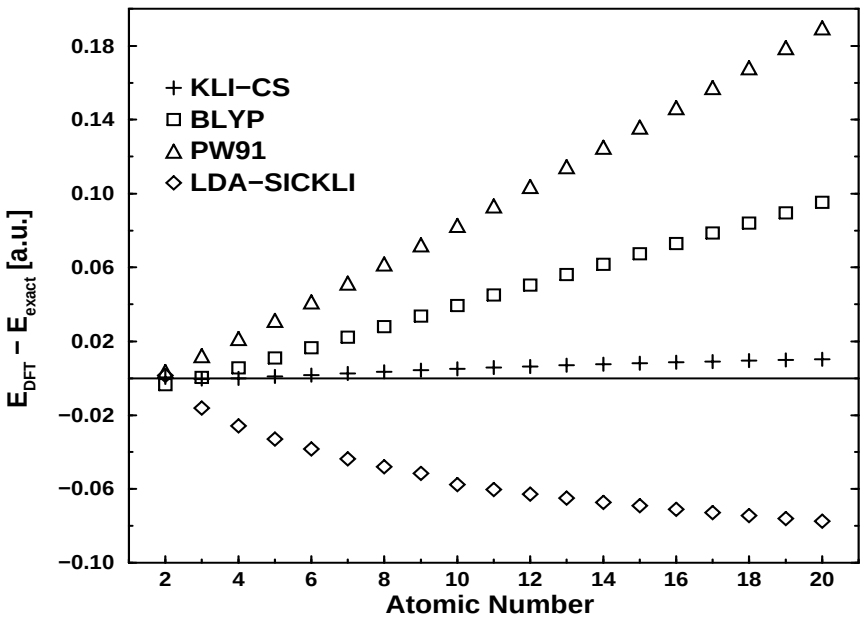

Figure 10: *Energy differences corresponding to Table 34.*

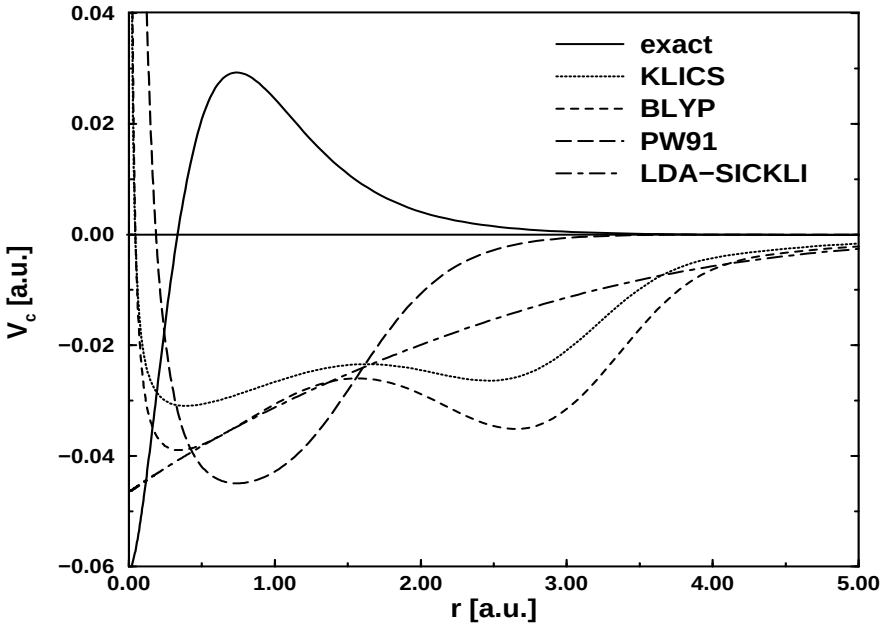

Figure 11: *Comparison of the exact and self consistently calculated correlation potentials of helium. Exact potential from [7].*

In Table 41 we display results for the bond lengths. It is apparent that the KLICS scheme leads to equilibrium distances which are generally too short, an effect present in

Table 36: *Total absolute ground-state energies for the Beryllium-isoelectronic series from various self-consistent calculations.* $\bar{\triangle}$ *denotes the mean absolute deviation from the exact values from [91] and* $\bar{\delta}$ *denotes* $|E_{\rm tot}^{\rm DFT} - E_{\rm tot}^{\rm exact}|/|E_{\rm tot}^{\rm exact}|$. *All numbers in atomic units.*

	KLICS	BLYP	PW91	exact
Be	14.6651	14.6615	14.6479	14.6674
B^{+}	24.3427	24.3366	24.3160	24.3489
C^{2+}	36.5224	36.5143	36.4881	36.5349
N^{3+}	51.2025	51.1927	51.1618	51.2228
O^{4+}	68.3825	68.3713	68.3362	68.4117
F^{5+}	88.0624	88.0499	88.0110	88.1011
Ne^{6+}	110.2420	110.2285	110.1859	110.2909
Na^{7+}	134.9216	134.9071	134.8610	134.9809
Mg^{8+}	162.1010	162.0857	162.0361	162.1710
Al^{9+}	191.7803	191.7642	191.7113	191.8613
Si^{10+}	223.9595	223.9427	223.8864	224.0516
P^{11+}	258.6387	258.6212	258.5616	258.7420
S^{12+}	295.8178	295.7996	295.7367	295.9324
Cl^{13+}	335.4968	335.4781	335.4119	335.6229
Ar^{14+}	377.6758	377.6566	377.5870	377.8134
K^{15+}	422.3548	422.3350	422.2621	422.5040
Ca^{16+}	469.5338	469.5134	469.4372	469.6946
Sc^{17+}	519.2127	519.1919	519.1122	519.3851
Ti^{18+}	571.3917	571.3703	571.2873	571.5757
V^{19+}	626.0708	626.0487	625.9623	626.2663
Cr^{20+}	683.2497	683.2271	683.1373	683.4570
Mn^{21+}	742.9286	742.9056	742.8123	743.1476
Fe^{22+}	805.1074	805.0840	804.9873	805.3382
Co^{23+}	869.7863	869.7624	869.6623	870.0289
Ni^{24+}	936.9652	936.9408	936.8373	937.2195
$\bar{\triangle}$	0.1183	0.1352	0.1973	
$\bar{\delta}$	0.0351	0.0443	0.0755	

the HF approximation as well. Most notable is the fact that the potential energy curve of Be_2 displays no local minimum in this approximation. Good agreement with experiment

Table 37: *Total absolute ground-state energies for the Neon-isoelectronic series from various self-consistent calculations.* $\bar{\triangle}$ *denotes the mean absolute deviation from the exact values from [91] and* $\bar{\delta}$ *denotes* $|E_{\rm tot}^{\rm DFT} - E_{\rm tot}^{\rm exact}|/|E_{\rm tot}^{\rm exact}|$. *All numbers in atomic units.*

	KLICS	BLYP	PW91	exact
Ne	128.9202	128.9730	128.9466	128.9376
Na^{+}	162.0645	162.0956	162.0668	162.0659
Mg^{2+}	199.2291	199.2448	199.2136	199.2204
Al^{3+}	240.4071	240.4102	240.3768	240.3914
$Si^{4}+$	285.5945	285.5867	285.5509	285.5738
P^{5+}	334.7888	334.7712	334.7331	334.7642
S^{6+}	387.9885	387.9616	387.9212	387.9608
Cl^{7+}	445.1922	445.1567	445.1138	445.1622
Ar^{8+}	506.3993	506.3554	506.3101	506.3673
K^{9+}	571.6091	571.5570	571.5092	571.5754
Ca^{10+}	640.8211	640.7610	640.7107	640.7861
Sc^{11+}	714.0350	713.9671	713.9141	713.9988
Ti^{12+}	791.2504	791.1748	791.1191	791.2132
V^{13+}	872.4671	872.3839	872.3255	872.4291
Cr^{14+}	957.6850	957.5942	957.5331	957.6463
Mn^{15+}	1046.9039	1046.8056	1046.7417	1046.8646
Fe^{16+}	1140.1237	1140.0179	1139.9511	1140.0838
Co^{17+}	1237.3440	1237.2309	1237.1613	1237.3039
Ni^{18+}	1338.5652	1338.4447	1338.3722	1338.5247
$\bar{\triangle}$	0.0293	0.0334	0.0694	
$\bar{\delta}$	0.0054	0.0067	0.0097	

is found only for Li_2. Except for this molecule, the PW91 values are clearly superior. In most cases even the LDA results are better than the KLICS values. With the exception of Li_2 and C_2, the GGA reduces the error of the LDA significantly.

Total absolute ground-state energies calculated at the bond lengths given in Table 41 are shown in Table 42. The exact values for the dimers are from [90], for the hydrides they are calculated by the same method using the exact nonrelativistic atomic ground-state energies in [91] and the experimental dissociation energies in [106]. For the lighter molecules H_2, Li_2, Be_2, LiH and BH the KLICS and PW91 results are of the same good quality, yielding errors of a few mHartrees. For the heavier molecules, however, the KLICS results are worse. Being the simplest approximation, it is not surprising that the LDA gives values for the total energies which show the largest errors.

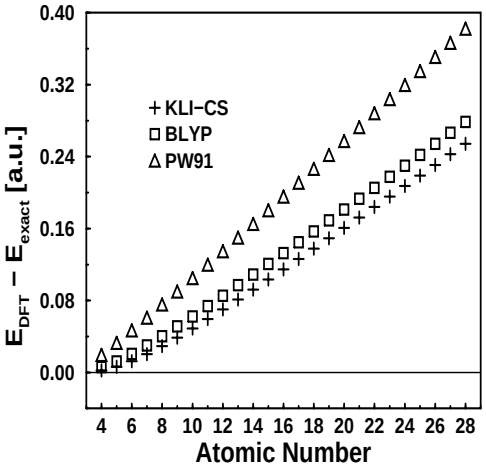

Figure 12: *Energy differences corresponding to Table 36.*

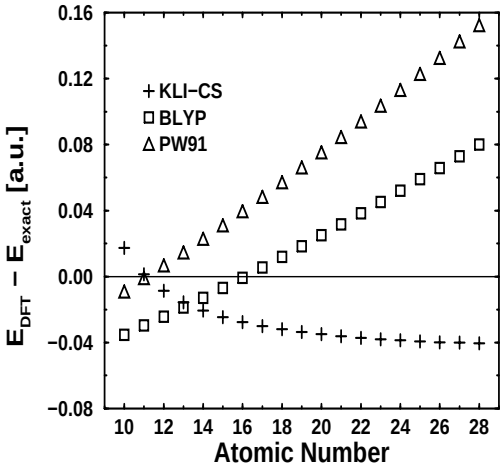

Figure 13: *Energy differences corresponding to Table 37.*

Apart from H_2 and LiH, the dissociation energies obtained within the KLICS approach are disappointing, as may be seen in Table 43. In most cases, the magnitude is underestimated considerably and for Be_2 and F_2 even the wrong sign is obtained. Since the corresponding *atomic* ground-state energies given in the previous section are of excellent quality, the error must be due to correlation effects present in molecules only. In particular, the left-right correlation error [110] well-known in HF theory also occurs in DFT when the exact Fock expression (27) for E_x is employed. Apparently, the error is not sufficiently corrected for by the CS functional. The LDA and PW91 results are clearly much better, the latter reducing the over-binding tendencies of the former.

Despite these shortcomings, the KLICS xc potential is of better quality than the conventional xc potentials. In Table 44 we list the absolute values of the highest occupied molecular orbital energies. In an *exact* implementation their values should be equal to the ionization potentials of the systems under consideration. It is evident that the conventional KS approaches represented by the LDA and PW91 functionals yield results which are typically 40 percent too high, while the KLICS values are much closer to the experimental results. As for atomic systems, this fact may be traced back to the correct asymptotic behavior of the KLICS xc potential for large r. In order to examine the quality of the KLICS potential in the region closer to the nuclei, we compare the orbital energies of FH obtained using the various DFT approximations with results from the Zhao-Parr (ZP) method [5] in Table 45. This scheme allows for the calculation of the Kohn-Sham potential which uniquely corresponds to a given density. Ingamells et. al. [10] have used accurate densities obtained within the coupled cluster approach and determined the orbital energies of FH shown in the last column of Table 45. Although these values are expected to be close to the exact ones, they still contain some errors. For example, the energy of the highest molecular orbital, -0.5996 Hartrees, is not equal to the experimentally observed ionization potential of -0.5894 Hartrees. Nevertheless, it is evident from the table that the KLICS results are much closer to the ZP values than the ones from the conventional DFT approaches. We

Table 38: *Ionization potentials from highest occupied Kohn-Sham orbital energies for the Beryllium-isoelectronic series from various self-consistent calculations. Exact nonrelativistic values calculated from [91] . All numbers in atomic units.*

	KLI	KLICS	BLYP	PW91	exact
	x-only	xc	xc	xc	
Be	0.3089	0.3294	0.2009	0.2072	0.3426
B^{+}	0.8732	0.8992	0.7129	0.7185	0.9243
C^{2+}	1.6933	1.7226	1.4804	1.4856	1.7594
N^{3+}	2.7659	2.7975	2.5000	2.5049	2.8459
O^{4+}	4.0898	4.1231	3.7706	3.7754	4.1832
F^{5+}	5.6644	5.6991	5.2918	5.2964	5.7708
Ne^{6+}	7.4896	7.5253	7.0633	7.0678	7.6087
Na^{7+}	9.5652	9.6017	9.0850	9.0894	9.6967
Mg^{8+}	11.8910	11.9281	11.3569	11.3611	12.0348
Al^{9+}	14.4669	14.5047	13.8788	13.8829	14.6230
Si^{10+}	17.2930	17.3312	16.6508	16.6548	17.4613
P^{11+}	20.3692	20.4078	19.6729	19.6768	20.5496
S^{12+}	23.6955	23.7345	22.9450	22.9487	23.8880
Cl^{13+}	27.2718	27.3111	26.4671	26.4707	27.4763
Ar^{14+}	31.0982	31.1378	30.2393	30.2427	31.3147
K^{15+}	35.1747	35.2145	34.2615	34.2647	35.4031
Ca^{16+}	39.5012	39.5412	38.5336	38.5367	39.7416
Sc^{17+}	44.0777	44.1179	43.0558	43.0587	44.3300
Ti^{18+}	48.9043	48.9447	47.8280	47.8307	49.1684
V^{19+}	53.9808	54.0214	52.8502	52.8527	54.2569
Cr^{20+}	59.3074	59.3481	58.1224	58.1247	59.5954
Mn^{21+}	64.8840	64.9249	63.6447	63.6467	65.1838
Fe^{22+}	70.7107	70.7516	69.4169	69.4187	71.0223
$Co^{23}+$	76.7873	76.8284	75.4391	75.4408	77.1108
Ni^{24+}	83.1140	83.1551	81.7113	81.7128	83.4493

conclude that the KLICS potential is a better approximation to the exact KS potential than any of the conventional approximations.

Table 39: *Ionization potentials from highest occupied Kohn-Sham orbital energies for the Neon-isoelectronic series from various self-consistent calculations. Exact nonrelativistic values calculated from [91]. All numbers in atomic units.*

	KLI	KLICS	BLYP	PW91	exact
	x-only	xc	xc	xc	
Ne	0.8494	0.8841	0.4914	0.4942	0.7945
Na^{+}	1.7959	1.8340	1.3377	1.3416	1.7410
Mg^{2+}	3.0047	3.0450	2.4531	2.4579	2.9499
Al^{3+}	4.4706	4.5125	3.8285	3.8339	4.4161
Si^{4+}	6.1912	6.2343	5.4601	5.4661	6.1371
P^{5+}	8.1651	8.2091	7.3458	7.3524	8.1112
S^{6+}	10.3914	10.4362	9.4846	9.4917	10.3378
Cl^{7+}	12.8696	12.9150	11.8757	11.8832	12.8162
Ar^{8+}	15.5992	15.6451	14.5185	14.5264	15.5460
K^{9+}	18.5800	18.6263	17.4126	17.4209	18.5270
Ca^{10+}	21.8118	21.8585	20.5579	20.5665	21.7589
Sc^{11+}	25.2943	25.3413	23.9541	23.9630	25.2416
Ti^{12+}	29.0274	29.0747	27.6010	27.6102	28.9748
V^{13+}	33.0112	33.0587	31.4986	31.5080	32.9586
$Cr^{14}+$	37.2453	37.2931	35.6467	35.6563	37.1929
Mn^{15+}	41.7299	41.7779	40.0453	40.0551	41.6776
$Fe^{16}+$	46.4649	46.5130	44.6943	44.7042	46.4126
Co^{17+}	51.4501	51.4984	49.5936	49.6037	51.3979
Ni^{18+}	56.6856	56.7341	54.7432	54.7535	56.6335

4.4 Solids

Few calculations applying OEP or KLI methods to solids have been reported in the literature [39, 40, 111, 112, 113, 114, 115, 116, 117, 118]. In this section we concentrate on materials for which more than one calculation has been reported, i.e. on Si, Ge and diamond. In Table 46 we show the energy gaps for Si at various high-symmetry points in the Brillouin zone. The results have been obtained with different computational techniques for the band structure calculation but they all make use of the exact, orbital-dependent exchange energy functional combined with the correlation energy functional in LDA. KKR-ASA denotes the Korringa-Kohn-Rostoker method in the atomic sphere approximation (ASA), LMTO-ASA is a linear-muffin-tin-orbital calculation in the same (ASA) approximation. Furthermore

Table 40: *Results for the Neon atom using various DFT approaches. 1D denotes the exact values obtained with our one-dimensional code, 2D the results from our 2D code with a bond distance of 1 a.u. and one nuclear charge set to zero. 1D calculations performed with a grid size of 800 points, 2D calculations with a grid size of 145 × 241 points. All numbers in atomic units.*

	KLICS		PW91		xcLDA	
	1D	2D	1D	2D	1D	2D
E_{tot}	-128.920235	-128.920234	-128.946580	-128.946580	-128.229914	-128.229915
ε_{1s}	-30.841442	-30.841447	-30.507920	-30.507920	-30.305770	-30.305770
ε_{2s}	-1.741044	-1.741044	-1.334970	-1.334970	-1.322601	-1.322601
$\varepsilon_{2p\sigma}$	-0.884057	-0.884057	-0.494228	-0.494228	-0.497847	-0.497847
$\varepsilon_{2p\pi}$	-0.884057	-0.884057	-0.494228	-0.494228	-0.497847	-0.497847
$< \frac{1}{r} >$	3.111736	3.111751	3.110075	3.110091	3.099824	3.099840
$< r >$	0.787235	0.787235	0.799878	0.799878	0.801547	0.801547
$< r^2 >$	0.931987	0.931987	0.982608	0.982608	0.985199	0.985200

Table 41: *Calculated bond lengths of the closed-shell-first-row dimers and hydrides. HF values taken from [105]. Experimental values from [106] except where noted. All values in atomic units. Taken from [104].*

	KLICS	PW91	xcLDA	HF	experiment
H_2	1.378	1.414	1.446	1.379	1.401[a]
Li_2	5.086	5.153	5.120	5.304	5.051
Be_2	-[b]	4.588	4.522	-	4.63[c]
C_2	2.306	2.367	2.354	-	2.3481
N_2	1.998	2.079	2.068	2.037	2.074
F_2	2.465	2.669	2.615	2.542	2.6682
LiH	2.971	3.030	3.030	3.092	3.0154
BH	2.274	2.356	2.373	-	2.3289
FH	1.684	1.756	1.761	1.722	1.7325

[a] *Exact value from [107]*
[b] *There is no local minimum in the electronic potential curve.*
[c] *From [90]*

Table 42: *Absolute total ground-state energies of the closed-shell-first-row dimers and hydrides calculated at the bond lengths given in Table 41. Estimates for exact values calculated using dissociation energies from Table 43 and nonrelativistic, infinite nuclear mass atomic ground-state energies from [91]. All numbers in atomic units. Taken from [104].*

	KLICS	PW91	xcLDA	exact
H_2	1.171444	1.170693	1.137692	1.174448[a]
Li_2	14.9982	14.9819	14.7245	14.9954
Be_2	29.3197[b]	29.3118	28.9136	29.3385
C_2	75.7736	75.8922	75.2041	75.922
N_2	109.4683	109.5449	108.6959	109.5424
F_2	199.4377	199.5699	198.3486	199.5299
LiH	8.0723	8.0625	7.9189	8.0705
BH	25.2857	25.2688	24.9770	25.29
FH	100.4241	100.4715	99.8490	100.4596

[a] *Exact value from [107]*
[b] *Calculated at the experimental bond length of 4.63 a.u.*

Table 43: *Dissociation energies of the closed-shell-first-row dimers and hydrides calculated at the bond lengths given in Table 41. HF values taken from [105]. All numbers in mHartrees. Taken from [104].*

	KLICS	PW91	xcLDA	HF	experiment
H_2	171.444	167.665	180.270	121.0	174.475[b]
Li_2	32.4	33.5	37.9	3.5	39.3[c]
Be_2	-10.5[a]	15.9	20.6	-	3.8[c]
C_2	75.6	239.2	267.5	-	232[d]
N_2	287.3	387.5	427.1	167.5	364.0[d]
F_2	-22.7	106.7	126.2	-54.7	62.1[d]
LiH	89.4	86.8	96.9	48.4	92.4[d]
BH	129.3	137.4	145.8	-	135[e]
FH	193.9	238.4	259.1	130.8	225.7[e]

[a] *Calculated at the experimental bond length 4.63 a.u.*
[b] *Exact value from [107]*
[c] *From [90]*
[d] *From [106]*
[e] *From [108]*

Table 44: *Absolute values for the highest occupied orbital energies of the closed-shell-first-row dimers and hydrides calculated at the bond lengths given in Table 41. Experimental values are the ionization potentials taken from [106]. All numbers in atomic units. Taken from [104].*

	KLICS	PW91	xcLDA	experiment
H_2	0.621563	0.382656	0.373092	0.5669
Li_2	0.1974	0.1187	0.1187	0.18
Be_2	0.2560[a]	0.1678	0.1660	-
C_2	0.4844	0.2942	0.2987	0.4465
N_2	0.6643	0.3804	0.3826	0.5726
F_2	0.6790	0.3512	0.3497	0.5764
LiH	0.3237	0.1621	0.1612	0.283[b]
BH	0.3692	0.2058	0.2041	0.359
FH	0.6803	0.3567	0.3594	0.5894

[a] *Calculated at the experimental bond length 4.63 a.u.*
[b] *From [109]*

Table 45: *Kohn-Sham orbital energies for FH using a bond length of* 1.6373 *a.u. ZP denotes results from the Zhao-Parr method using accurate densities from coupled cluster calculations, taken from [10]. These numbers are close to the exact ones. All values in atomic units.*

	KLICS	PW91	xcLDA	ZP
$\varepsilon_{1\sigma}$	-24.5479	-24.2671	-24.0863	-24.6209
$\varepsilon_{2\sigma}$	-1.4492	-1.1234	-1.1114	-1.3732
$\varepsilon_{3\sigma}$	-0.8220	-0.5080	-0.5085	-0.7418
$\varepsilon_{1\pi}$	-0.6835	-0.3622	-0.3655	-0.5996

we report several calculations using pseudopotentials (PP). The abbreviations EXX and KLI stand for exact exchange and KLI exchange, both combined with LDA correlation.

For comparison, we show in Table 47 the LDA gaps obtained with the same computational methods. This comparison serves two purposes: first it can be seen that the LDA band gaps from the different methods agree pretty well. In contrast, the corresponding EXX (and KLI) band gaps show somewhat larger discrepancies among each other, although the agreement is still reasonable. Second we recognize the general trend of the EXX and KLI calculations to enhance the gaps significantly over the LDA values, thus achieving considerably better agreement with the experimental results. This can be attributed to the fact that EXX and KLI calculations have no self-interaction errors in the exchange potentials. Comparison of the results of the KLI calculation (column 5 of Table 46) with the exact exchange calculations obtained by also employing a local pseudopotential (column 3 of Table 46) suggests that the KLI approximation yields somewhat smaller band gaps than exact exchange.

In Tables 48 and 49 we report band gaps for Ge and diamond, respectively. The general findings from the calculations on Si are preserved in both cases: compared to LDA the band gaps obtained with exact exchange are significantly enhanced, but not as much as for Si.

Städele et.al. [118] also studied the x-only derivative discontinuity which should be taken into account in a rigorous calculation of the band gap (see Eq. (179)). They found that this discontinuity is roughly twice as large as the Kohn-Sham band gap obtained by simply taking the difference of the KS eigenvalues. This leads to total gaps close to the Hartree-Fock band gaps. The discontinuity in the correlation potential must therefore cancel a large part of the exchange discontinuity to reproduce the experimentally observed gaps. This demonstrates the importance of finding a good, orbital-dependent correlation energy functional. LDA correlation has no discontinuity and is therefore not able to do this job.

All the calculations discussed so far employed the exact exchange energy functional combined with LDA correlation. Städele et.al. [118] also performed a self-consistent exchange-only calculation, i.e. employing the exact exchange potential without adding any correlation potential. The resulting exchange potential, being the exact exchange potential of x-only DFT, was compared for silicon with approximate exchange functionals. Their results are shown in Fig. 14. In the physically important bonding region between the

Si atoms the LDA potential significantly underestimates the spatial variations of the exact exchange. In this region the GGA exchange potential of Becke [75] is clearly superior to the LDA, while in the low-density regions the GGA potential is far too large.

In this self-consistent x-only calculation for Si, Städele et.al. [118] determined the total energy per atom as well as the exchange energy per atom to be -104.75 eV and -29.40 eV, respectively. Similar to the results reported for atoms and molecules in the previous sections, these total-energy results agree very closely with the corresponding Hartree-Fock values [118] of -104.87 eV and 29.61 eV.

Table 46: *Kohn-Sham energy gaps for Si (in eV) from various calculations using the exact exchange functional*

	KKR-ASA	LMTO-ASA	local PP	nonlocal PP	KLI-PP [c]	
	EXX [a]	EXX [a]	EXX [b]	EXX [b]	KLI [c]	expt.
E_g	1.12	1.25	1.43	1.44	-	1.17 [d]
L	1.98	2.09	2.36	2.30	1.82	2.4 [e]
Γ	2.87	2.95	3.46	3.29	2.87	3.05 [f]
X	1.24	1.38	-	1.58	0.94	

[a] *from reference [111]*
[b] *from reference [118]*
[c] *from reference [117]*
[d] *from reference [119]*
[e] *from reference [120]*
[f] *from reference [121]*

Table 47: *Kohn-Sham energy gaps for Si (in eV) from various LDA calculations*

	KKR-ASA	LMTO-ASA	local PP	nonlocal PP	PP	
	LDA [a]	LDA [a]	LDA [b]	LDA [b]	LDA [c]	expt.
E_g	0.54	0.55	0.52	0.49	-	1.17 [d]
L	1.43	1.43	1.54	1.45	1.43	2.4 [e]
Γ	2.57	2.57	2.79	2.55	2.57	3.05 [f]
X	0.66	0.66	-	-	0.60	

[a] *from reference [111]*
[b] *from reference [118]*
[c] *from reference [116]*
[d] *from reference [119]*
[e] *from reference [120]*
[f] *from reference [121]*

Table 48: *Kohn-Sham energy gaps for Ge (in eV) from various calculations*

	KKR-ASA EXX [a]	LMTO-ASA EXX [a]	KKR- or LMTO-ASA LDA [a]	PP KLI [b]	PP LDA [b]	expt.[c]
L (E_g)	1.03	1.12	0.40	0.77	0.42	0.84
Γ	1.57	1.67	0.60	1.26	0.82	1.00
X	1.24	1.34	0.78	0.87	0.57	1.3 $\pm$ 0.2

[a] *from reference [111]*
[b] *from reference [117]*
[c] *from reference [119]*

Table 49: *Kohn-Sham energy gaps for diamond (in eV) from various calculations*

	KKR-ASA EXX [a]	LMTO-ASA EXX [a]	PP EXX [b]	PP LDA [b]	expt. [c]
E_g	4.58	4.65	5.06	4.16	5.47
L	8.63	8.68	9.19	8.42	-
Γ	5.87	5.92	6.28	5.57	7.3

[a] *from reference [111]*
[b] *from reference [118]*
[b] *from reference [122]*

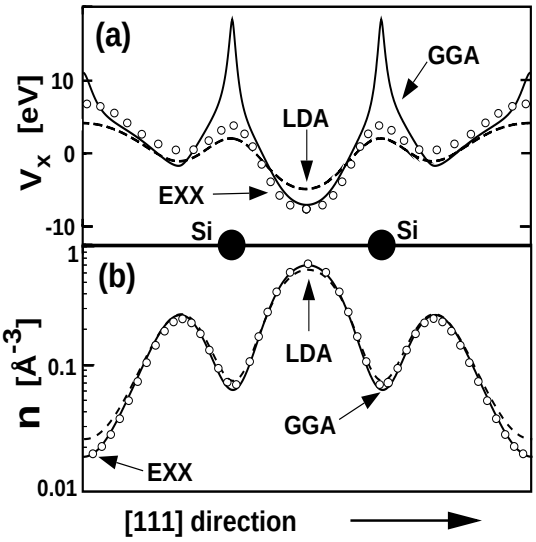

Figure 14: *(a) Comparison of the calculated exact exchange potential (open circles), in eV, along the [111] direction in Si with the approximate LDA (dashed line) and GGA (solid line) [75] exchange potentials. The filled black circles correspond to the positions of the Si atoms. The LDA and GGA potentials were evaluated at the exchange-only EXX density and the local ionic pseudopotential was employed. The mean values of all exchange potentials have been set equal to zero. (b) Self-consistent charge densities computed with the indicated exchange-only functionals; taken from [118].*

For metals the exact exchange functional is not expected to give good results. Kotani and Akai [112] found for transition metals such as Fe that the exact exchange plus LDA correlation potential yields the occupied bands too deep relative to the s bands and leads to magnetizations too large compared with experiment. In order to rectify this problem Kotani [113] has recently combined the exact exchange potential with a full (inhomogeneous) RPA for the correlation potential. It was found for the transition metals that the RPA correlation potential has a large contribution opposite in sign to the exchange potential. The resulting band structures and magnetizations are rather close to LDA results and to the experimental numbers. The magnetization of Fe, for example, is found to be 2.02 μ_B in the EXX+RPA calculation in contrast to 3.27 μ_B in the EXX+LDA calculation. The corresponding LDA and experimental values are 2.13 μ_B and 2.12 μ_B, respectively.

5 Beyond the OEP - a connection with Many-Body Perturbation Theory

We have discussed in detail the connection between the OEP method and the conventional density functional approach. The OEP method, where the xc energy is expressed as a functional of the orbitals, allows for more flexibility in approximating the xc energy, while preserving important properties of the exact KS potential such as the derivative discontinuities and the absence of spurious self-interactions. Apart from the use of the Colle-Salvetti functional in the OEP procedure as described in previous chapters, several approaches have been reported in the literature to derive approximations to the correlation-

energy functional suitable for the OEP method. Görling and Levy [123, 32] proposed a scheme to derive a correlation-energy functional from a coupling-constant perturbation expansion. Casida [124] on the other hand, used an approximate perturbative expression for the ground-state energy to include correlation in the OEP scheme.

The purpose of the present chapter is to establish a connection between the OEP method and many-body perturbation theory which may serve to construct correlation energy functionals in a systematic way. We first derive exact equations for the xc potential and the xc energy in terms of the Green function and self-energy of the system by using a particular perturbative expansion of the interacting Hamiltonian. Then we demonstrate that the x-only OEP method is equivalent to the first-order approximation of this expansion. On the basis of this observation we then propose an iterative scheme to include correlation which relies on the Kohn-Sham Green function rather than on the Kohn-Sham orbitals.

The starting point of our discussion is the Hamiltonian of the system of interacting electrons (see Eq. (1)) written in second quantized notation:

$$\hat{H} = \hat{T} + \hat{V}_0 + \hat{W}_{\mathrm{Clb}} \tag{304}$$

where

$$\hat{T} = \sum_\sigma \int \mathrm{d}^3 r \; \hat{\psi}^\dagger_\sigma(\mathbf{r}) \left(-\frac{\nabla^2}{2} \right) \hat{\psi}_\sigma(\mathbf{r}) \tag{305}$$

is the kinetic energy operator,

$$\hat{V}_0 = \sum_\sigma \int \mathrm{d}^3 r \; \hat{\psi}^\dagger_\sigma(\mathbf{r}) v_0(\mathbf{r}) \hat{\psi}_\sigma(\mathbf{r}) \tag{306}$$

is the operator of the external (nuclear) potential and

$$\hat{W}_{\mathrm{Clb}} = \frac{1}{2} \sum_{\sigma,\sigma'} \int \mathrm{d}^3 r \int \mathrm{d}^3 r' \; \hat{\psi}^\dagger_\sigma(\mathbf{r}) \hat{\psi}^\dagger_{\sigma'}(\mathbf{r}') \frac{1}{|\mathbf{r}-\mathbf{r}'|} \hat{\psi}_{\sigma'}(\mathbf{r}') \hat{\psi}_\sigma(\mathbf{r}) \tag{307}$$

is the Coulomb interaction of the electrons.

The central idea is now to formally rewrite Eq. (304) by addition and subtraction of the exact Hartree and xc potentials in the following way:

$$\hat{H} = \hat{T} + \hat{V}_0 + \hat{V}_{\mathrm{H}} + \hat{V}_{\mathrm{xc}} + (\hat{W}_{\mathrm{Clb}} - \hat{V}_{\mathrm{H}} - \hat{V}_{\mathrm{xc}}) =: \hat{H}_{KS} + \hat{H}_1 \quad . \tag{308}$$

Here $\hat{V}_{\mathrm{H}}$ and $\hat{V}_{\mathrm{xc}}$ are the operators of the Hartree and xc potentials defined in analogy to Eq. (306) with $v_0(\mathbf{r})$ replaced by

$$v_{\mathrm{H}}(\mathbf{r}) = \int \mathrm{d}^3 r \; \frac{\rho(\mathbf{r}')}{|\mathbf{r}-\mathbf{r}'|} \tag{309}$$

and $V_{\mathrm{xc}\sigma}(\mathbf{r})$, respectively.

$$\hat{H}_{KS} = \hat{T} + \hat{V}_0 + \hat{V}_{\mathrm{H}} + \hat{V}_{\mathrm{xc}} \tag{310}$$

is the Hamiltonian of non-interacting electrons moving in the spin-dependent KS potential

$$V_{S\sigma}(\mathbf{r}) = v_0(\mathbf{r}) + v_{\mathrm{H}}(\mathbf{r}) + V_{\mathrm{xc}\sigma}(\mathbf{r}) \tag{311}$$

and will serve as the unperturbed reference Hamiltonian while

$$\hat{H}_1 = \hat{W}_{\mathrm{Clb}} - \hat{V}_{\mathrm{H}} - \hat{V}_{\mathrm{xc}} \tag{312}$$

will be treated as a perturbation to $\hat{H}_{KS}$. It has to be emphasized that the xc potential $V_{\mathrm{xc}\sigma}(\mathbf{r})$ – and hence the unperturbed Hamiltonian $\hat{H}_{KS}$ – is not known at this stage and has to be determined by further arguments. Its uniqueness, on the other hand, is guaranteed by the Hohenberg-Kohn theorem. We also note that the perturbative approach based on the proposed splitting (308) of the interacting Hamiltonian is *not* equivalent to a Taylor expansion in powers of e^2 with e being the elementary charge. This is due to the fact that the unperturbed Hamiltonian $\hat{H}_{KS}$ through the exact KS potential $V_{\mathrm{xc}\sigma}$ already contains e^2 up to infinite order.

Application of the techniques of many-body perturbation theory to Hamiltonian (308) in the described way, i.e. treating $\hat{H}_1$ as a perturbation to the KS Hamiltonian $\hat{H}_{KS}$, leads to the Dyson equation

$$G_\sigma(\mathbf{r},\mathbf{r}',\omega) = G_\sigma^{KS}(\mathbf{r},\mathbf{r}',\omega) + \int \mathrm{d}^3y \int \mathrm{d}^3y' \; G_\sigma^{KS}(\mathbf{r},\mathbf{y},\omega)\Sigma_\sigma(\mathbf{y},\mathbf{y}',\omega)G_\sigma(\mathbf{y}',\mathbf{r}',\omega) \tag{313}$$

which relates the Green function G_σ of the interacting system to the KS Green function

$$G_\sigma^{KS}(\mathbf{r},\mathbf{r}',\omega) = \lim_{\eta\to 0^+} \sum_j \varphi_{j\sigma}(\mathbf{r})\varphi_{j\sigma}^*(\mathbf{r}') \left(\frac{\Theta(\varepsilon_{j\sigma}-\varepsilon_F)}{\omega-\varepsilon_{j\sigma}+i\eta} + \frac{\Theta(\varepsilon_F-\varepsilon_{j\sigma})}{\omega-\varepsilon_{j\sigma}-i\eta} \right) \quad . \tag{314}$$

$\Sigma_\sigma(\mathbf{r},\mathbf{r}',\omega)$ is the irreducible self-energy corresponding to the perturbation $\hat{H}_1$. Since this perturbation contains the unknown xc potential one can write the self-energy as a functional of $V_{\mathrm{xc}\sigma}(\mathbf{r})$:

$$\Sigma_\sigma(\mathbf{r},\mathbf{r}',\omega) = \Sigma_\sigma[V_{\mathrm{xc}\sigma}](\mathbf{r},\mathbf{r}',\omega) \quad . \tag{315}$$

Explicit approximations of this functional can be found, e.g., by evaluating all self-energy diagrams up to a given order in the perturbation. An example for this strategy will be discussed below.

In order to determine $V_{\mathrm{xc}\sigma}(\mathbf{r})$ we finally make use of the fact that – due to the KS theorem – the spin density of the interacting system can be obtained both via the Green function G_σ and the KS Green function G_σ^{KS} by the expression

$$\rho_\sigma(\mathbf{r}) = -i \int \frac{\mathrm{d}\omega}{2\pi} \; G_\sigma(\mathbf{r},\mathbf{r},\omega) = -i \int \frac{\mathrm{d}\omega}{2\pi} \; G_\sigma^{KS}(\mathbf{r},\mathbf{r},\omega) \quad . \tag{316}$$

Using Dyson's equation (313) one is thus led to the integral equation

$$\int \frac{\mathrm{d}\omega}{2\pi} \int \mathrm{d}^3y \int \mathrm{d}^3y' \; G_\sigma^{KS}(\mathbf{r},\mathbf{y},\omega)\Sigma_\sigma(\mathbf{y},\mathbf{y}',\omega)G_\sigma(\mathbf{y}',\mathbf{r},\omega) = 0 \quad . \tag{317}$$

Writing the self-energy as

$$\Sigma_\sigma(\mathbf{r},\mathbf{r}',\omega) = \Sigma_{\mathrm{xc}\sigma}(\mathbf{r},\mathbf{r}',\omega) - \delta(\mathbf{r}-\mathbf{r}')V_{\mathrm{xc}\sigma}(\mathbf{r}) \tag{318}$$

one obtains

$$\begin{aligned} &\int \mathrm{d}^3y \; V_{\mathrm{xc}\sigma}(\mathbf{y}) \int \frac{\mathrm{d}\omega}{2\pi} \; G_\sigma^{KS}(\mathbf{r},\mathbf{y},\omega)G_\sigma(\mathbf{y},\mathbf{r},\omega) = \\ &= \int \mathrm{d}^3y \int \mathrm{d}^3y' \int \frac{\mathrm{d}\omega}{2\pi} \; G_\sigma^{KS}(\mathbf{r},\mathbf{y},\omega)\Sigma_{\mathrm{xc}\sigma}(\mathbf{y},\mathbf{y}',\omega)G_\sigma(\mathbf{y}',\mathbf{r},\omega) \quad . \end{aligned} \tag{319}$$

This exact integral equation relating the xc potential to the xc part $\Sigma_{\mathrm{xc}\sigma}(\mathbf{r},\mathbf{r}',\omega)$ of the irreducible self-energy was first derived by Sham and Schlüter [50, 54].

Sham also derived an exact expression for the xc energy in terms of the Green function and the self-energy by using the techniques of Luttinger and Ward [125]. This expression reads

$$\begin{aligned} E_{xc}[\rho_\uparrow,\rho_\downarrow] &= i\sum_\sigma \int \frac{\mathrm{d}\omega}{2\pi} \int \mathrm{d}^3 r \; \log\left(1 - G_\sigma^{KS}\Sigma_\sigma\right)(\mathbf{r},\mathbf{r},\omega) \\ &\quad + i\sum_\sigma \int \frac{\mathrm{d}\omega}{2\pi} \int \mathrm{d}^3 r \int \mathrm{d}^3 r' \; \Sigma_\sigma(\mathbf{r},\mathbf{r}',\omega) G_\sigma(\mathbf{r}',\mathbf{r},\omega) + \sum_{n=1}^{\infty} Y^{(n)} \end{aligned} \tag{320}$$

where the logarithm of some integral operator $C(\mathbf{r},\mathbf{r}')$ has to be read as

$$\log(1-C)(\mathbf{r},\mathbf{r}') = -\sum_{n=1}^{\infty} \frac{1}{n} \left(C(\mathbf{r},\mathbf{r}')\right)^n \tag{321}$$

with

$$\left(C(\mathbf{r},\mathbf{r}')\right)^n = \int \mathrm{d}^3 x_1 \ldots \int \mathrm{d}^3 x_{n-1} C(\mathbf{r},\mathbf{x}_1) C(\mathbf{x}_1,\mathbf{x}_2) \ldots C(\mathbf{x}_{n-1},\mathbf{r}') \; . \tag{322}$$

The quantities $Y^{(n)}$ are defined by

$$Y^{(n)} = -\frac{i}{2n} \sum_\sigma \int \frac{\mathrm{d}\omega}{2\pi} \int \mathrm{d}^3 r \int \mathrm{d}^3 r' \; \Sigma^{(n)}_{\sigma,\mathrm{dressed}}(\mathbf{r},\mathbf{r}',\omega) G_\sigma(\mathbf{r}',\mathbf{r},\omega) \tag{323}$$

where, for $n \geq 2$, $\Sigma^{(n)}_{\sigma,\mathrm{dressed}}(\mathbf{r},\mathbf{r}',\omega)$ is the sum of all dressed skeleton diagrams of order n, while for $n = 1$ it is given solely by the nonlocal first-order dressed skeleton diagram, i.e.,

$$\Sigma^{(1)}_{\sigma,\mathrm{dressed}}(\mathbf{r},\mathbf{r}') = i \int \frac{\mathrm{d}\omega}{2\pi} \frac{G_\sigma(\mathbf{r},\mathbf{r}',\omega)}{|\mathbf{r}-\mathbf{r}'|} \; . \tag{324}$$

As a consequence of the logarithm of integral operators, Eq. (320) is rather difficult to handle. In the following we derive a much simpler, though still exact, expression for E_{xc}. We begin with the standard expression [126] for the total ground state energy of the interacting system:

$$\begin{aligned} E_{GS} &= -\frac{i}{2}\sum_\sigma \int \frac{\mathrm{d}\omega}{2\pi} \int \mathrm{d}^3 r \lim_{\mathbf{r}'\to\mathbf{r}} \left(\omega - \frac{\nabla^2_{\mathbf{r}}}{2} + v_0(\mathbf{r})\right) G_\sigma(\mathbf{r},\mathbf{r}',\omega) \\ &= -\frac{i}{2}\sum_\sigma \int \frac{\mathrm{d}\omega}{2\pi} \int \mathrm{d}^3 r \lim_{\mathbf{r}'\to\mathbf{r}} \left(\omega - h^{KS}_\sigma(\mathbf{r}) + 2h^{KS}_\sigma(\mathbf{r})\right) G_\sigma(\mathbf{r},\mathbf{r}',\omega) \\ &\quad -\frac{1}{2}\sum_\sigma \int \mathrm{d}^3 r \left(v_H(\mathbf{r}) + v_{xc\sigma}(\mathbf{r})\right) \rho_\sigma(\mathbf{r}) \\ &= -i\sum_\sigma \int \frac{\mathrm{d}\omega}{2\pi} \int \mathrm{d}^3 r \lim_{\mathbf{r}'\to\mathbf{r}} \left(-\frac{\nabla^2_{\mathbf{r}}}{2}\right) G_\sigma(\mathbf{r},\mathbf{r}',\omega) + \int \mathrm{d}^3 r v_0(\mathbf{r})\rho(\mathbf{r}) \\ &\quad +\frac{1}{2}\int \mathrm{d}^3 r \int \mathrm{d}^3 r' \frac{\rho(\mathbf{r})\rho(\mathbf{r}')}{|\mathbf{r}-\mathbf{r}'|} - \frac{i}{2}\sum_\sigma \int \frac{\mathrm{d}\omega}{2\pi} \int \mathrm{d}^3 r \int \mathrm{d}^3 r' \Sigma_{xc\sigma}(\mathbf{r},\mathbf{r}',\omega) G_\sigma(\mathbf{r}',\mathbf{r},\omega) \end{aligned} \tag{325}$$

where we used Dyson's equation (313) and the equation of motion for the KS Green function

$$(\omega - h^{KS}_\sigma(\mathbf{r})) G^{KS}_\sigma(\mathbf{r},\mathbf{r}',\omega) = \delta(\mathbf{r}-\mathbf{r}') \; , \tag{326}$$

with the KS single-particle Hamiltonian

$$h^{KS}_\sigma(\mathbf{r}) = -\frac{\nabla^2}{2} + V_{S\sigma}(\mathbf{r}) \; . \tag{327}$$

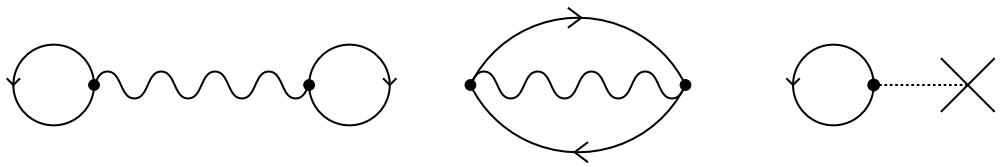

Figure 15: *Energy diagrams of first order in $\hat{H}_1$. Straight lines represent the KS Green function, wavy lines represent the bare Coulomb interaction. Diagram c) originates from the local part $-\hat{V}_{\rm H} - \hat{V}_{\rm xc}$ of the perturbation.*

Comparison of Eq. (325) with the defining equation for E_{xc},

$$E_{GS}[\rho_\uparrow,\rho_\downarrow] = T_s[\rho_\uparrow,\rho_\downarrow] + \int \mathrm{d}^3 r v_0(\mathbf{r})\rho(\mathbf{r}) + \frac{1}{2}\int \mathrm{d}^3 r \int \mathrm{d}^3 r' \frac{\rho(\mathbf{r})\rho(\mathbf{r}')}{|\mathbf{r}-\mathbf{r}'|} + E_{xc}[\rho_\uparrow,\rho_\downarrow] \quad , \tag{328}$$

leads to the desired result

$$\begin{aligned} & E_{xc}[\rho_\uparrow,\rho_\downarrow] \\ &= -\frac{i}{2}\sum_\sigma \int \frac{\mathrm{d}\omega}{2\pi} \int \mathrm{d}^3 r \int \mathrm{d}^3 r' \Sigma_{xc\sigma}(\mathbf{r},\mathbf{r}',\omega) G_\sigma(\mathbf{r}',\mathbf{r},\omega) + T[\rho_\uparrow,\rho_\downarrow] - T_s[\rho_\uparrow,\rho_\downarrow] \quad , \end{aligned} \tag{329}$$

where

$$T[\rho_\uparrow,\rho_\downarrow] = -i\sum_\sigma \int \frac{\mathrm{d}\omega}{2\pi} \int \mathrm{d}^3 r \lim_{\mathbf{r}'\to\mathbf{r}} \left(-\frac{\nabla_{\mathbf{r}}^2}{2}\right) G_\sigma(\mathbf{r},\mathbf{r}',\omega) \tag{330}$$

is the kinetic energy of the interacting system while

$$T_s[\rho_\uparrow,\rho_\downarrow] = -i\sum_\sigma \int \frac{\mathrm{d}\omega}{2\pi} \int \mathrm{d}^3 r \lim_{\mathbf{r}'\to\mathbf{r}} \left(-\frac{\nabla_{\mathbf{r}}^2}{2}\right) G_\sigma^{KS}(\mathbf{r},\mathbf{r}',\omega) \tag{331}$$

is the kinetic energy of the non-interacting KS system.

Sham noted that Eq. (319) reduces to the integral equation of the exchange-only OEP method if one approximates $\Sigma_{{\rm xc}\sigma}$ by the Fock self-energy

$$\Sigma_{{\rm xc}\sigma}(\mathbf{r},\mathbf{r}',\omega) \approx \Sigma_\sigma^F(\mathbf{r},\mathbf{r}') = -\sum_{j,\varepsilon_{j\sigma}\le\varepsilon_F} \frac{\varphi_{j\sigma}(\mathbf{r})\varphi_{j\sigma}^*(\mathbf{r}')}{|\mathbf{r}-\mathbf{r}'|} \tag{332}$$

and simultaneously replaces the Green function G_σ of the interacting system by the KS Green function G_σ^{KS}. This can easily be understood within the above framework by performing a perturbative analysis of the ground-state energy of the interacting system in terms of the proposed splitting (308) of the original Hamiltonian. The energy of the unperturbed KS reference system is

$$\begin{aligned} E^{(0)} &= T_s[\rho] + \sum_\sigma \int \mathrm{d}^3 r \; V_{S\sigma}(\mathbf{r})\rho_\sigma(\mathbf{r}) \\ &= T_s[\rho] + \int \mathrm{d}^3 r \; v_0(\mathbf{r})\rho(\mathbf{r}) + \int \mathrm{d}^3 r \; v_{\rm H}(\mathbf{r})\rho(\mathbf{r}) + \sum_\sigma \int \mathrm{d}^3 r \; V_{{\rm xc}\sigma}(\mathbf{r})\rho_\sigma(\mathbf{r}) \quad . \end{aligned} \tag{333}$$

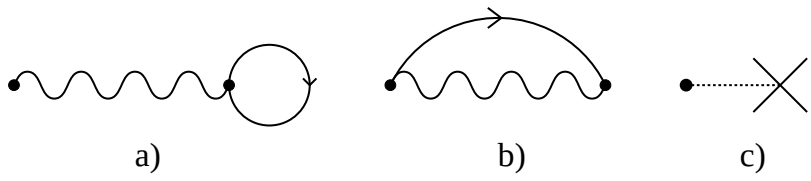

Figure 16: *Self-energy diagrams of first order in* $\hat{H}_1$.

The first-order correction to the energy can be expressed in terms of the Feynman diagrams shown in Fig. 15 where the last diagram, Fig. 15c originates from the local part $(-\hat{V}_{\rm H}-\hat{V}_{\rm xc})$ of the perturbation $\hat{H}_1$. The sum of these diagrams yields

$$\begin{aligned}\Delta E^{(1)} &= \frac{1}{2}\int \mathrm{d}^3r \int \mathrm{d}^3r' \; \frac{\rho(\mathbf{r})\rho(\mathbf{r}')}{|\mathbf{r}-\mathbf{r}'|} \\ &\quad -\frac{1}{2}\sum_\sigma \sum_{\substack{i,j \\ \mathrm{occ}}} \int \mathrm{d}^3r \int \mathrm{d}^3r' \; \frac{\varphi^*_{i\sigma}(\mathbf{r})\varphi_{i\sigma}(\mathbf{r}')\varphi_{j\sigma}(\mathbf{r})\varphi^*_{j\sigma}(\mathbf{r}')}{|\mathbf{r}-\mathbf{r}'|} \\ &\quad -\sum_\sigma \int \mathrm{d}^3r \;\; (v_{\rm H}(\mathbf{r}) + V_{{\rm xc}\sigma}(\mathbf{r}))\, \rho_\sigma(\mathbf{r}) \;, \end{aligned} \tag{334}$$

so that

$$\begin{aligned} E^{(1)} &= E^{(0)} + \Delta E^{(1)} \\ &= T_s[\rho] + \int \mathrm{d}^3r \; v_0(\mathbf{r})\rho(\mathbf{r}) + \frac{1}{2}\int \mathrm{d}^3r \int \mathrm{d}^3r' \; \frac{\rho(\mathbf{r})\rho(\mathbf{r}')}{|\mathbf{r}-\mathbf{r}'|} \\ &\quad -\frac{1}{2}\sum_\sigma \sum_{\substack{i,j \\ \mathrm{occ}}} \int \mathrm{d}^3r \int \mathrm{d}^3r' \; \frac{\varphi^*_{i\sigma}(\mathbf{r})\varphi_{i\sigma}(\mathbf{r}')\varphi_{j\sigma}(\mathbf{r})\varphi^*_{j\sigma}(\mathbf{r}')}{|\mathbf{r}-\mathbf{r}'|} \end{aligned} \tag{335}$$

which is identical to the energy functional used in the x-only OEP case.

Returning to Eq. (317) we note that its lowest-order approximation is obtained by replacing the self-energy Σ_σ by its first-order approximation $\Sigma^{(1)}_\sigma$ and, simultaneously, the Green function G_σ by the zeroth order Green function $G^{\rm KS}_\sigma$. $\Sigma^{(1)}_\sigma$ is expressed diagrammatically by the three diagrams depicted in Fig. 16. But the diagram 16a, by virtue of the KS theorem, is canceled exactly by the Hartree potential contained in the diagram 16c, so that

$$\Sigma^{(1)}_\sigma(\mathbf{r},\mathbf{r}') = \Sigma^F_\sigma(\mathbf{r},\mathbf{r}') - V_{{\rm xc}\sigma}(\mathbf{r})\delta(\mathbf{r}-\mathbf{r}') \tag{336}$$

with the Fock self-energy Σ^F_σ already defined in Eq. (332).

As has been already discussed (see Eq. (315)), the self-energy is an explicit functional of $V_{{\rm xc}\sigma}$ and we see from Eq. (336) that an explicit approximation to this functional can be obtained in a rather natural way by applying our perturbative approach. It is also evident that the first-order approximation Eq. (336) and Sham's approximation Eq. (332) for the xc-part of the self-energy, $\Sigma_{{\rm xc}\sigma}$, are identical. The latter approximation is known to lead to the x-only OEP integral equation and the energy functional in first order, Eq. (335), is also identical to the energy functional of the x-only OEP method. Therefore we conclude that the x-only OEP method and our first-order perturbative approach are equivalent in the sense that one uses the first-order approximation to Sham's integral equation (319) to

determine the corresponding xc potential. It may be worth noting that while the x-only OEP method – by the arguments given above – may be interpreted as a particular, *purely first order* perturbation theory, the Hartree-Fock approach is equivalent to a *self-consistent* perturbation theory of first order, i.e. an infinite sum of certain diagrams is taken into account [126].

There are now several possible routes to go beyond the x-only case by including higher orders in the perturbation. In view of the foregoing discussion one could evaluate Eq. (317) up to a given order. The resulting integral equation then has to be solved self-consistently for $V_{\mathrm{xc}\sigma}(\mathbf{r})$ together with the corresponding KS equation and the corresponding xc-energy functional which could also be obtained by perturbative analysis of the energy diagrams up to the same order. Solution of the integral equation for $V_{\mathrm{xc}\sigma}$ in higher orders can be expected to be a highly non-trivial task since this equation will be non-linear in the unknown xc potential. Moreover, not only the occupied but also the unoccupied KS orbitals and orbital energies will enter that equation.

Instead of using Eq. (317) one could also perform a perturbative analysis of the energy in higher orders (similar to the first-order analysis of Eqs. (334) and (335)) and use the resulting energy functional in higher orders in the standard OEP procedure, i.e. determine that local potential minimizing this energy functional. Again one faces the problem that the xc energy functional depends on the occupied as well as the unoccupied KS orbitals and on the corresponding KS energies. In addition, the xc functional in higher orders also explicitly depends on the unknown xc potential, i.e. we have for the xc-energy functional in n-th order

$$E_{\mathrm{xc}}^{(n)} = E_{\mathrm{xc}}^{(n)}[\{\varphi_{j\sigma}\}, \{\varepsilon_{j\sigma}\}, V_{\mathrm{xc}\sigma}] \ . \tag{337}$$

Due to this fact the resulting integral equation for $V_{\mathrm{xc}\sigma}$ will not only contain the unknown xc potential but also the equally unknown xc kernel $f_{\mathrm{xc}}^{\sigma\sigma'}$ defined as functional derivative of the xc potential:

$$f_{\mathrm{xc}}^{\sigma\sigma'}(\mathbf{r}, \mathbf{r}') = \frac{\delta V_{\mathrm{xc}\sigma}(\mathbf{r})}{\delta \rho_{\sigma'}(\mathbf{r}')} = \frac{\delta^2 E_{\mathrm{xc}}}{\delta \rho_{\sigma}(\mathbf{r}) \delta \rho_{\sigma'}(\mathbf{r}')} \ . \tag{338}$$

Although it would be very interesting to obtain information on the xc kernel, the equation determining $f_{\mathrm{xc}}^{\sigma\sigma'}$ and $V_{\mathrm{xc}\sigma}$ can be expected to be *extremely* difficult to solve in practice. One should note that in the x-only method (i.e. for $n = 1$) the xc potential as well as the KS energies enter the energy functional only implicitly via the occupied KS orbitals and the resulting integral equation does not contain the xc kernel.

In the following we propose a third approach which might be more practical. The central idea of this scheme is to approximate the xc part $\Sigma_{\mathrm{xc}\sigma}$ of the self-energy as a functional of the full Green function and then solve Dyson's equation (313) for G_σ together with Sham's integral equation (319) for $V_{\mathrm{xc}\sigma}$ in a self-consistent fashion. To achieve this we first derive an *exact* diagrammatic representation of $\Sigma_{\mathrm{xc}\sigma}$ in terms of the full Green function G_σ. To this end we return to the standard formulation of many-body perturbation theory and treat the interaction $\hat{W}_{\mathrm{Clb}}$ as a perturbation to the non-interacting Hamiltonian $\hat{H}_0 = \hat{T} + \hat{V}_0$. In this case Dyson's equation of course reads

$$G_\sigma(\mathbf{r}, \mathbf{r}', \omega) = G_\sigma^{(0)}(\mathbf{r}, \mathbf{r}', \omega) + \int \mathrm{d}^3 y \int \mathrm{d}^3 y' \ G_\sigma^{(0)}(\mathbf{r}, \mathbf{y}, \omega) \tilde{\Sigma}_\sigma(\mathbf{y}, \mathbf{y}', \omega) G_\sigma(\mathbf{y}', \mathbf{r}', \omega) \tag{339}$$

with the Green function $G_\sigma^{(0)}$ corresponding to $\hat{H}_0$ and the irreducible self-energy $\tilde{\Sigma}_\sigma$ corresponding to the perturbation $\hat{W}_{\mathrm{Clb}}$. $\tilde{\Sigma}_\sigma$ can exactly be expressed as the sum of the two

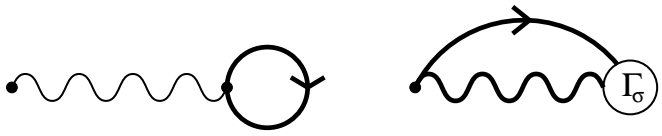

Figure 17: *The two self-consistent diagrams which constitute the self-energy $\tilde{\Sigma}_\sigma$ of Eq. (339). The thick straight lines represent the Green function of the interacting system, the thick wavy line is the screened interaction and Γ_σ is the irreducible vertex function. The xc self-energy $\Sigma_{\mathrm{xc}\sigma}$ can exactly be represented solely by diagram b).*

diagrams shown in Fig. 17 where Γ_σ is the irreducible vertex function and W_σ is the effective screened interaction [126].

The non-interacting Green function $G_\sigma^{(0)}$ is the solution of the equation of motion

$$(\omega - h^{(0)}(\mathbf{r}))G_\sigma^{(0)}(\mathbf{r},\mathbf{r}',\omega) = \delta(\mathbf{r}-\mathbf{r}') \tag{340}$$

with

$$h^{(0)}(\mathbf{r}) = -\frac{\nabla^2}{2} + v_0(\mathbf{r}) \; . \tag{341}$$

Operating with $(\omega - h^{(0)})$ on Eq. (339) yields

$$(\omega - h^{(0)}(\mathbf{r}))G_\sigma(\mathbf{r},\mathbf{r}',\omega) = \delta(\mathbf{r}-\mathbf{r}') + \int \mathrm{d}^3y' \; \tilde{\Sigma}_\sigma(\mathbf{r},\mathbf{y}',\omega)G_\sigma(\mathbf{y}',\mathbf{r}',\omega) \; . \tag{342}$$

In a similar manner, by using the equation of motion (326) of the KS Green function one obtains from Eq. (313)

$$\begin{aligned}(\omega - h_\sigma^{KS}(\mathbf{r}))G_\sigma(\mathbf{r},\mathbf{r}',\omega) &= \delta(\mathbf{r}-\mathbf{r}') + \int \mathrm{d}^3y' \; \Sigma_\sigma(\mathbf{r},\mathbf{y}',\omega)G_\sigma(\mathbf{y}',\mathbf{r}',\omega) \\ &= \delta(\mathbf{r}-\mathbf{r}') - V_{\mathrm{xc}\sigma}(\mathbf{r})G_\sigma(\mathbf{r},\mathbf{r}',\omega) + \int \mathrm{d}^3y' \; \Sigma_{\mathrm{xc}\sigma}(\mathbf{r},\mathbf{y}',\omega)G_\sigma(\mathbf{y}',\mathbf{r}',\omega)\end{aligned} \tag{343}$$

where we used Eq. (318) in the last step. Eq. (343) can be rewritten as

$$\begin{aligned}&(\omega - h^{(0)}(\mathbf{r}))G_\sigma(\mathbf{r},\mathbf{r}',\omega) \\ &= \delta(\mathbf{r}-\mathbf{r}') + v_{\mathrm{H}}(\mathbf{r})G_\sigma(\mathbf{r},\mathbf{r}',\omega) + \int \mathrm{d}^3y' \; \Sigma_{\mathrm{xc}\sigma}(\mathbf{r},\mathbf{y}',\omega)G_\sigma(\mathbf{y}',\mathbf{r}',\omega) \; .\end{aligned} \tag{344}$$

Comparison of Eqs. (344) and (342) relates the self-energy $\tilde{\Sigma}_\sigma$ to $\Sigma_{\mathrm{xc}\sigma}$ via

$$\tilde{\Sigma}_\sigma(\mathbf{r},\mathbf{r}',\omega) = v_{\mathrm{H}}(\mathbf{r})\delta(\mathbf{r}-\mathbf{r}') + \Sigma_{\mathrm{xc}\sigma}(\mathbf{r},\mathbf{r}',\omega) \; . \tag{345}$$

As mentioned before, $\tilde{\Sigma}_\sigma$ can be represented by the sum of the two diagrams of Fig. 17. Since the diagram of Fig. 17 a) yields $v_{\mathrm{H}}(\mathbf{r})\delta(\mathbf{r}-\mathbf{r}')$, the xc-part of the self-energy $\Sigma_{\mathrm{xc}\sigma}$ can be represented solely by diagram 17 b). Since one can express the self-energy $\tilde{\Sigma}_\sigma$ also in terms of skeleton diagrams [126], $\Sigma_{\mathrm{xc}\sigma}$ can alternatively be represented as the sum of all fully dressed skeleton diagrams except the diagram of Fig. 17 a). This diagrammatic representation of the xc-part of the self-energy can then easily be used to approximate $\Sigma_{\mathrm{xc}\sigma}$ as a functional of the full Green function G_σ. One possible approximation would be to use

only the dressed skeleton diagrams up to a certain order, e.g., by the first-order skeleton diagram given by Eq. (324).

In the following we assume that some approximation to $\Sigma_{\mathrm{xc}\sigma}$ as a functional of G_σ has been specified:

$$\Sigma_{\mathrm{xc}\sigma}(\mathbf{r},\mathbf{r}',\omega) \approx \Sigma_{\mathrm{xc}\sigma}^{\mathrm{approx}}[G_\sigma](\mathbf{r},\mathbf{r}',\omega) \tag{346}$$

Using this approximation we propose the following iterative scheme:

1. Start with an approximation to $V_{\mathrm{xc}\sigma}$ (e.g. the x-only $V_{\mathrm{xc}}^{\mathrm{OEP}}$) and calculate the corresponding KS Green function G_σ^{KS}.

2. Solve Dyson's equation (313) for the Green function G_σ with Σ_σ approximated by

$$\Sigma_\sigma(\mathbf{r},\mathbf{r}',\omega) \approx \Sigma_{\mathrm{xc}\sigma}^{\mathrm{approx}}[G_\sigma](\mathbf{r},\mathbf{r}',\omega) - \delta(\mathbf{r}-\mathbf{r}')V_{\mathrm{xc}\sigma}(\mathbf{r}) \; . \tag{347}$$

3. With the solution G_σ of Dyson's equation and the corresponding self-energy solve Sham's integral equation (319) for $V_{\mathrm{xc}\sigma}$. Use that xc-potential to calculate the corresponding KS Green function G_σ^{KS}.

4. Return to point 2. and iterate until self-consistency is achieved.

5. Calculate the ground state energy of the interacting system via Eq. (325).

We emphasize that the only approximation in the above scheme is the approximation to the functional $\Sigma_{\mathrm{xc}\sigma}[G_\sigma]$. Even for the simplest approximation to the xc self-energy, namely using only the first-order dressed skeleton diagram, the converged result of the above scheme goes far beyond the x-only OEP solution since in this case, as discussed at the beginning of this chapter, the xc self-energy is expressed as the first-order skeleton diagram using the *bare* KS Green function instead of using the dressed Green function. Therefore we hope that the above iterative scheme might have the merit of including the important part of electron correlation already through low-order approximations of the xc self-energy. Of course one could in principle also use more sophisticated approximations of the xc self-energy such as the GW approximation [127], but due to the necessity of solving the integral equation for $V_{\mathrm{xc}\sigma}$ in each iteration cycle this would result in a very high computational effort.

Since in the x-only case of the OEP method the KLI approximation to the integral equation for the xc potential has proven to be extremely useful, an analogous approximation for Sham's integral equation seems highly desirable.

The proposed iterative scheme has another desirable feature: a converged solution of that scheme not only gives an approximate xc potential, it also yields an approximation of the Green function of the interacting system. This Green function yields the ground-state energy of the interacting system via Eq. (325), but it also allows for the calculation of photoemission and inverse photoemission spectra of the interacting system.

Acknowledgments

We thank Eberhard Engel for providing us with his KS and RKS computer codes, and John Perdew for his PW91 xc subroutine, Dage Sundholm and Pekka Pyykkö for their two-dimensional Xα code for molecules and for the warm hospitality during a stay of one of us (T.G.) in Helsinki. The entire manuscript was read by Kieron Burke, who deserves special

thanks for numerous comments. T.K. gratefully acknowledges a fellowship of the Studienstiftung des deutschen Volkes. Numerous discussions with Dage Sundholm, Eberhard Engel, Klaus Capelle, Martin Petersilka and Martin Lüders are gratefully acknowledged. This work was supported in part by the Deutsche Forschungsgemeinschaft.

References

[1] *Density Functional Theory*, Vol. 337 of *NATO ASI Series B*, edited by E.K.U. Gross and R.M. Dreizler (Plenum Press, New York, 1995).

[2] R.M. Dreizler and E.K.U. Gross, *Density Functional Theory* (Springer, Berlin, 1990).

[3] R.G. Parr and W. Yang, *Density-Functional Theory of Atoms and Molecules* (Oxford University Press, New York, 1989).

[4] P. Hohenberg and W. Kohn, Phys. Rev. **136**, B864 (1964).

[5] Q. Zhao and R.G. Parr, Phys. Rev. A **46**, 2337 (1992).

[6] C.J. Umrigar and X. Gonze, in *High Performance Computing and its Application to the Physical Sciences*, edited by D.A. Browne et al (World Scientific, Singapore, 1993).

[7] C.J. Umrigar and X. Gonze, Phys. Rev. A **50**, 3827 (1994).

[8] R. van Leeuwen and E.J. Baerends, Phys. Rev. A **49**, 2421 (1994).

[9] A. Görling and M. Ernzerhof, Phys. Rev. A **51**, 4501 (1995).

[10] V.E. Ingamells and N.C. Handy, Chem. Phys. Lett. **248**, 373 (1996).

[11] W. Kohn and L.J. Sham, Phys. Rev. **140**, A1133 (1965).

[12] R.T. Sharp and G.K. Horton, Phys. Rev. **90**, 317 (1953).

[13] J.D. Talman and W.F. Shadwick, Phys. Rev. A **14**, 36 (1976).

[14] J.B. Krieger, Y. Li, and G.J. Iafrate, Phys. Rev. A **46**, 5453 (1992).

[15] Y. Li, J.B. Krieger, and G.J. Iafrate, Phys. Rev. A **47**, 165 (1993).

[16] J.B. Krieger, Y. Li, and G.J. Iafrate, in *Density Functional Theory*, edited by R.M. Dreizler and E.K.U. Gross (Plenum Press, New York, 1995), p. 191.

[17] J.B. Krieger, Y. Li, and G.J. Iafrate, Phys. Lett. A **146**, 256 (1990).

[18] J.B. Krieger, Y. Li, M.R. Norman, and G.J. Iafrate, Phys. Rev. B **44**, 10437 (1991).

[19] J.B. Krieger, Y. Li, and G.J. Iafrate, Phys. Rev. A **45**, 101 (1992).

[20] J.B. Krieger, Y. Li, and G.J. Iafrate, Int. J. Quantum Chem. **41**, 489 (1992).

[21] Y. Li, J.B. Krieger, and G.J. Iafrate, Chem. Phys. Lett. **191**, 38 (1992).

[22] J.B. Krieger, J. Chen, Y. Li, and G.J. Iafrate, Int. J. Quantum Chem. Symp. **29**, 79 (1995).

[23] C.A. Ullrich, U.J. Gossmann, and E.K.U. Gross, Phys. Rev. Lett. **74**, 872 (1995).

[24] C.A. Ullrich, S. Erhard, and E.K.U. Gross, in *Super Intense Laser Atom Physics IV*, edited by H.G. Muller and M.V. Fedorov (Kluwer, Dordrecht, 1996), p. 267.

[25] M. Petersilka, U.J. Gossmann, and E.K.U Gross, Phys. Rev. Lett. **76**, 1212 (1996).

[26] E.K.U. Gross, J.F. Dobson, and M. Petersilka, in *Density Funktional Theory II*, Vol. 181 of *Topics in Current Chemistry*, edited by R.F. Nalewajski (Springer, Berlin, 1996), p. 81.

[27] K. Burke and E.K.U. Gross, in *Density Functionals: Theory and Applications*, Vol. 500 of *Lecture Notes in Physics*, edited by D. Joubert (Springer, Berlin, 1998).

[28] V.A. Khodel, V.R. Shaginyan, and V.V. Khodel, Phys. Rep. **249**, 1 (1994).

[29] U. von Barth and L. Hedin, J. Phys. C **5**, 1629 (1972).

[30] M.M. Pant and A.K. Rajagopal, Sol. State Commun. **10**, 1157 (1972).

[31] V.R. Shaginyan, Phys. Rev. A **47**, 1507 (1993).

[32] A. Görling and M. Levy, Phys. Rev. A **50**, 196 (1994).

[33] M.R. Norman and D.D. Koelling, Phys. Rev. B **30**, 5530 (1984).

[34] T. Grabo and E.K.U. Gross, Chem. Phys. Lett. **240**, 141 (1995).

[35] V. Sahni, J. Gruenebaum, and J.P. Perdew, Phys. Rev. B **26**, 4371 (1982).

[36] J.P. Perdew and M.R. Norman, Phys. Rev. B **26**, 5445 (1982).

[37] E. Engel and S.H. Vosko, Phys. Rev. A **47**, 2800 (1993).

[38] K. Aashamar, T.M. Luke, and J.D. Talman, At. Data Nucl. Data Tables **22**, 443 (1978).

[39] T. Kotani, Phys. Rev. B **50**, 14816 (1994), and Phys. Rev. B **51**, 13903 (1995)(E).

[40] T. Kotani, Phys. Rev. Lett. **74**, 2989 (1995).

[41] T. Kotani and H. Akai, Phys. Rev. B **52**, 17153 (1995).

[42] J.B. Krieger, Y. Li, and G.J. Iafrate, Phys. Lett. A **148**, 470 (1990).

[43] J. Chen, J.B. Krieger, Y. Li, and G.J. Iafrate, Phys. Rev. A **54**, 3939 (1996).

[44] J.B. Krieger, Y. Li, Y. Liu, and G.J. Iafrate, Int. J. Quantum Chem. **61**, 273 (1997).

[45] T. Kreibich, S. Kurth, T. Grabo, and E.K.U. Gross, Adv. Quantum Chem. (1997), in press.

[46] C. Filippi, C.J. Umrigar, and X. Gonze, Phys. Rev. A **54**, 4810 (1996).

[47] C.O. Almbladh and U. von Barth, Phys. Rev. B **31**, 3231 (1985).

[48] N.C. Handy, M.T. Marron, and H.J. Silverstone, Phys. Rev. **180**, 45 (1969).

[49] M. Levy and A. Görling, Phys. Rev. A **53**, 3140 (1996).

[50] L. Sham, Phys. Rev. B **32**, 3876 (1985).

[51] M. K. Harbola and V. Sahni, Phys. Rev. Lett. **62**, 489 (1989).

[52] E. Engel, J.A. Chevary, L.D. MacDonald, and S.H. Vosko, Z. Phys. D **23**, 7 (1992).

[53] J.P. Perdew, R.G. Parr, M. Levy, and J.L. Balduz, Phys. Rev. Lett. **49**, 1691 (1982).

[54] M. Schlüter L.J. Sham, Phys. Rev. Lett. **51**, 1888 (1983).

[55] M. Schlüter L.J. Sham, Phys. Rev. B **32**, 3883 (1985).

[56] R. van Leeuwen, O.V. Gritsenko, and E.J. Baerends, Z. Phys. D **33**, 229 (1995).

[57] M. Petersilka and E.K.U Gross, Int. J. Quantum Chem. **60**, 181 (1996).

[58] M. Petersilka, U.J. Gossmann, and E.K.U Gross, in *Electronic Density Functional Theory: Recent Progress and New Directions*, edited by J.F. Dobson, G. Vignale, and M.P. Das (Plenum, New York, 1997), p. 177.

[59] P. Pyykkö, Chem. Rev. **88**, 563 (1988).

[60] O.K. Andersen, Phys. Rev. B **2**, 883 (1970).

[61] A. K. Rajagopal and J. Callaway, Phys. Rev. B **7**, 1912 (1973).

[62] E. Engel, H. Müller, C. Speicher, and R.M. Dreizler, in *Density Functional Theory*, edited by E.K.U. Gross and R.M. Dreizler (Plenum Press, New York, 1995), p. 65.

[63] E. Engel and R.M. Dreizler, in *Density Functional Theory II*, Vol. 181 of *Topics in Current Chemistry*, edited by R.F. Nalewajski (Springer, Berlin, 1996), p. 1.

[64] E. Engel, S. Keller, A. Facco Bonetti, H. Müller, and R.M. Dreizler, Phys. Rev. A **52**, 2750 (1995).

[65] A. K. Rajagopal, J. Phys. C **11**, L943 (1978).

[66] A.H. MacDonald and S.H. Vosko, J. Phys. C **12**, 2977 (1979).

[67] C. Itzykson and J.-B. Zuber, *Quantum Field Theory* (McGraw-Hill, New York, 1980).

[68] T. Kreibich, E.K.U. Gross, and E. Engel, Phys. Rev. A **57**, (1998), in press.

[69] B.A. Shadwick, J.D. Talman, and M.R. Norman, Comput. Phys. Commun. **54**, 95 (1989).

[70] E. Engel, S. Keller, and R.M. Dreizler, Phys. Rev. A **53**, 1367 (1996).

[71] E. Engel and S.H. Vosko, Phys. Rev. B **47**, 13164 (1993).

[72] J.D. Talman, Comput. Phys. Commun. **54**, 85 (1989).

[73] Y. Wang, J.P. Perdew, J.A. Chevary, L.D. Macdonald, and S.H. Vosko, Phys. Rev. A **41**, 78 (1990).

[74] Y. Li, J.B. Krieger, J.A. Chevary, and S.H. Vosko, Phys. Rev. A **43**, 5121 (1991).

[75] A.D. Becke, Phys. Rev. A **38**, 3098 (1988).

[76] J.P. Perdew, in *Electronic Structure of Solids '91*, edited by P. Ziesche and H. Eschrig (Akademie Verlag, Berlin, 1991), p. 11.

[77] J.P. Perdew, K. Burke, and Y. Wang, Phys. Rev. B **54**, 16533 (1996).

[78] K. Burke, J.P. Perdew, and Y. Wang, in *Electronic Density Functional Theory: Recent Progress and New Directions*, edited by J.F. Dobson, G. Vignale, and M.P. Das (Plenum, New York, 1997).

[79] C. Froese Fischer, *The Hartree-Fock method for atoms* (Wiley, New York, 1977).

[80] J.C. Slater, *Structure of Molecules and Solids* (McGraw-Hill, New York, 1960), Vol. 4.

[81] E.K.U. Gross, M. Petersilka, and T. Grabo, in *Chemical Applications of Density Functional Theory, ACS Symposium Series 629*, edited by B.B Laird, R.B. Ross, and T. Ziegler (American Chemical Society, Washington, DC, 1996), p. 42.

[82] D. Heinemann, A. Rosén, and B. Fricke, Phys. Scr. **42**, 692 (1990).

[83] L. Laaksonen, P. Pyykkö, and D. Sundholm, Int. J. Quantum Chem. **23**, 309 (1983).

[84] L. Laaksonen, P. Pyykkö, and D. Sundholm, Int. J. Quantum Chem. **23**, 319 (1983).

[85] L. Laaksonen, D. Sundholm, and P. Pyykkö, Int. J. Quantum Chem. **28**, 601 (1985).

[86] L. Laaksonen, P. Pyykkö, and D. Sundholm, Comp. Phys. Reports **4**, 313 (1986).

[87] J.C. Slater, Phys. Rev. **81**, 385 (1951).

[88] T. Grabo and E.K.U. Gross, Int. J. Quantum Chem. **64**, 95 (1997).

[89] C. Jamorski, M.E. Casida, and D.R. Salahub, J. Chem. Phys. **104**, 5134 (1996).

[90] C. Filippi and C.J. Umrigar, J. Chem. Phys. **105**, 213 (1996).

[91] S.J. Chakravorty, S.R. Gwaltney, E.R. Davidson, F.A. Parpia, and C. Froese Fischer, Phys. Rev. A **47**, 3649 (1993).

[92] J.B. Krieger, J. Chen, and G.J. Iafrate, Bull. Am. Phys. Soc. **41**, 748 (1996).

[93] J. Chen, J.B. Krieger, and G.J. Iafrate, Bull. Am. Phys. Soc. **41**, 748 (1996).

[94] J.D. Bjorken and S.D. Drell, *Relativistic Quantum Fields* (McGraw-Hill, New York, 1965).

[95] E. Engel, S. Keller, and R.M. Dreizler, in *Electronic Density Functional Theory: Recent Progress and New Directions*, edited by J.F. Dobson, G. Vignale, and M.P.Das (Plenum, New York, 1997), p. 149.

[96] K. Hikasa et al. (Particle Data Group), Phys. Rev. D **45**, S1 (1992).

[97] R. Colle and D. Salvetti, Theoret. Chim. Acta **37**, 329 (1975).

[98] R. Colle and D. Salvetti, Theoret. Chim. Acta **53**, 55 (1979).

[99] C. Lee, W. Yang, and R.G. Parr, Phys. Rev. B **37**, 785 (1988).

[100] J.P. Perdew and Y. Wang, Phys. Rev. B **45**, 13244 (1992).

[101] J.A. Montgomery, J.W. Ochterski, and G.A. Petersson, J. Chem. Phys. **101**, 5900 (1994).

[102] E.R. Davidson, S.A. Hagstrom, S.J. Chakravorty, V.M. Umar, and C. Froese Fischer, Phys. Rev. A **44**, 7071 (1991).

[103] A.A. Radzig and B.M. Smirnov, *Reference Data on Atoms and Molecules* (Springer, Berlin, 1985).

[104] T. Grabo, T.Kreibich, and E.K.U. Gross, Mol. Engineering (1997), in press.

[105] B.G. Johnson, P.M.W. Gill, and J.A. Pople, J. Chem. Phys. **98**, 5612 (1993).

[106] K.P. Huber and G. Herzberg, *Molecular Spectra and Molecular Structure: IV. Constants of Diatomic Molecules* (Van Nostrand Reinhold, New York, 1979).

[107] W. Kolos and L. Wolniewicz, J. Chem. Phys. **49**, 404 (1968).

[108] K. A. Peterson, R. A. Kendall, and T. H. Dunning, J. Chem. Phys. **99**, 1930 (1993).

[109] O.V. Gritsenko, R. van Leeuwen, and E.J. Baerends, J. Chem. Phys. **104**, 8535 (1996).

[110] M.A. Buijse and E.J. Baerends, in *Density Functional Theory of Molecules, Clusters and Solids*, edited by D.E. Ellis (Kluwer Academic Publishers, Amsterdam, 1995), p. 1.

[111] T. Kotani and H. Akai, Phys. Rev. B **54**, 16502 (1996).

[112] T. Kotani and H. Akai, Physica B (1997), in press.

[113] T. Kotani, (1997), submitted.

[114] D. M. Bylander and L. Kleinman, Phys. Rev. Lett. **74**, 3660 (1994).

[115] D. M. Bylander and L. Kleinman, Phys. Rev. B **52**, 14566 (1995).

[116] D. M. Bylander and L. Kleinman, Phys. Rev. B **54**, 7891 (1996).

[117] D.M. Bylander and L. Kleinman, Phys. Rev. B **55**, 9432 (1997).

[118] M. Städele, J. A. Majewski, P. Vogl, and A. Görling, Phys. Rev. Lett. **79**, 2089 (1997).

[119] *Numerical Data and Functional Relationships in Science and Technology,* edited by K.-H. Hellwege, Landolt-Börnstein, *New Series, Group III, Vol 17*, edited by O. Madelung amd M. Schulz and H. Weiss (Springer, Berlin, 1982).

[120] D. Straub, L. Ley, and F.J. Himpsel, Phys. Rev. Lett. **54**, 142 (1985).

[121] J.E. Ortega and F.J. Himpsel, Phys. Rev. B **47**, 2130 (1993).

[122] A. Mainwood, in *Properties and Growth of Diamond*, edited by G. Davies (Electronic Materials Information Service, London, 1994), p. 3.

[123] A. Görling and M. Levy, Phys. Rev. B **47**, 13105 (1993).

[124] M.E. Casida, Phys. Rev. A **51**, 2005 (1995).

[125] J. Luttinger and J. Ward, Phys. Rev. **118**, 1417 (1960).

[126] E.K.U. Gross, E. Runge, and O. Heinonen, *Many-Particle Theory* (Adam Hilger, Bristol, 1991).

[127] L. Hedin and S. Lundqvist, Solid State Physics **23**, 1 (1969).